Characterization of the antibodies and antibody technologies to improve the pharmaceutical activity

Daisuke Shinmi

2018

Preface

The studies presented in this thesis had been carried out at Kyowa Hakko Kirin Co., Ltd. (formerly known as Kirin Pharma Company, Limited) during July 2007 to December 2016. This thesis aims to characterize the antibodies and antibody technologies which are able to improve the potency and efficacy of antibody therapeutics.

It is the author's great pleasure to express sincere gratitude to Professor Yasuo Mori for his guidance, valuable suggestion, heartfelt education and endless encouragement.

The author also expresses hearty thanks to Dr. Taro Tamada, Dr. Yasushi Yonezawa and Dr. Ryota Kuroki, Quantum Beam Science Center, Japan Atomic Energy Agency, Dr. Shiro Kataoka, Business Development, Anaeropharma Science.

The author is also deeply grateful to Dr. Kazuhiro Motoki, Oncology R&D Management Office, R&D Division, Kyowa Hakko Kirin Co., Ltd., Dr. Kazuhiro Masuda, Innovative Technology Laboratories, Research Functions Unit, R&D Division, Kyowa Hakko Kirin Co., Ltd., Dr. Yasuhisa Shiraishi, R&D Planning Department, R&D Division, Kyowa Hakko Kirin Co., Ltd., Dr. Kazuma Tomizuka, Innovative Technology Laboratories, Research Functions Unit, R&D Division, Kyowa Hakko Kirin Co., Ltd., Dr. Emi Arakawa, Fuji Research Park, R&D Division, Kyowa Hakko Kirin Co., Ltd., Dr. Junichi Enokizono, Kyowa Hakko Kirin (Singapore) Pte. Ltd., Dr. Eiji Mori, R&D Planning Department, R&D Division, Kyowa Hakko Kirin Co., Ltd., Ryosuke Nakano, Research Core Function Laboratories, Research Functions Unit, R&D Division, Kyowa Hakko

Kirin Co., Ltd.

The accomplishments described in this thesis could not have been achieved without the efforts of many colleagues. The author should be emphasized that the contribution of Dr. Eri Taguchi, Research Core Function Laboratories, Research Functions Unit, R&D Division, Kyowa Hakko Kirin Co., Ltd., Minami Suzuki-Imaizumi, Translational Research Unit, R&D Division, Kyowa Hakko Kirin Co., Ltd., Masahiro Ikeda, Immunology & Allergy Research Laboratories, R&D Division, Kyowa Hakko Kirin Co., Ltd., Junko Iwano, Research Core Function Laboratories, Research Functions Unit, R&D Division, Kyowa Hakko Kirin Co., Ltd., Yuya Isoda, Innovative Technology Laboratories, Research Functions Unit, R&D Division, Kyowa Hakko Kirin Co., Ltd., Tsuyoshi Yamaguchi, Bio Process Research and Development Laboratories, Production Division, Kyowa Hakko Kirin Co., Ltd., Keisuke Mitamura, Oncology Research Laboratories, Oncology R&D Unit, R&D Division, Kyowa Hakko Kirin Co., Ltd., who participated in some work presented here, are greatly appreciated.

Many thanks to my family and my friends who have been supported me to complete my thesis, for their kind understanding of my career decision and heartwarming assistance.

Daisuke Shinmi

Research Core Function Laboratories

Research Functions Unit

R&D Division

Kyowa Hakko Kirin Co., Ltd.

Contents

General introduction

Monoclonal antibody therapeutics

Monoclonal antibody therapy is one of the most successful and important strategies for treating patients with many types of diseases. Currently, more than 40 therapeutic antibodies are on the market to treat cancers as well as immunological and other diseases, such as Adalimumab (anti-tumor necrosis factor [TNF]-α antibody), Rituximab (anti-CD20 antibody), Bevacizumab (anti-vascular endothelial growth factor [VEGF] antibody), Trastuzumab (anti-HER2 antibody), Palivizumab (anti-respiratory syncytial virus [RSV] antibody), Omalizumab (anti-immunoglobulin E [IgE] antibody) and (anti-epidermal growth factor receptor [EGFR] antibody)[1-8].

Antibodies, which are also called immunoglobulins, are large proteins used by the immune system to identify and neutralize foreign objects such as bacteria and viruses. Immunoglobulins are composed of two identical heavy chains and two identical light chains, linked by disulfide bonds. Light chains fold into a variable domain (VL) and a constant domain (CL), whereas heavy chains are composed of one variable domain (VH) and three constant domains (CH1-3). The antigen-binding sites at the tip of the Fab regions are formed from the variable domains of both the heavy and light chains. The Fc region mediates interaction with effector molecules, such as complement and Fc receptors. There are five types of immunoglobulins or antibodies in the blood: IgG, IgA, IgM, IgD and IgE. IgG is present in the largest amount, followed by IgM and IgA. IgD is much lower, and IgE is present in only minute amounts[9]. All of the approved therapeutic antibodies are IgGs.

Current modern era of therapeutic antibodies originated with the invention of

hybridoma technology to generate mouse monoclonal antibodies in 1975[10]. Then, immunogenicity: major limitations of mouse antibodies as therapeutic agents, lack of effector functions and short serum half-life, were subsequently identified and largely overcome by the advent of antibody chimerization and, later, humanization technologies in the 1980s[11]. Furthermore, fully human sequence antibodies isolated from either phage display or transgenic mouse platforms have been approved for therapeutic use[12].

Monoclonal antibody drugs that bind directly to target cells can mediate their therapeutic effects through various mechanisms. Monoclonal antibodies can promote antibody-dependent cellular cytotoxicity (ADCC) and tumor cell destruction by immune effector cells, such as natural killer cells, monocytes, macrophages, neutrophils, eosinophils and dendritic cells through binding to the Fc gamma receptors (FcγRs) expressed on these cells[13]. Complement-dependent cytotoxicity (CDC) can directly result in target cell death through the development of a membrane attack complex[14]. Monoclonal antibodies can also have direct effects on target cells by inhibiting or activating receptor signal pathway. Blocking an activation signal by monoclonal antibodies is induced by binding to the ligand and preventing interaction with receptor, binding the ligand-binding site of the receptor and preventing interaction with ligand, and preventing dimerization domain or sterically blocking the interaction[15-17]. Whereas, activating receptor signal or inducing an apoptotic signal is induced by crosslinking a receptor[18,19]. Such crosslinking of the receptor can be enhanced when a monoclonal antibody is bound to Fc receptor-expressing cells.

Global sales revenue for all monoclonal antibody products such as described above was nearly $75 billion in 2013, representing approximately half of the total sales of all biopharmaceutical products[1]. However, despite the clinical success of these antibodies,

many clinical trials, especially in the field of oncology, have failed to show a benefit in patients owing to lack of efficacy. To improve the efficacy of antibody therapeutics, various new technologies have been subject to considerable research. For example, Fc engineering such as POTELLIGENT® developed by Kyowa Hako Kirin is one of the emerging technologies which can enhance binding affinity to FcγR, leading to improved ADCC[20,21].

Survey of this thesis

This thesis consists of the following three chapters on evaluation technologies or characters which have possibilities of improving the potency and efficacy of antibody therapeutics.

Antibody-drug conjugate. Antibody-drug conjugate (ADC) is another technology which can enhance activity of antibodies. ADCs are monoclonal antibodies attached to biologically active drugs by chemical linkers and have a mechanism for selective delivery of the cytotoxic agent to cancer cells via the specific binding of the antibody to cancer-selective cell surface molecules[22]. The first two approved ADCs and many other ADC candidates which are under clinical investigation are heterogeneous products from the aspect of drug loading. This heterogeneity might be lead to affect the pharmacokinetics, efficacy, and therapeutic index of the resulting ADC[23]. The first chapter describes a novel and facile preparation method of ADC to prepare a homogeneous product by using an antibody variant which genetically introduces unpaired cysteine residues.

Soluble antigen uncompetitive antibody. Carcinoembryonic antigen (CEA) is highly

expressed and released by most tumors of gastrointestinal origin. Therefore, soluble CEA released by tumors is present in the circulation of patients with cancer, where it is used as a marker for cancer progression[24]. However its use as a target for tumor therapy by antibodies might be impeded by the high levels of soluble CEA that are found circulating in the blood of cancer patients because of competition between membrane-bound and soluble form of CEA. The second chapter shows about a novel anti-CEA antibody which exhibit strong binding to membrane-bound form and poor affinity for soluble form to overcome the competition.

Direct agonistic antibody. Anti-TNF-related apoptosis-inducing ligand receptor 2 (TRAIL-R2) antibody exhibits agonist activity, and is able to induce apoptosis of TRAIL-R2 expressing tumor cells[25]. Common bivalent IgG antibodies can induce the efficient apoptosis by mimicking the natural ligands but only after these antibodies are further oligomerized by crosslinking by Fc receptor-expressing cells[26]. However, the effector function of such endogenous cross-linkers might be variable in individual patients due to immunosuppressive therapies and polymorphism of Fc receptor[27-29]. KMTR2 is a "direct agonist antibody" against TRAIL-R2 that is capable of inducing apoptosis without cross-linking and elucidated its mode of action and efficacy[30]. The last chapter describes how this antibody oligomerizes and induces apoptosis to the cancer cells by using X-ray crystal structure analysis of KMTR2.

References

1 Ecker, D. M., Jones, S. D. & Levine, H. L. The therapeutic monoclonal antibody market. *MAbs* **7**, 9-14, doi:10.4161/19420862.2015.989042 (2015).

2 van de Putte, L. B. *et al.* Efficacy and safety of adalimumab as monotherapy in patients with rheumatoid arthritis for whom previous disease modifying antirheumatic drug treatment has failed. *Annals of the rheumatic diseases* **63**, 508-516, doi:10.1136/ard.2003.013052 (2004).

3 McLaughlin, P. *et al.* Rituximab chimeric anti-CD20 monoclonal antibody therapy for relapsed indolent lymphoma: half of patients respond to a four-dose treatment program. *Journal of clinical oncology : official journal of the American Society of Clinical Oncology* **16**, 2825-2833, doi:10.1200/jco.1998.16.8.2825 (1998).

4 Hurwitz, H. *et al.* Bevacizumab plus irinotecan, fluorouracil, and leucovorin for metastatic colorectal cancer. *N Engl J Med* **350**, 2335-2342, doi:10.1056/NEJMoa032691 (2004).

5 Cobleigh, M. A. *et al.* Multinational study of the efficacy and safety of humanized anti-HER2 monoclonal antibody in women who have HER2-overexpressing metastatic breast cancer that has progressed after chemotherapy for metastatic disease. *Journal of clinical oncology : official journal of the American Society of Clinical Oncology* **17**, 2639-2648, doi:10.1200/jco.1999.17.9.2639 (1999).

6 Makari, D., Jensen, K. M., Harris, B. & Jafri, H. S. Randomized, Double-Blind Study of the Safety of the Liquid Versus Lyophilized Formulation of Palivizumab in Premature Infants and Children with Chronic Lung Disease of Prematurity. *Infectious diseases and therapy* **3**, 339-347, doi:10.1007/s40121-014-0033-y

(2014).

7 Corren, J., Casale, T., Deniz, Y. & Ashby, M. Omalizumab, a recombinant humanized anti-IgE antibody, reduces asthma-related emergency room visits and hospitalizations in patients with allergic asthma. *The Journal of allergy and clinical immunology* **111**, 87-90 (2003).

8 Cunningham, D. *et al.* Cetuximab monotherapy and cetuximab plus irinotecan in irinotecan-refractory metastatic colorectal cancer. *N Engl J Med* **351**, 337-345, doi:10.1056/NEJMoa033025 (2004).

9 Schroeder, H. W., Jr. & Cavacini, L. Structure and function of immunoglobulins. *The Journal of allergy and clinical immunology* **125**, S41-52, doi:10.1016/j.jaci.2009.09.046 (2010).

10 Kohler, G. & Milstein, C. Continuous cultures of fused cells secreting antibody of predefined specificity. *Nature* **256**, 495-497 (1975).

11 Almagro, J. C. & Fransson, J. Humanization of antibodies. *Frontiers in bioscience : a journal and virtual library* **13**, 1619-1633 (2008).

12 Lonberg, N. Fully human antibodies from transgenic mouse and phage display platforms. *Current opinion in immunology* **20**, 450-459, doi:10.1016/j.coi.2008.06.004 (2008).

13 Nimmerjahn, F. & Ravetch, J. V. Fcgamma receptors: old friends and new family members. *Immunity* **24**, 19-28, doi:10.1016/j.immuni.2005.11.010 (2006).

14 Zipfel, P. F. & Skerka, C. Complement regulators and inhibitory proteins. *Nat Rev Immunol* **9**, 729-740, doi:10.1038/nri2620 (2009).

15 Sunada, H., Magun, B. E., Mendelsohn, J. & MacLeod, C. L. Monoclonal antibody against epidermal growth factor receptor is internalized without

stimulating receptor phosphorylation. *Proceedings of the National Academy of Sciences of the United States of America* **83**, 3825-3829 (1986).

16 Li, S. *et al.* Structural basis for inhibition of the epidermal growth factor receptor by cetuximab. *Cancer Cell* **7**, 301-311, doi:10.1016/j.ccr.2005.03.003 (2005).

17 Chen, J. S., Lan, K. & Hung, M. C. Strategies to target HER2/neu overexpression for cancer therapy. *Drug resistance updates : reviews and commentaries in antimicrobial and anticancer chemotherapy* **6**, 129-136 (2003).

18 Shan, D., Ledbetter, J. A. & Press, O. W. Apoptosis of malignant human B cells by ligation of CD20 with monoclonal antibodies. *Blood* **91**, 1644-1652 (1998).

19 Pedersen, I. M., Buhl, A. M., Klausen, P., Geisler, C. H. & Jurlander, J. The chimeric anti-CD20 antibody rituximab induces apoptosis in B-cell chronic lymphocytic leukemia cells through a p38 mitogen activated protein-kinase-dependent mechanism. *Blood* **99**, 1314-1319 (2002).

20 Ishida, T. *et al.* Defucosylated anti-CCR4 monoclonal antibody (KW-0761) for relapsed adult T-cell leukemia-lymphoma: a multicenter phase II study. *Journal of clinical oncology : official journal of the American Society of Clinical Oncology* **30**, 837-842, doi:10.1200/jco.2011.37.3472 (2012).

21 Cartron, G. *et al.* Obinutuzumab (GA101) in relapsed/refractory chronic lymphocytic leukemia: final data from the phase 1/2 GAUGUIN study. *Blood* **124**, 2196-2202, doi:10.1182/blood-2014-07-586610 (2014).

22 Chari, R. V., Miller, M. L. & Widdison, W. C. Antibody-drug conjugates: an emerging concept in cancer therapy. *Angew Chem Int Ed Engl* **53**, 3796-3827, doi:10.1002/anie.201307628 (2014).

23 Hamblett, K. J. *et al.* Effects of drug loading on the antitumor activity of a

monoclonal antibody drug conjugate. *Clin Cancer Res* **10**, 7063-7070, doi:10.1158/1078-0432.ccr-04-0789 (2004).

24 Cooper, E. H., Turner, R., Steele, L., Neville, A. M. & Mackay, A. M. The contribution of serum enzymes and carcinoembryonic antigen to the early diagnosis of metastatic colorectal cancer. *Br J Cancer* **31**, 111-117 (1975).

25 Almasan, A. & Ashkenazi, A. Apo2L/TRAIL: apoptosis signaling, biology, and potential for cancer therapy. *Cytokine & growth factor reviews* **14**, 337-348 (2003).

26 Mori, E. *et al.* Human normal hepatocytes are susceptible to apoptosis signal mediated by both TRAIL-R1 and TRAIL-R2. *Cell Death Differ* **11**, 203-207, doi:10.1038/sj.cdd.4401331 (2004).

27 Weng, W. K. & Levy, R. Two immunoglobulin G fragment C receptor polymorphisms independently predict response to rituximab in patients with follicular lymphoma. *Journal of clinical oncology : official journal of the American Society of Clinical Oncology* **21**, 3940-3947, doi:10.1200/jco.2003.05.013 (2003).

28 Kono, K. *et al.* Impaired antibody-dependent cellular cytotoxicity mediated by herceptin in patients with gastric cancer. *Cancer Res* **62**, 5813-5817 (2002).

29 Cartron, G. *et al.* Therapeutic activity of humanized anti-CD20 monoclonal antibody and polymorphism in IgG Fc receptor FcgammaRIIIa gene. *Blood* **99**, 754-758 (2002).

30 Motoki, K. *et al.* Enhanced apoptosis and tumor regression induced by a direct agonist antibody to tumor necrosis factor-related apoptosis-inducing ligand receptor 2. *Clin Cancer Res* **11**, 3126-3135, doi:10.1158/1078-0432.ccr-04-1867 (2005).

Chapter 1

One-step conjugation method for site-specific antibody-drug conjugates through reactive cysteine engineered antibodies

Abstract

Engineered cysteine residues are particularly convenient method for the site-specific conjugation of antibody drug conjugates (ADC), because no cell engineering and additives required. In general, cysteine residues of the cysteine engineered antibody usually form mixed disulfides with glutathione or other cysteine during production of therapeutic proteins from Chinese hamster ovary (CHO) cells, therefore, additional reduction and reoxidization steps are required prior to conjugation. In this study, we prepared light chain (Lc)-Q124C variants of IgG and examined conjugation efficiency. Intriguingly, Lc-Q124C exhibited high thiol reactivity and generated site-specific ADC without any pretreatment (named active thiol antibody: Actibody). Most of the cysteine-maleimide conjugates including Lc-Q124C showed retro-Michael reaction with cysteine 34 in plasma albumin and were decomposed over time. In order to acquire resistance to such a maleimide exchange reaction, the facile procedure for succinimide hydrolysis on anion exchange resin was generated. Hydrolyzed Lc-Q124C conjugate prepared with anion exchange procedure retained high stability in plasma. Recently, various stable linkage schemes for cysteine conjugation have been reported. Combination with Actibody technology and stable linker technology could enable to generate stable site-specific ADCs by simple

method. Actibody technology open the new way of cysteine-based conjugation, and contribute to drop entry barriers to preparation and evaluation of ADCs.

Introduction

Antibody-drug conjugates (ADCs) are new class of highly potent drug modalities that equip antibodies with potent cytotoxic payloads and attract much interest in cancer therapy in the last few years. Targeted delivery of a cytotoxic drug to the target cells by antibody decreases the minimum effective dose and at the same time elevates the maximum tolerated dose. ADCs have shown significant progress in oncology field through the two FDA approved-drugs, ado-trastuzumab emtansine (KADCYLA®) and brentuximab vedotin (ADCETRIS®). Furthermore, many ADCs prepared with various combinations of antibodies and linker-drugs have currently undergone clinical studies[1].

Conjugation of the drug payload to the antibody needs a controlled chemical reaction with specific amino acid residues exposed on the surface of the antibody. Most of the current ADC products generally apply a chemical reaction of lysine ε-amino groups or cysteine sulfhydryl groups activated by reducing the inter-chain disulfide bonds of antibody[2]. These conjugation chemistries produce heterogeneous products at the molecular level, lead to affect the different pharmacokinetics, efficacy, and therapeutic index. Especially, the ADCs with an average of two to four drug-to-antibody ratios (DARs) have been shown to be suitable for exerting maximal *in vivo* efficacy[3].

Site-specific conjugation is one of the most effectual techniques to reduce heterogeneity of current ADC[4]. In recent years, the site specific modification of antibodies has been achieved by protein engineering strategies such as introducing cysteine residues in the antibody sequence[5-9], incorporating sugars[10,11], unnatural amino acid with bio-orthogonal reactivity[12,13], or genetic encoding of peptide tags for further enzymatic modification[14,15]. The engineered antibodies with additional cysteine residues such as THIOMAB technology offer a particularly convenient method, in that no cell-

engineering and additional reagents are required. However, the introduced cysteine residues in IgG generally formed mixed disulfides with cysteine or glutathione, possibly during the fermentation process in Chinese hamster ovary (CHO) cells. Therefore, complicated reduction and reoxidation steps are required in order to produce unpaired, reactive sulfhydryl groups prior to drug conjugation (Scheme 1A)[6,16].

We previously reported that several engineered cysteine residues at less exposed positions of Fab fragment showed high conjugation efficiency with various-sized molecules. Among them, Fab-Lc-Q124C, which was introduced engineered cysteine residues at the position with the lowest Accessible Surface Area (ASA)[17], exhibited the highest thiol reactivity. In order to confirm the versatility and potency of Lc-Q124C, IgG-Lc-Q124C was produced through fermentation in CHO cells and compared with other variant such as IgG-Hc-A118C and IgG-Lc-V205C with THIOMAB technology[16]. Here, we disclosed that IgG-Lc-Q124C (named active thiol antibody: Actibody) retained high thiol reactivity itself and made it possible to perform one-step conjugation without any pretreatment (Scheme 1B). Furthermore, we examined possibility of application to site-specific ADC.

Scheme 1. General strategy for synthesis of site-specific antibody-drug conjugates with common cysteine-engineered antibody technology (A). Simple strategy for synthesis of site-specific antibody-drug conjugates with Actibody technology (B)

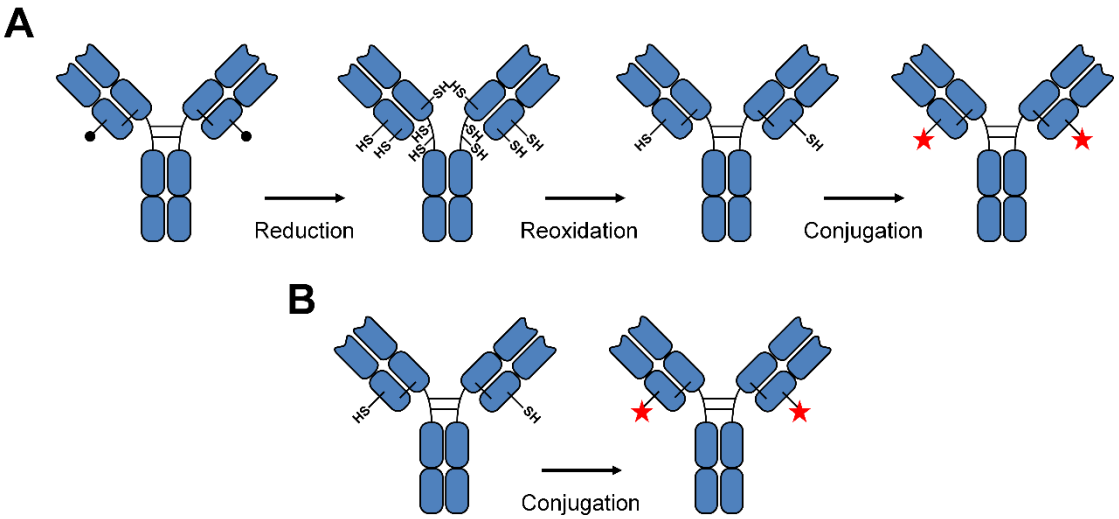

Results

Comparison of thiol reactivity of cysteine positional variants. Trastuzumab (Tra) was used as a model antibody in this study. Yields of all of Tra-IgG cysteine positional variants were similar to that of Tra-WT and existed mainly as monomer (Figure 1). We examined thiol reactivity and drug-antibody ratio (DAR) of four selected clones (Tra-IgG-WT, -Lc-Q124C, -Lc-V205C, and -Hc-A118C) without any reduction procedure using 4-PDS assay and Alexa 488 conjugates (Table 1). Tra-IgG-Lc-V205C and -Hc-A118C using THIOMAB technology were well-known for production of site-specific antibody-drug conjugates[6,16]. As in the previous case of Tra-Fab[17], selected cysteine positional variants existed as monomer and possessed similar binding affinity to that of Tra-IgG-WT (data not shown). Tra-IgG-WT showed less thiol reactivity evaluated by 4-PDS assay and Alexa 488-antibody ratio (0.074 and 0.17). Tra-IgG-Lc-V205C and -Hc-A118C exhibited a little thiol reactivity (0.48 and 0.36), which was far from theoretical value: 2.0. In addition, Alexa 488-antibody ratios were also low (0.44 and 0.37), which was consistent with low thiol reactivity. On the other hand, Tra-IgG-Lc-Q124C retained much higher thiol reactivity and Alexa 488-antibody ratio, which were similar to theoretical value. In order to examine the differences in thiol reactivity and Alexa 488-antibody ratios, we determined molecular weight of selected clones by LC-MS analysis (Figure 2). Tra-IgG-Lc-V205C and -Hc-A118C showed broaden peaks which were located at higher molecular weight than those of estimated values as previously reported[6]. To the contrary, Tra-IgG-Lc-Q124C showed single peak corresponding to the estimated value as in the case of Tra-IgG-WT.

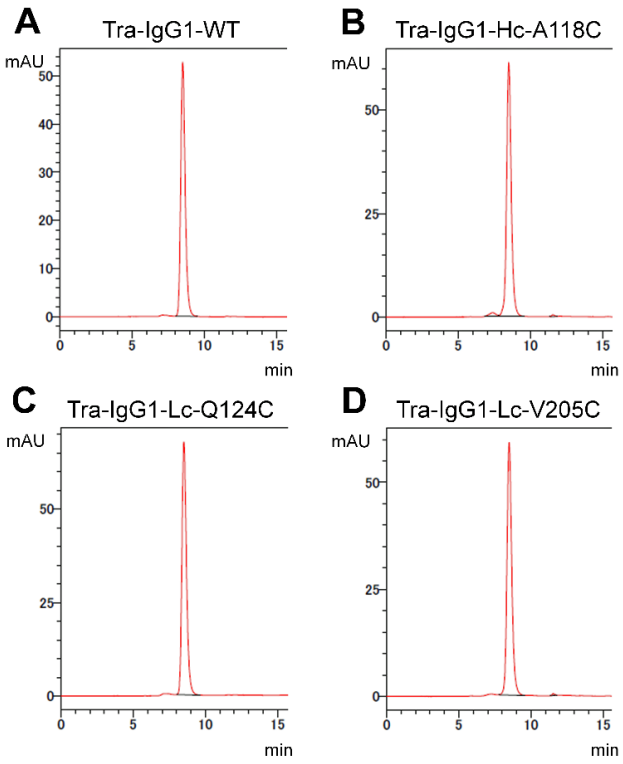

Figure 1. Size-exclusion chromatograms of Tra-IgG-WT (A), Tra-IgG-Hc-A118C (B), Tra-IgG-Lc-Q124C (C), and Tra-IgG-Lc-V205C (D).

Table 1. Thiol reactivity and Alexa 488-antibody ratios of selected clones.

Variant	Thiol Reactivity[a]	Alexa488[a]
Tra-IgG-WT	0.074 ± 0.0022	0.17 ± 0.0087
Tra-IgG-Lc-Q124C	2.0 ± 0.016	2.0 ± 0.013
Tra-IgG-Hc-A118	0.36 ± 0.0025	0.37 ± 0.060
Tra-IgG-Lc-V205C	0.48 ± 0.0040	0.44 ±0.0057

[a]Thiol reactivity and Alexa 488-antibody ratios were determined by three independent assays. Each value was shown as mean value ± standard deviation (SD).

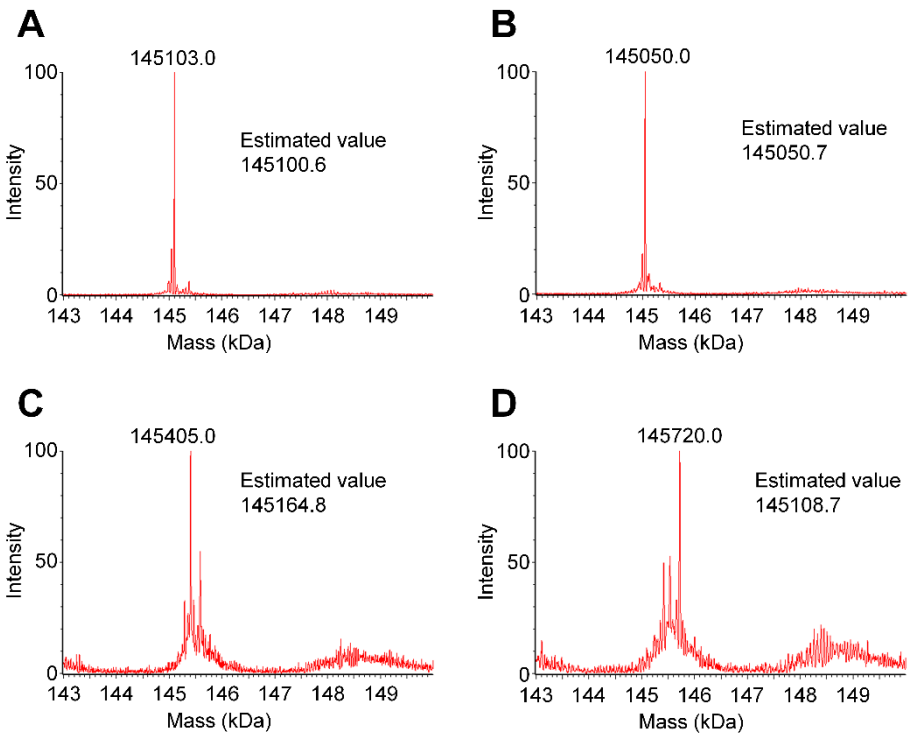

Figure 2. Deconvoluted mass spectra of naked Tra-IgG-WT (A), Tra-IgG-Lc-Q124C (B), Tra-IgG-Hc-A118C (C), and Tra-IgG-Lc-V205C (D). The most intense peak in each mass spectrum corresponds to the molecular weight of the antibody.

Preparation and evaluation of Tra-IgG- vcMMAE conjugates. Three-quarters of the ADCs in the current clinical trials utilize either auristatin or maytansine derivatives, which are developed by Seattle Genetics and ImmunoGen[18]. Auristatin derivative: vcMMAE has been designed to link to antibody via maleimide-thiol chemistry. In consideration to high thiol reactivity and DAR of Alexa 488 conjugate, Tra-IgG-Lc-Q124C was directly conjugated with vcMMAE for producing site-specific ADC (Scheme 1B). Tra-IgG-Lc-V205C-vcMMAE and –Hc-A118C-vcMMAE were prepared as control through reduction/reoxidization procedure shown in previous report (Scheme 1A)[19]. As

shown in Figure 3, all of the Tra-IgG-vcMMAE conjugates existed mainly as population with DAR: 2.0. We confirmed that Tra-IgG-Lc-Q124C-vcMMAE existed mainly as monomers by size exclusion chromatography (SEC) analysis (Figure 4). Hence, we confirmed that Tra-IgG-Lc-Q124C could produce site-specific conjugate by one-step procedure as shown in Scheme 1B.

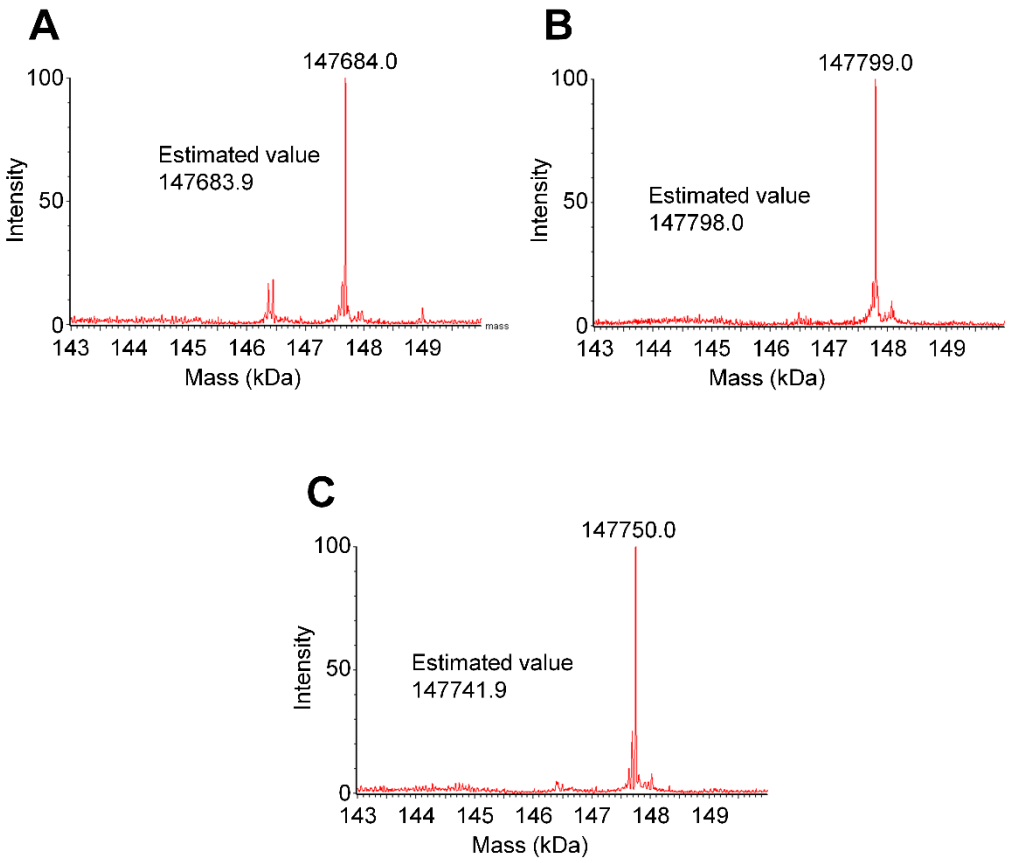

Figure 3. Deconvoluted mass spectra of Tra-IgG-Lc-Q124C-vcMMAE (A), Tra-IgG-Hc-A118C-vcMMAE (B), and Tra-IgG-Lc-V205-vcMMAE (C). Tra-IgG-Lc-Q124C-vcMMAE was produced by direct approach (Scheme 1B), on the other hand, Tra-IgG-Hc-A118C-vcMMAE and -Lc-V205C-vcMMAE were prepared by common route (Scheme 1A).

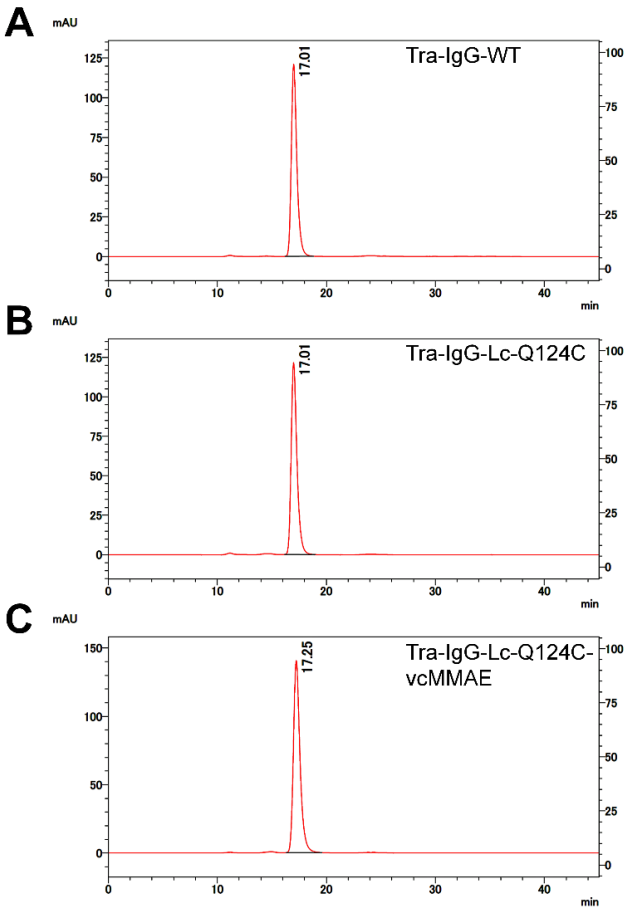

Figure 4. Size-exclusion chromatograms of Tra-IgG-WT (A), Tra-IgG-Lc-Q124C (B) and Tra-IgG-Lc-Q124C-vcMMAE (C).

In order to compare the ADC derived from Tra-IgG-Lc-Q124C with those derived from Tra-IgG-Lc-V205C and -Hc-A118C, we assessed cytotoxicity against Her2 expressing SK-BR-3, BT-474 and NCI-N87 cells using CellTiter-Glo assay[17]. Tra-IgG-Lc-Q124C-vcMMAE exerted similar cytotoxicity to those of Tra-IgG-Hc-A118C-vcMMAE and -Lc-V205C-vcMMAE against SK-BR-3 cells *in vitro* (Figure 5A). Similar results were observed in BT-474 and NCI-N87 cells (Figure 5B, C). IC_{50} values of Tra-IgG-vcMMAE conjugates were shown in Table 2. We confirmed that control-IgG-Lc-

Q124C-vcMMAE had no cytotoxicity between 0.32 and 1000 ng/mL (Figure 6).

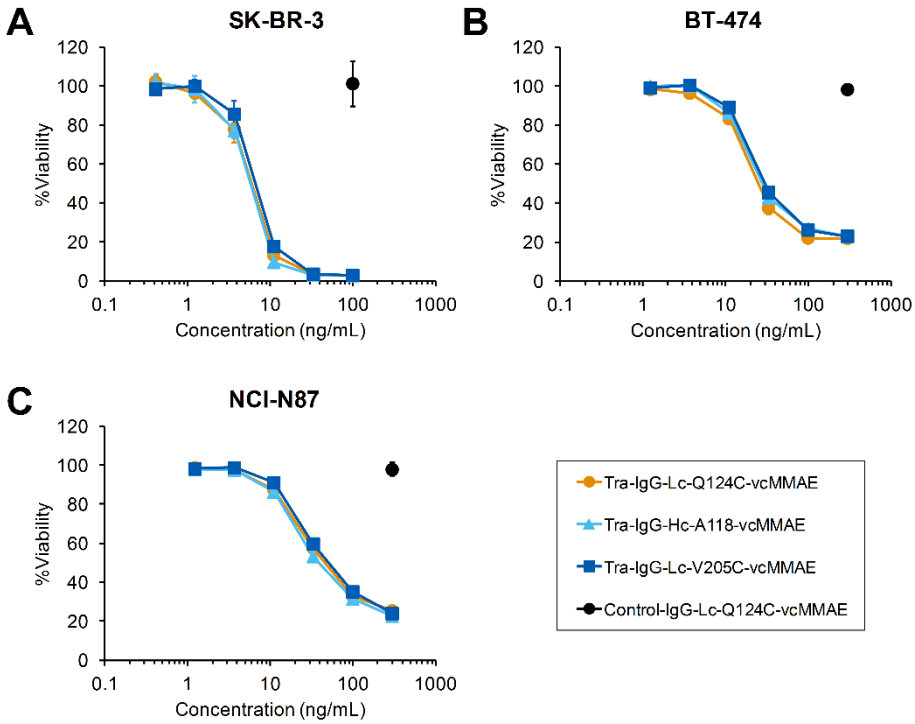

Figure 5. *In vitro* cytotoxicity of Tra-IgG-Lc-Q124C-vcMMAE, Tra-IgG-Hc-A118-vcMMAE, Tra-IgG-Lc-V205-vcMMAE, and control-IgG1-Lc-Q124C-vcMMAE on Her2-positive breast cancer cell lines, SK-BR-3 (A), BT-474 (B), and NCI-N87 (C).

Table 2. Cytotoxic activity (IC_{50} values) of Q124C, A118C and V205C conjugates.

Cys variant	Cytotoxicity in tumor cell lines IC_{50} (ng/mL)		
	SK-BR-3	BT-474	NCI-N87
Tra-IgG-Lc-Q124C-vcMMAE	5.62 ± 0.58	24.1 ±1.5	41.4 ± 1.2
Tra-IgG-Hc-A118C-vcMMAE	5.28 ± 0.24	27.7 ± 1.4	38.0 ± 0.96
Tra-IgG-Lc-V205C-vcMMAE	6.57 ± 0.63	29.9 ± 0.31	47.0 ± 2.5

IC_{50} values were determined by three independent assays and calculated using XLfit software. Each value was shown as mean value ± standard deviation (SD).

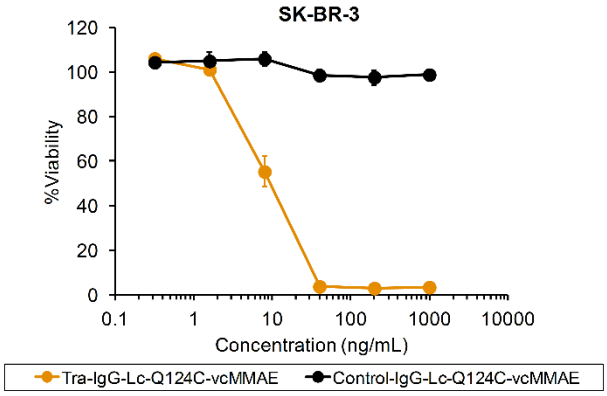

Figure 6. *In vitro* cytotoxicity of Tra-IgG-Lc-Q124C-vcMMAE and control-IgG-Lc-Q124C-vcMMAE on HER2-positive breast cancer cell lines, SK-BR-3.

Analysis of drug-linker stability in vitro. To confirm the stability depending on the conjugation site, Tra-IgG-Lc-Q124C-Alexa 488, -Lc-V205C-Alexa 488 and -Hc-A118C-Alexa 488 were incubated in human plasma for 96 hours followed by size-exclusion chromatographic analysis by detecting Alexa 488 fluorescence. As reported by Shen's group[16], the fluorescent peak of Tra-IgG-Lc-V205C-Alexa 488 was almost retained throughout 24 hours incubation period, whereas that of Tra-IgG-Hc-A118C-Alexa 488 modestly decreased and new peak appeared at lower molecular weight at 24 hours, which corresponded to albumin-Alexa 488 conjugate (Figure 7A and B). On the contrary, the fluorescent intensity of Tra-IgG-Lc-Q124C-Alexa 488 was dramatically moved to the lower molecular weight peak at 24 hours (Figure 7C). The time course of the ratio of Tra-IgG-Alexa 488 conjugate was plotted (Figure 8), which also exhibited dramatic reduction caused by retro-Michael Reaction in Tra-IgG-Lc-Q124C-Alexa 488 conjugate.

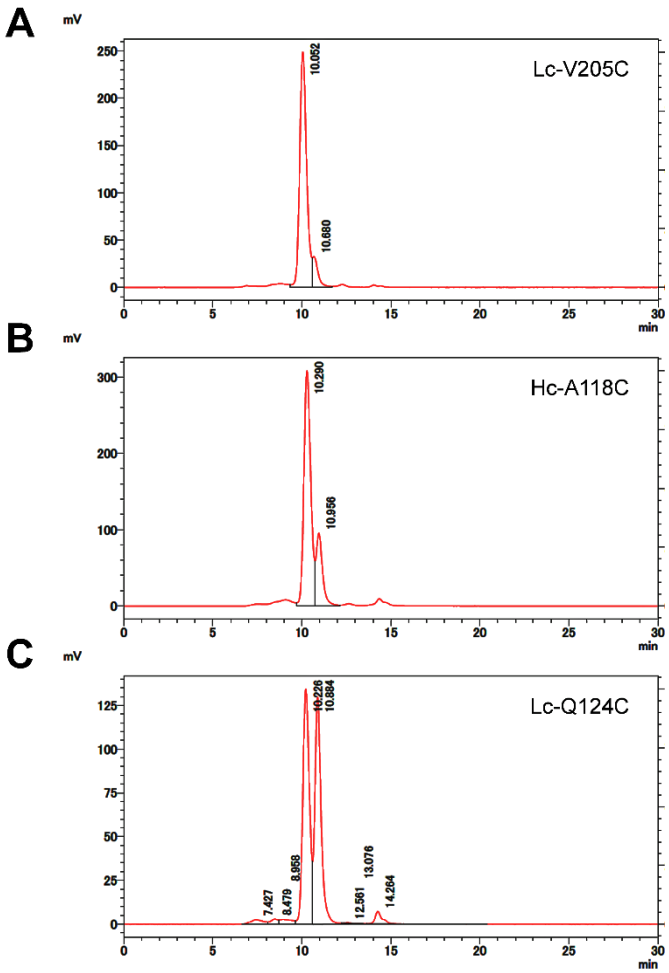

Figure 7. Fluorescence-detection size-exclusion chromatograms of Tra-IgG-Lc-V205C-Alexa 488 (A), Tra-IgG-Hc-A118C- Alexa 488 (B), and Tra-IgG-Lc-Q124C- Alexa 488 (C) after 24 hours incubation in human plasma.

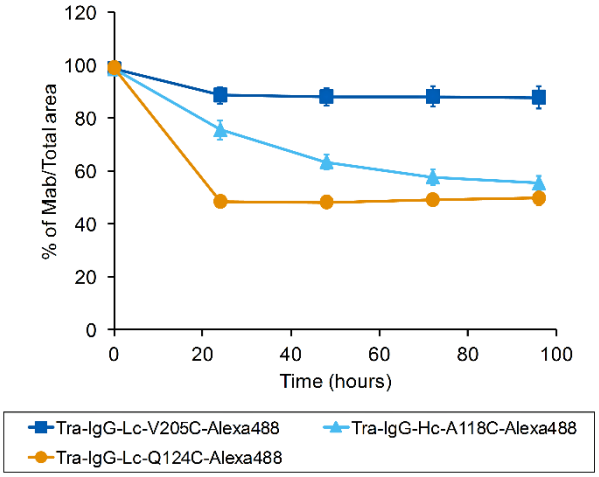

Figure 8. Stability of Tra-IgG-Lc-Q124C-Alexa 488, Tra-IgG-Hc-A118-Alexa 488, and Tra-IgG-Lc-V205-Alexa 488 in human plasma. Measurement of Tra-IgG-Alexa 488 conjugate concentration was conducted by Fluorescence-detection size-exclusion chromatography.

Linker stabilization on anion exchange resin and evaluation of stabilized ADC. Recent studies demonstrated that retro-Michael type mediated transfer of linker-payload portion was induced by exposure of high concentration of free thiols such as cysteine, glutathione, and serum albumin[20]. Hydrolysis of succinimide ring in alkaline medium allowed prevention of retro and reversible maleimide transfer[21-23]. In this study, we applied anion exchange chromatography techniques to induce succinimide ring-opening under an alkaline condition in solid phase system (Scheme 2). Succinimide hydrolysis of Tra-IgG-Tra-IgG-Lc-Q124C-vcMMAE (hy-Tra-IgG-Lc-Q124C-vcMMAE) was confirmed by using LC-MS analysis (Figure 9). The binding and cytotoxic activities of hy-Tra-IgG-Lc-Q124C-vcMMAE were maintained (Table 3, Figure 10). The hy-Tra-IgG-Lc-Q124C-Alexa488 which was produced by the same procedure retained the linker-drug portion in human plasma during the 96 hours incubation period (Figure. 11).

Scheme 2. Mechanism of drug transfer from an antibody to albumin through the maleimide exchange reaction and prevention of drug transfer by succinimide hydrolysis with anion exchange chromatography techniques.

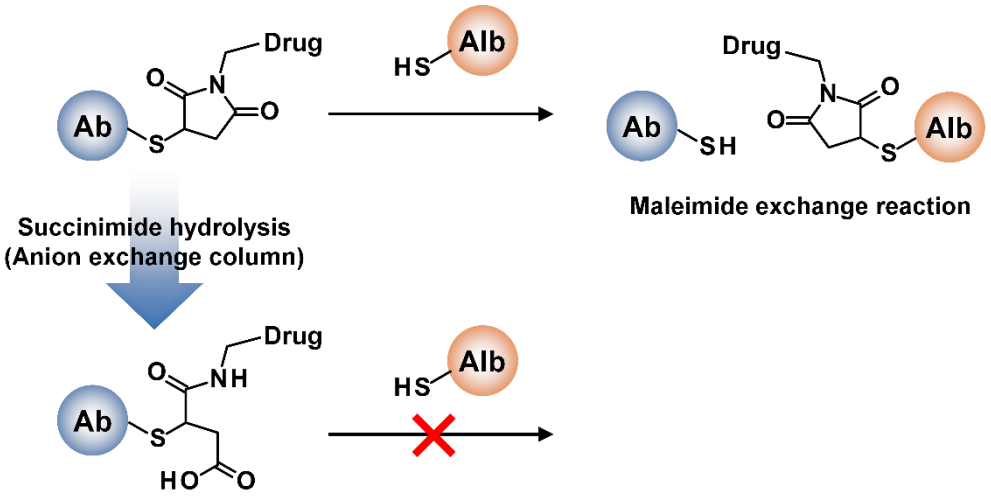

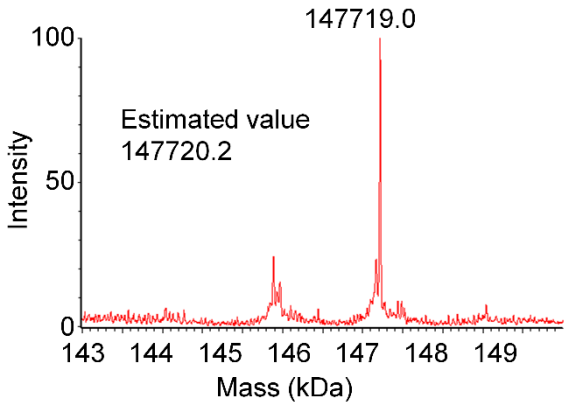

Figure 9. Deconvoluted mass spectra of hy-Tra-IgG-Lc-Q124C- vcMMAE.

Table 3. Binding kinetics of succinimide-hydrolyzed Trastuzumab-Lc-Q124C conjugates compared with nontreated conjugate and naked antibody.

ADC or antibody	KD (nM)
Tra-IgG-WT	2.77 ± 0.042
Tra-IgG-Lc-Q124C-Alexa488	2.75 ± 0.071
hy-Tra-IgG-Lc-Q124C-Alexa488	3.68 ± 0.069
Tra-IgG-Lc-Q124C-vcMMAE	2.60 ± 0.042
hy-Tra-IgG-Lc-Q124C-vcMMAE	3.62 ± 0.080

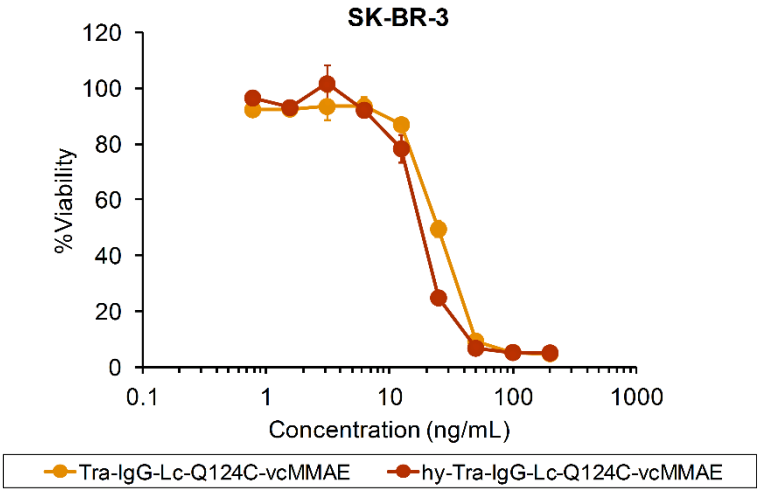

Figure 10. *In vitro* cytotoxicity of Tra-IgG-Lc-Q124C-vcMMAE and hy-Tra-IgG-Lc-Q124C-vcMMAE on HER2-positive breast cancer cell lines, SK-BR-3.

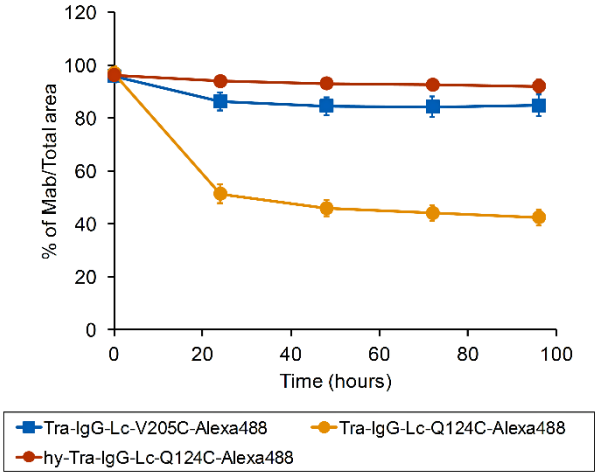

Figure 11. Evaluation of succinimide hydrolyzed Tra-IgG-Lc-Q124C-Alexa 488. Stability of hy-Tra-IgG-Lc-Q124C conjugate, nontreated Tra-IgG-Lc-Q124C conjugate and Tra-IgG-Lc-V205C conjugate in human plasma

---

Antitumor activity of Tra-IgG-Lc-Q124C-vcMMAE. In Drake's and Jackson's reports[14,24], NCI-N87 tumor xenograft model was used for evaluation of efficacy of Tra-based ADC. To evaluate whether differences in linker stability *in vitro* correlate with differences in antitumor activity, Tra-IgG-Lc-Q124C-vcMMAE, hy-Tra-IgG-Lc-Q124C-vcMMAE and Tra-IgG-Lc-V205C-vcMMAE were intravenously administered once into tumor bearing mice at doses of 0.3 and 1 mg/kg (Figure 12). All Tra-IgG-vcMMAE conjugates showed partial inhibition in tumor growth at 0.3 mg/kg. The tumor growth rates of both hy-Tra-IgG-Lc-Q124C-vcMMAE and Tra-IgG-Lc-V205C-vcMMAE treated mice were slower than that of Tra-IgG-Lc-Q124C-vcMMAE. At a dosing of 1 mg/kg, there were no differences in efficacy between these three treatment groups until day 63. However, tumor volume in mice treated with Tra-IgG-Lc-Q124C-vcMMAE stared to regrow, which was about three-fold larger than those of hy-Tra-IgG-Lc-Q124C-

vcMMAE and Tra-IgG-Lc-V205C-vcMMAE treated mice at day 83.

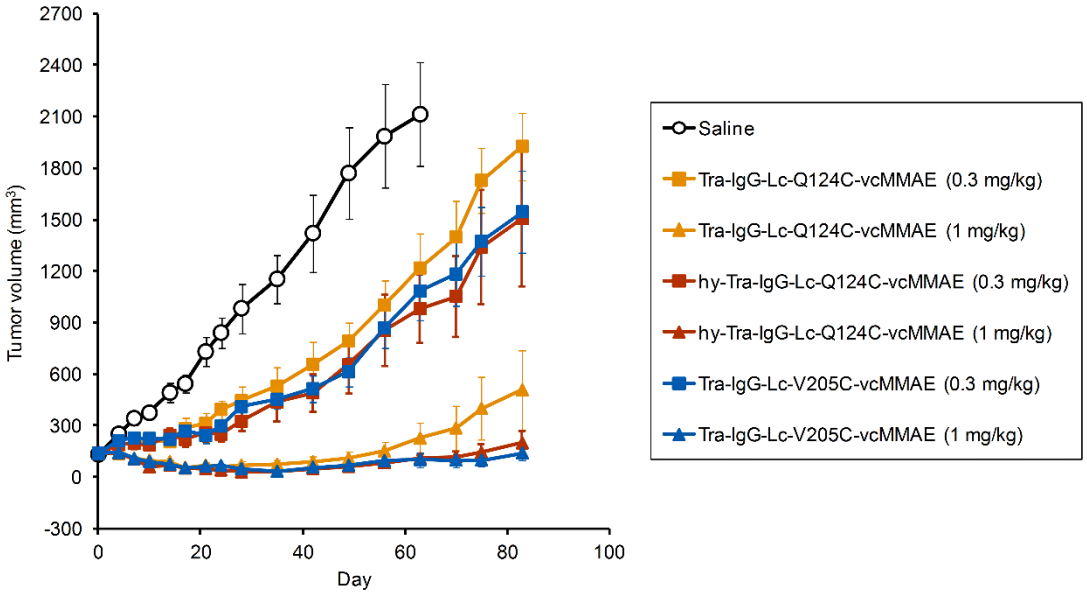

Figure 12. *In vivo* efficacy of Tra-IgG-Lc-Q124C-vcMMAE, hy-Tra-IgG-Lc-Q124C-vcMMAE and Tra-IgG-Lc-V205-vcMMAE in a xenograft model. Male SCID mice were injected subcutaneously with NCI-N87 cells. Tra-IgG-Lc-Q124C-vcMMAE, hy-Tra-IgG-Lc-Q124C-vcMMAE and Tra-IgG-Lc-V205-vcMMAE were dosed intravenously at 0.3 and 1 mg/kg on day 0.

Discussion

Various types of site-specific conjugation technology have been reported, which mainly consist of recombinant[4,6,10-15] and nonrecombinant methods[25,26]. Engineered cysteine technology is convenient way in that cell engineering or special additives are not required. On the other hand, a reduction and reoxidation process are necessary for producing free and reactive cysteines. Alternative nonrecombinant methods have developed for construction of homogeneous ADC, in which bi-functional linkers such as bis-sulfone linker and bifunctional dibromomaleimide are used for reaction with two adjacent cysteine thiol groups on antibody[25,26]. However, these methods also need full reduction process prior to conjugation that can potentially lead to misfolding events and yield several conjugate isoforms. From the point of view of no pretreatment, utilization of unnatural amino acid is superior to other methods[12,13], however, it needs cell engineering and expensive unnatural amino acid additives. Considering these characteristics, engineered cysteine technology without oxidization would provide an ideal way of site-specific conjugation.

Hc-A118C and Lc-V205C variants showed high thiol reactivity when they were produced in *E. coli*[7], while their thiol reactivity was almost lost when they were produced in mammalian cells[6]. Based on the observation that Tra-IgG-Hc-A118C IgG and -Lc-V205C exhibited broad peaks in LC-MS analysis, free cysteine and glutathione might be conjugated with introduced cysteines during incubation, resulting in the thiol capping of engineered cysteine[6]. Surprisingly, the result presented here demonstrated that the engineered cysteine residues in Tra-IgG-Lc-Q124C exist as reduced form and exhibit higher thiol reactivity, which defies the common recognition that cysteine mutants are easily capped. Serum albumin is one of the most well-known native proteins with a single

unpaired cysteine residue as Lc-Q124C[27]. Cys34 of human serum albumin (HSA) in blood is mainly present in reduced form (75%) under aerobic conditions[28]. Intriguingly, ASA value of Cys34 is very low (0.7%), which is similar to Lc-Q124C (1.1%)[17]. The crystal structure of HSA[27] suggest that the sulfur atom of Cys34 is protected by the side chains of surrounding amino acids. On the other hand, ASA values of A118C (39.9%) and V205C (30.6%), which are calculated by the previous procedure[17], are much higher than that of Lc-Q124C. Based on these facts, location at a buried position or orientation of side-chain would contribute to protecting the engineered cysteine from oxidization. In order to understand the detail mechanism of Lc-Q124C, further study such as structural analysis could be needed.

Site-specific Lc-Q124C-IgG conjugates (MMAE and Alexa 488) were able to be produced by direct conjugation without any pretreatment. Tra-IgG-Lc-Q124C-vcMMAE exhibited *in vitro* cytotoxicy similar to that of Tra-IgG-Lc-V205C-vcMMAE conjugate through reduction-reoxidization process, suggesting that IgG-Lc-Q124C could be applied to site-specific ADC. In addition, IgG-Lc-Q124C variant showed high thiol reactivity in the case of transient and stable expression in CHO cells. Furthermore we confirmed high thiol reactivity also in the case of preliminary fed-batch fermentation procedure (approx. 1 g/L). From our previous report[17], Fab-Lc-Q124C showed the highest thiol reactivity among selected engineered cysteine mutants, and could produce 1:1 conjugates with various sized functional molecules such as MMAE and branched PEG (20 kDa × 2). In this regard, both Fab and IgG of Lc-Q124C can provide site-specific conjugates with something desired by simple one-step procedure.

Thiosuccinimide linkage, which was formed by the reaction of maleimide electrophiles with thiol of engineered cysteine residues, could cause the maleimide

exchange reaction with Cys34 in serum albumin, leading to the linker instability in blood and consequent low efficacy *in vivo*. Recent study revealed that the basic environment surrounding conjugation site such as Lc-V205C undergoes spontaneous succinimide hydrolysis, resulting in the resistance to maleimide exchange reaction[16]. In fact, Tra-IgG-Lc-V205C-Alexa 488 was stable in human plasma, while Tra-IgG-Lc-Q124C-Alexa 488 and -Hc-A118C-Alexa 488 were decomposed over time. Tumey et al. demonstrated that the reaction at pH 9.2 at 37°C intentionally proceed succinimide hydrolysis[22], however, this aqueous method yielded only about 50% of hydrolyzed product in the case of maleimidocaproyl linker. In order to enhance the stability of Lc-Q124C-conjugates, we created a simple and efficient method based on this approach, in which reaction is performed on anion exchange resin at pH 9.5. As a result, hydrolyzed Lc-Q124C (hy-Lc-Q124C) conjugate was produced after short time exposure (6 hours), and buffer exchange was easily completed as elution procedure.

We found that hy-Tra-IgG-Lc-Q124C-Alexa 488 enhanced higher stability than original Tra-IgG-Lc-Q124C-Alexa 488, and no differences in stability was detected between hy-Tra-IgG-Lc-Q124C-Alexa 488 and Tra-IgG-Lc-V205C-Alexa 488. Additionally, hy-Tra-IgG-Lc-Q124C-vcMMAE exhibited similar efficacy than that of Tra-IgG-Lc-V205C-vcMMAE. Altogether, these results suggest that the instability of maleimide-thiol linker of Lc-Q124C-conjugate could be overcome by alkaline hydrolysis or substitution of more stable linkers. Bromoacetamidecaproyl[29] and methylsuifonylbenzothiazole[30,31] linkers were developed as alternative reagent for stable thioether conjugation. In addition, it was demonstrated that the thiosuccinimide linkage was automatically hydrolyzed even under a neutral condition by the incorporation of a basic functional group adjacent to the maleimide[21,23]. Recently, the newly palladium

reagents were developed for thiol specific conjugation of biomolecules[32]. Combination with Lc-Q124C variants and these linker technologies could provide stable antibody-drug conjugate.

In conclusion, Lc-Q124C (Actibody) is prepared as reduced form in the case of Fab in *E. coli* and IgG in mammalian cell line, which was contrary to the fact that engineered cysteine is easily oxidized. Actibody is easily prepared by just substituion with cystein at Gln124 (Kabat numbering) in light chain of aimed antibody and incubation, and has high capacity for payload size. These findings together suggest that Actibody, based on our new concept for introducing cysteine residues with low ASA values, provides easy way for preparing and analyzing site-specific conjugate, and shed light on the progress on analysis of functional molecules as in the form of antibody-conjugated.

Experimental Procedures

Materials. 4,4'-Dithiodipyridine (4-PDS) was obtained from Nacalai Tesque (Kyoto, Japan). Maleimidocaproyl-valine-citrulline-p-aminobenzoyloxycarbonyl-monomethyl auristatin E (vcMMAE) was obtained from MedChem Express (Princeton, NJ). Alexa Fluor 488 C5 Maleimide was purchased from Thermo Fisher Scientific (Waltham, MA). Chinese hamster ovary (CHO)-K1 cell line was obtained from European Collection of Cell Cultures and cultured at 37°C with 5% CO2 in EXCELL325PF (SAFC Biosciences, Lenexa, KS) supplemented with 4 mM L-glutamine、50 μg/mL gentamicin. Reaction buffer was composed of 20 mM citrate (pH 6.0) and 150 mM NaCl. The composition of conjugation buffer was 50 mM Tris-HCl (pH 7.5) and 5 mM EDTA. All cancer cell lines were obtained from American Type Culture Collection (Manassas, VA). SK-BR-3 was cultured at 37°C with 5% CO2 in McCoy's 5A supplemented with 10% fetal bovine serum (FBS). BT-474 was cultured at 37°C with 5% CO2 in RPMI1640 supplemented with 10% FBS and 10 μg/ml bovine insulin. NCI-N87 was cultured at 37°C with 5% CO2 in RPMI1640 supplemented with 10% FBS.

Animals. C.B17/Icr-scid Jcl (SCID) mice were purchased from Clea (Tokyo, Japan). All animal studies were performed in accordance with Standards for Proper Conduct of Animal Experiments at Kyowa Hakko Kirin Co., Ltd. under the approval of the company’s Institutional Animal Care and Use Committee (protocol number APS15J0135 and APS15J0233). Fuji Research Park and Tokyo Research Park of Kyowa Hakko Kirin co., Ltd. are fully accredited by the Association for the Assessment and Accreditation of Laboratory Animal Care, International.

Expression and purification of cysteine engineered Tra-IgG. The light or heavy chain genes of Tra-IgG which contained cysteine mutations were cloned into mammalian expression vector. Cysteine positions in Cκ light chain (Lc) and CH1 heavy chain (Hc) constant regions were defined by Kabat number and EU number, respectively. Each cysteine engineered Tra-IgG (Tra-IgG-Lc-Q124C, –Lc-V205C, and -Hc-A118C) was stably expressed in CHO-K1 and these transfectants were incubated for about one week. The culture supernatant was applied onto 1 mL Mab Select SuRe Protein A resin (GE Healthcare, Piscataway, NJ). The resin was washed with 20 mL of D-PBS. The bound antibody was eluted with 5 mL of 100 mM glycine-HCl (pH 3.5) and neutralized using 1 M Tris-HCl (pH 8.0). The buffer exchange into reaction buffer was accomplished using Amicon Ultra 4 device (Merck Millipore, Billerica, MA).

Thiol Reactivity Analysis by 4-PDS. 4-PDS reacts with the thiol groups under weak acidic conditions to form 4-mercaptopyridine with an absorbance at 324 nm[33]. Purified Tra-IgG were mixed with the reaction buffer, containing 4-PDS, such that the final solution contained 50 μM IgG and 500 μM of 4-PDS. A standard curve was derived from the titration of N-acetyl-L-cysteine with 4-PDS. The reaction for 30 min at room temperature was followed by monitoring the absorption at 324 nm. Thiol reactivity was calculated as the ratio of measured value and theoretical value at 50 μM of N-acetyl-L-cysteine, obtained from the standard curve. Theoretically, thiol reactivity of a molecule with one free thiol is 2.0.

Size Exclusion Chromatography (SEC). SEC was performed using Prominence (SHIMADZU, Kyoto, Japan). Approximately 200-pmol samples were injected into the

TSKgel G3000SWXL columns (TOSOH, Tokyo, Japan). The mobile phase was the reaction buffer. The flow rate was 1 mL/min for 30 min. Detection was conducted by recording absorbance at 280 nm.

Binding Analysis by Biacore. Binding affinity and kinetics analyses were conducted using the Biacore T100 (GE Healthcare). To circumvent errors from different sample concentrations, each Tra-IgG conjugate was immobilized on a CM5 sensor chip by using Human Antibody Capture Kit (GE Healthcare), then a range of concentrations of Her2-flag were passed as following procedures. 1 mg/mL of Tra-IgG or each Tra IgG-Lc-Q124C conjugate in HBS-EP+ running buffer (10 mM HEPES, pH 7.4, 150 mM NaCl, 3 mM EDTA, 0.005% surfactant P20) was captured for 40 sec at a flow rate of 10 µL/min. A range of concentrations of Her2-flag in HBS-EP+ running buffer were passed over the immobilized Tra-IgG or each Tra IgG-Lc-Q124C conjugate for 180 sec at a flow rate of 30 µL/min during the association phase. At the dissociation phases, HBS-EP+ running buffer was exposed for 600 sec at a flow rate of 30 µL/min. Chip regeneration was accomplished by exposure to 3 M magnesium chloride for 30 sec at a flow rate of 20 µL/min. All kinetic measurements were conducted at 25°C. Binding kinetic parameters, including the ka, kd, and KD values, were calculated using Biacore evaluation software.

Preparation of Tra-IgG-Alexa 488 and vcMMAE conjugates. Tra-IgG-Lc-Q124C, -Lc-V205C, and -Hc-A118C were adjusted to 50 µM with reaction buffer and conjugated with 10-fold molar excess of Alexa Fluor 488 C5 maleimide at 4°C for overnight. The excess Alexa Fluor 488 C5 maleimide was purified and buffer-exchanged with reaction buffer using Amicon Ultra 4 device. The concentrations antibody Alexa 488 conjugates were

calculated according to the manufacturer's instructions. Tra-IgG-Lc-Q124C was adjusted to 30 µM with reaction buffer and conjugated with 10-fold molar excess of vcMMAE in the presence of 20 % v/v of acetonitrile at 4°C for overnight. The excess vcMMAE was purified and buffer-exchanged with D-PBS using Amicon Ultra 4 device. Tra-IgG Lc-V205C and –Hc-A118C were required to reduce their introduced cysteine residues before conjugation. Tra-IgG-Lc-V205C and -Hc-A118C were adjusted to 5 mg/mL with conjugation buffer and reacted with 40-fold molar excess of dithiothreitol (DTT) to reduce the cysteine residues at room temperature for 16 hours. The excess DTT was removed and buffer-exchanged with reaction buffer using Amicon Ultra 4 device. To reoxidation of interchain disulfide bonds, reduced antibodies were adjusted to 50 µM and reacted with 15-fold molar excess of (L)-Dehydroascorbic acid (DHAA) at room temperature for 3 hours. Reoxidized antibodies were conjugated with 2.5-fold molar excess of vcMMAE in the presence of 20% v/v of acetonitrile at room temperature for 1 hour. The excess vcMMAE was purified and buffer-exchanged as described above. Formation of MMAE conjugate was confirmed by LC-MS analysis. The concentrations and the averages drug to antibody ratio (DAR) was accomplished by UV-VIS analysis and equations which was described by Hamblett et al[3].

Mass spectrometric analysis. All of the Tra-IgG-vcMMAE conjugates were treated with 5 units of PNGase F (Roche Diagnostics, Germany) at 4°C for overnight. Samples were separated by isocratic high performance liquid chromatography (HPLC) on ACQUITY UPLC BEH200 SEC column (Waters Corporation, Milford, MA) and identified by positive time-of-flight synapt high-definition mass spectrometry (Waters Corporation). Data collection and processing were controlled by MassLynx 4.1 software.

In vitro cytotoxicity. SK-BR-3 (3,000 cells/well), BT-474 and NCI-N87 (10,000 cells/well) were seeded in clear bottom, white wall 96 well plates (Greiner Bio-One, Kremsmünster, Austria). After 24 hours, serial dilution of trastuzumab vcMMAE conjugates were added to cells and incubated at 37°C for 120 hours. Cell viability was then determined using the Cell Titer-Glo luminescent assay (Promega Corp, Madison, WI) following the manufacturer's instructions.

In vitro plasma stability. Before sample preparation, human plasma was centrifuged at 20,400 g for 10 min followed by filtering through a 0.22 µm filter unit (Merck Millipore). Tra-IgG-Alexa 488 conjugates and -vcMMAE conjugates were diluted at 100 µg/mL with human plasma and incubated at 37°C for 0 hour, 24 hours, 48 hours, 72 hours and 96 hours. After incubation, each sample was kept frozen until analysis. The 0 hour samples were immediately frozen after the conjugate dilution. Tra-IgG-Alexa 488 conjugates were detected by Fluorescence-detection size exclusion chromatography using Prominence HPLC system (SHIMADZU, Kyoto, Japan). Approximately 90 pmol were injected into the TSKgel G3000SWXL columns (TOSOH, Tokyo, Japan). The mobile phase was the reaction buffer. The flow rate was 1 mL/min for 20 min. The % mean stability was calculated by dividing the peak area of Tra-IgG-Alexa 488 conjugate by total fluorescence area.

Stabilization of Tra-IgG-Lc-Q124C conjugate. Stabilization of Tra-IgG-Lc-Q124C conjugates was conducted on anion exchange resin. Tra-IgG-Lc-Q124C conjugates were diluted 5 times with 20 mM Bis-tris propane (pH 9.5). Each diluted sample was injected

onto 1 mL HiTrap Q column (GE Healthcare) equilibrated in 20 mM Bis-tris propane (pH 9.5). Columns were left at room temperature for 6 hours. Stabilized Tra-IgG-Lc-Q124C conjugates were then eluted with 20 mM Bis-tris propane (pH 9.5) and, 1 M NaCl and then buffer-exchanged with D-PBS using Amicon Ultra 4 device (Merck Millipore).

In vivo efficacy. *In vivo* efficacy of Tra-IgG-vcMMAE conjugates was evaluated in NCI-N87 human gastric carcinoma xenograft model. NCI-N87 cells were subcutaneously inoculated into right flank of SCID mice at 5×10^6 cells per mice. Seven or 8 days after implantation, mice bearing palpable tumor were assigned into groups so that average tumor volume/group would be equivalent. Vehicle and Tra-IgG-vcMMAE conjugates were intraveneously administered into mice on day 0 at dosages of 0.3, 1, and 3 mg/kg. Tumor mass were measured by calipers twice weekly, and tumor volume was calculated as: tumor volume (mm^3) = (length × width × width) /2.

References

1 Mullard, A. Maturing antibody-drug conjugate pipeline hits 30. *Nat Rev Drug Discov* **12**, 329-332, doi:10.1038/nrd4009 (2013).

2 Chari, R. V., Miller, M. L. & Widdison, W. C. Antibody-drug conjugates: an emerging concept in cancer therapy. *Angew Chem Int Ed Engl* **53**, 3796-3827, doi:10.1002/anie.201307628 (2014).

3 Hamblett, K. J. *et al.* Effects of drug loading on the antitumor activity of a monoclonal antibody drug conjugate. *Clin Cancer Res* **10**, 7063-7070, doi:10.1158/1078-0432.ccr-04-0789 (2004).

4 Agarwal, P. & Bertozzi, C. R. Site-specific antibody-drug conjugates: the nexus of bioorthogonal chemistry, protein engineering, and drug development. *Bioconjug Chem* **26**, 176-192, doi:10.1021/bc5004982 (2015).

5 Voynov, V. *et al.* Design and application of antibody cysteine variants. *Bioconjug Chem* **21**, 385-392, doi:10.1021/bc900509s (2010).

6 Junutula, J. R. *et al.* Site-specific conjugation of a cytotoxic drug to an antibody improves the therapeutic index. *Nat Biotechnol* **26**, 925-932, doi:10.1038/nbt.1480 (2008).

7 Junutula, J. R. *et al.* Rapid identification of reactive cysteine residues for site-specific labeling of antibody-Fabs. *Journal of immunological methods* **332**, 41-52, doi:10.1016/j.jim.2007.12.011 (2008).

8 Stimmel, J. B. *et al.* Site-specific conjugation on serine right-arrow cysteine variant monoclonal antibodies. *The Journal of biological chemistry* **275**, 30445-30450, doi:10.1074/jbc.M001672200 (2000).

9 Lyons, A. *et al.* Site-specific attachment to recombinant antibodies via introduced

surface cysteine residues. *Protein engineering* **3**, 703-708 (1990).

10 Zhou, Q. *et al.* Site-specific antibody-drug conjugation through glycoengineering. *Bioconjug Chem* **25**, 510-520, doi:10.1021/bc400505q (2014).

11 Li, X., Fang, T. & Boons, G. J. Preparation of well-defined antibody-drug conjugates through glycan remodeling and strain-promoted azide-alkyne cycloadditions. *Angew Chem Int Ed Engl* **53**, 7179-7182, doi:10.1002/anie.201402606 (2014).

12 Zimmerman, E. S. *et al.* Production of site-specific antibody-drug conjugates using optimized non-natural amino acids in a cell-free expression system. *Bioconjug Chem* **25**, 351-361, doi:10.1021/bc400490z (2014).

13 Tian, F. *et al.* A general approach to site-specific antibody drug conjugates. *Proceedings of the National Academy of Sciences of the United States of America* **111**, 1766-1771, doi:10.1073/pnas.1321237111 (2014).

14 Drake, P. M. *et al.* Aldehyde tag coupled with HIPS chemistry enables the production of ADCs conjugated site-specifically to different antibody regions with distinct in vivo efficacy and PK outcomes. *Bioconjug Chem* **25**, 1331-1341, doi:10.1021/bc500189z (2014).

15 Dennler, P. *et al.* Transglutaminase-based chemo-enzymatic conjugation approach yields homogeneous antibody-drug conjugates. *Bioconjug Chem* **25**, 569-578, doi:10.1021/bc400574z (2014).

16 Shen, B. Q. *et al.* Conjugation site modulates the in vivo stability and therapeutic activity of antibody-drug conjugates. *Nat Biotechnol* **30**, 184-189, doi:10.1038/nbt.2108 (2012).

17 Shiraishi, Y. *et al.* Identification of highly reactive cysteine residues at less

exposed positions in the Fab constant region for site-specific conjugation. *Bioconjug Chem* **26**, 1032-1040, doi:10.1021/acs.bioconjchem.5b00080 (2015).

18 Hamilton, G. S. Antibody-drug conjugates for cancer therapy: The technological and regulatory challenges of developing drug-biologic hybrids. *Biologicals : journal of the International Association of Biological Standardization* **43**, 318-332, doi:10.1016/j.biologicals.2015.05.006 (2015).

19 Bhakta, S., Raab, H. & Junutula, J. R. Engineering THIOMABs for site-specific conjugation of thiol-reactive linkers. *Methods in molecular biology (Clifton, N.J.)* **1045**, 189-203, doi:10.1007/978-1-62703-541-5_11 (2013).

20 Baldwin, A. D. & Kiick, K. L. Tunable degradation of maleimide-thiol adducts in reducing environments. *Bioconjug Chem* **22**, 1946-1953, doi:10.1021/bc200148v (2011).

21 Fontaine, S. D., Reid, R., Robinson, L., Ashley, G. W. & Santi, D. V. Long-term stabilization of maleimide-thiol conjugates. *Bioconjug Chem* **26**, 145-152, doi:10.1021/bc5005262 (2015).

22 Tumey, L. N. *et al.* Mild method for succinimide hydrolysis on ADCs: impact on ADC potency, stability, exposure, and efficacy. *Bioconjug Chem* **25**, 1871-1880, doi:10.1021/bc500357n (2014).

23 Lyon, R. P. *et al.* Self-hydrolyzing maleimides improve the stability and pharmacological properties of antibody-drug conjugates. *Nat Biotechnol* **32**, 1059-1062, doi:10.1038/nbt.2968 (2014).

24 Jackson, D. *et al.* In vitro and in vivo evaluation of cysteine and site specific conjugated herceptin antibody-drug conjugates. *PLoS One* **9**, e83865, doi:10.1371/journal.pone.0083865 (2014).

25 Behrens, C. R. *et al.* Antibody-Drug Conjugates (ADCs) Derived from Interchain Cysteine Cross-Linking Demonstrate Improved Homogeneity and Other Pharmacological Properties over Conventional Heterogeneous ADCs. *Mol Pharm* **12**, 3986-3998, doi:10.1021/acs.molpharmaceut.5b00432 (2015).

26 Badescu, G. *et al.* Bridging disulfides for stable and defined antibody drug conjugates. *Bioconjug Chem* **25**, 1124-1136, doi:10.1021/bc500148x (2014).

27 Sugio, S., Kashima, A., Mochizuki, S., Noda, M. & Kobayashi, K. Crystal structure of human serum albumin at 2.5 A resolution. *Protein engineering* **12**, 439-446 (1999).

28 Turell, L., Radi, R. & Alvarez, B. The thiol pool in human plasma: the central contribution of albumin to redox processes. *Free radical biology & medicine* **65**, 244-253, doi:10.1016/j.freeradbiomed.2013.05.050 (2013).

29 Alley, S. C. *et al.* Contribution of linker stability to the activities of anticancer immunoconjugates. *Bioconjug Chem* **19**, 759-765, doi:10.1021/bc7004329 (2008).

30 Patterson, J. T., Asano, S., Li, X., Rader, C. & Barbas, C. F., 3rd. Improving the serum stability of site-specific antibody conjugates with sulfone linkers. *Bioconjug Chem* **25**, 1402-1407, doi:10.1021/bc500276m (2014).

31 Toda, N., Asano, S. & Barbas, C. F., 3rd. Rapid, stable, chemoselective labeling of thiols with Julia-Kocienski-like reagents: a serum-stable alternative to maleimide-based protein conjugation. *Angew Chem Int Ed Engl* **52**, 12592-12596, doi:10.1002/anie.201306241 (2013).

32 Vinogradova, E. V., Zhang, C., Spokoyny, A. M., Pentelute, B. L. & Buchwald, S. L. Organometallic palladium reagents for cysteine bioconjugation. *Nature* **526**,

687-691, doi:10.1038/nature15739 (2015).

33 Grassetti, D. R. & Murray, J. F., Jr. Determination of sulfhydryl groups with 2,2'- or 4,4'-dithiodipyridine. *Archives of biochemistry and biophysics* **119**, 41-49 (1967).

Chapter 2

Novel anticarcinoembryonic antigen antibody-drug conjugate has antitumor activity in the existence of soluble antigen

Abstruct

Carcinoembryonic antigen (CEA or CEACAM5) is a classic tumor specific antigen and that is overexpressed in the several cancers such as gastric cancer. Although some anti-CEA antibodies have been be tested in a clinical trial, there is no clinically approved anti-CEA antibody therapeutics until now. Among this circumstance, we have created the novel anti- CEA antibody, 15-1-32, which is able to bind strongly to membrane-bound CEA on the cancer cells compared with existing anti-CEA antibodies. 15-1-32 also shows poor affinity for soluble CEA, thus the binding activity of 15-1-32 to the membrane-bound CEA is not influenced by soluble CEA. Furthermore, we constructed 15-1-32- monomethyl auristatin E conjugate (15-1-32-vcMMAE) to improve therapeutic efficacy of 15-1-32. 15-1-32-vcMMAE showed enhanced anti-tumor activity against gastric cancer cell line. Additionally, unlike the existing anti-CEA antibody, anti-tumor activity of 15-1-32-vcMMAE was retained even in the existence of high concentration soluble CEA.

Introduction

Carcinoembryonic antigen (CEA or CEACAM5) is a 180 kDa glycosylated protein that is expressed on the cell surface membrane in many types of cancers, and widely used as a clinical diagnosis maker for various tumors, such as colorectal, gastric, liver and other cancer[1-3]. Thus, CEA is considered as an attractive target for the cancer therapy, especially for the antibody therapy. Currently, several anti-CEA antibodies are under clinical trial, however no CEA targeted antibody is not marketed so far[4-7]. There are two major problems for the cancer immunotherapy of CEA targeted antibodies. First, the functional significance of CEA in tumorigenesis is thought to be limited because CEA is glycophosphatidylinositol (GPI) anchor protein and has no intracellular domain that is required for signal transduction. Many anti-CEA antibodies have been reported, however there are few reports about anti-CEA antibodies which possess inhibition activity of tumor function. Second, CEA is highly cleaved from the cell surface as a soluble form[8]. This property of CEA is useful as a clinical maker[9,10], however, this does not fit for the target of therapeutic antibody. Because highly secreted soluble CEA around tumor and in serum may disturb the therapeutic antibody binding to the membrane form CEA, therefore accumulation of therapeutic anti-CEA antibody in tumor is limited for the enough clinical efficacy.

Antibody-drug conjugate (ADC) is currently established antibody therapeutics format that covalently link cytotoxic agent to antibodies that recognize tumor antigens to enhance the anti-tumor potency of antibody therapeutics[11,12]. Antibodies conjugated with the cytotoxic agent bind to the tumor tissue depending on the expression of tumor antigen, internalize to intracellular space, then release the payload to inside the cell. Two ADCs are already on the market, including CD30-targeted brentuximab vedotin (ADCETRIS®)

for relapsed Hodgkin lymphoma and anaplastic large cell lymphoma[13], and Her2-targeted ado-trastuzumab emtansine (KADCYLA®) for refractory Her2-expressing breast cancers[14]. More than 40 ADCs are under clinical trial including anti-CEA ADC, IMMU-130 (labetuzumab-SN-38), which are now in phase II clinical trials for the colorectal cancers[4].

15-1-32 is fully human antibody that strongly recognizes membrane-bound CEA. 15-1-32 shows high binding affinity for membrane-bound CEA compared with other CEA antibodies and is little influenced by soluble form CEA. Although another group also reported that anti-CEA antibody, PR1A3, binds only membrane-bound CEA[15-18], our antibody recognizes different epitope and shows much higher binding activity to the membrane-bound CEA. Despite the unique binding property, 15-1-32 retained same reactivity for the tumor tissue compared with existing CEA antibodies. In this study, we constructed 15-1-32-drug conjugate (15-1-32-vcMMAE) to improve therapeutic efficacy of 15-1-32 and investigated the antitumor effects.

Results

Isolation of an anti-CEA antibody, 15-1-32. We firstly aimed to identify the anti-CEA antibodies with high affinity only for the membrane-bound CEA. To isolate anti-CEA antibodies, KM mouse were immunized with CEA-expressing L929 trasnfectant[19]. Hybridoma cells produced from spleen cells were selected through flow cytometry. One of these anti-CEA antibodies which we obtained was 15-1-32, fully human anti-CEA antibody. 15-1-32 bound to CEA expressing MKN-45 and KATO-III cells in the same manner as labetuzumab and mouse anti-human CEA antibody, 12-140-1, which is commercially available, whereas did not bind to CEA negative Raji cells (Figure 1A). These results indicated that 15-1-32 displayed strong and specific binding to membrane-bound CEA. Another group has reported that anti-CEA antibody, PR1A3, binds only membrane-bound CEA. PR1A3 recognized the B3 domain that located C-terminal of CEA[16]. For exploration of a 15-1-32 binding epitope, we conducted competition experiments against existing anti-CEA antibody, such as PR1A3, labetuzumab and other anti-CEA antibodies by flow cytometry analysis (Figure 1B). PR1A3 did not inhibit 15-1-32 binding, but 12-140-1 that recognized N domain of CEA inhibited 15-1-32 binding[20]. These results suggested 15-1-32 targeted N-terminal domain of CEA and recognition epitope is different from that of PR1A3.

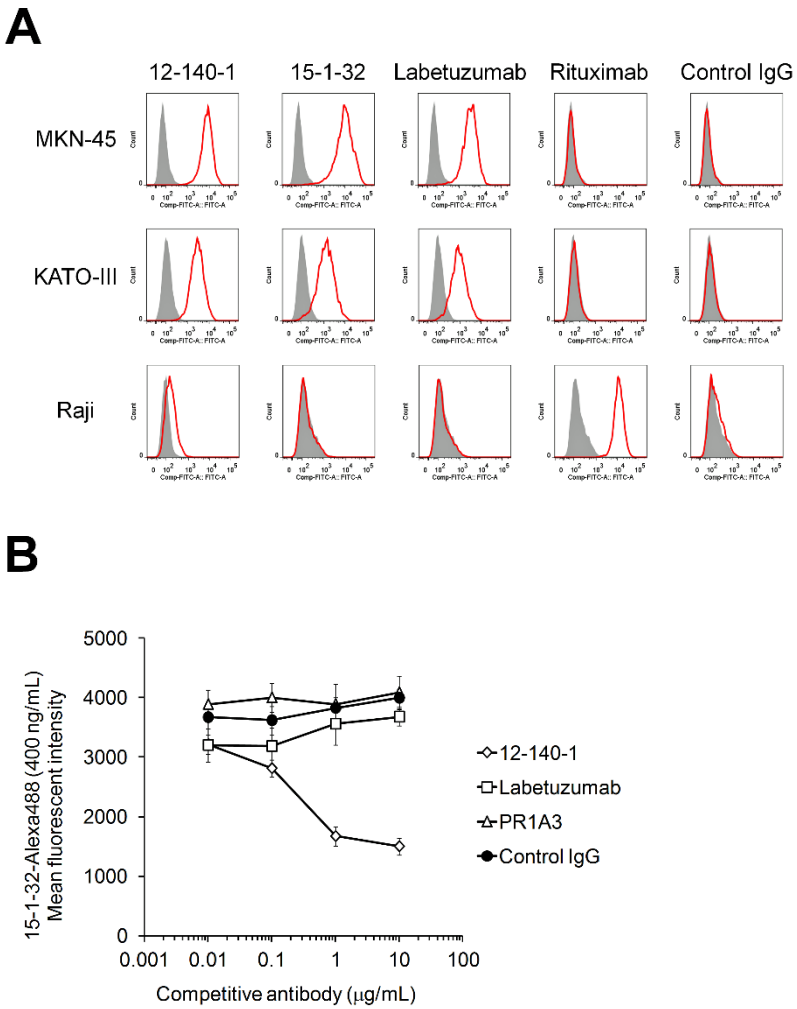

Figure 1. (A) Histograms of antibody binding to carcinoembryonic antigen (CEA) expressing MKN-45 and KATO-III, CEA negative Raji cells by flow cytometry (red histograms). The secondary antibody only served as controls (gray-filled histograms). (B) Competitive flow cytometric analysis with Alexa 488-labeled 15-1-32 against CEA-expressing MKN-45 cells. 12-140-1 (open rhombus), labetuzumab (open square), and PR1A3 (open triangle) were used as competitors.

Binding property of 15-1-32. Next, we validated the binding activity to membrane-bound CEA of 15-1-32 compared with PR1A3 and labetuzumab which is parental antibody of labetuzumab-SN-38 with or without soluble CEA by flow cytometry analysis. As shown Figure 2, 15-1-32 showed much higher binding activity to membrane-bound CEA expressed on MKN-45 than other two anti-CEA antibodies. In the presence of soluble CEA, labetuzumab reduced binding activity to cell surface CEA. However, there was slightly reduction in reactivity of PR1A3 and 15-1-32 with MKN-45 even in the presence of 10 μg/mL soluble CEA. The reactivity of 15-1-32 with MKN-45 is almost ten times higher than PR1A3 in this condition.

The binding kinetics of the 15-1-32, PR1A3 and labetuzumab to soluble CEA were analyzed on a Biacore biosensor in order to clarify the mechanism of binding property of 15-1-32. The sensorgrams and kinetic parameters for antibody-soluble CEA interactions are shown in Figure 3 and Table 1. The correct kinetic parameters of PR1A3 could not be calculated because of the poor reactivity to soluble CEA. Equilibrium dissociation constant (KD) of 15-1-32 had only an approximately fourfold difference compared with labetuzumab; however, binding property of 15-1-32 is significantly difference from labetuzumab. 15-1-32 had an approximately threefold higher association rate constant (ka) for soluble CEA than labetuzumab, whereas 15-1-32 had an approximately 12-fold higher dissocation constant (kd). These results indicated that 15-1-32 showed week binding property against soluble CEA.

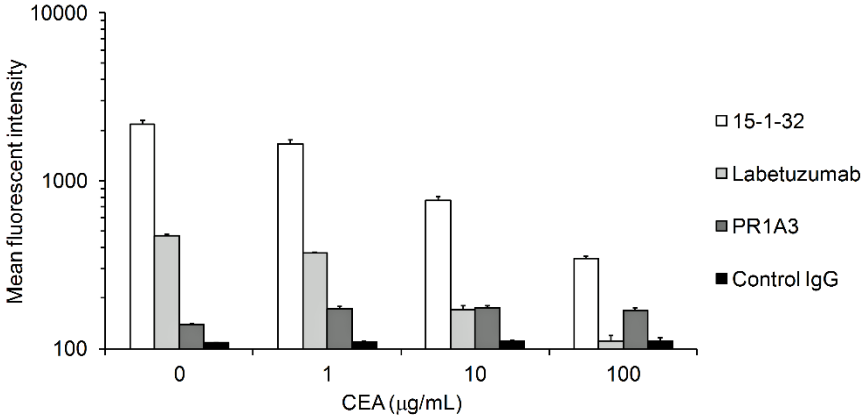

Figure 2. Binding activity of anti-carcinoembryonic antigen (CEA) antibodies to membrane-bound CEA on MKN-45 under the presence or absence of soluble CEA.

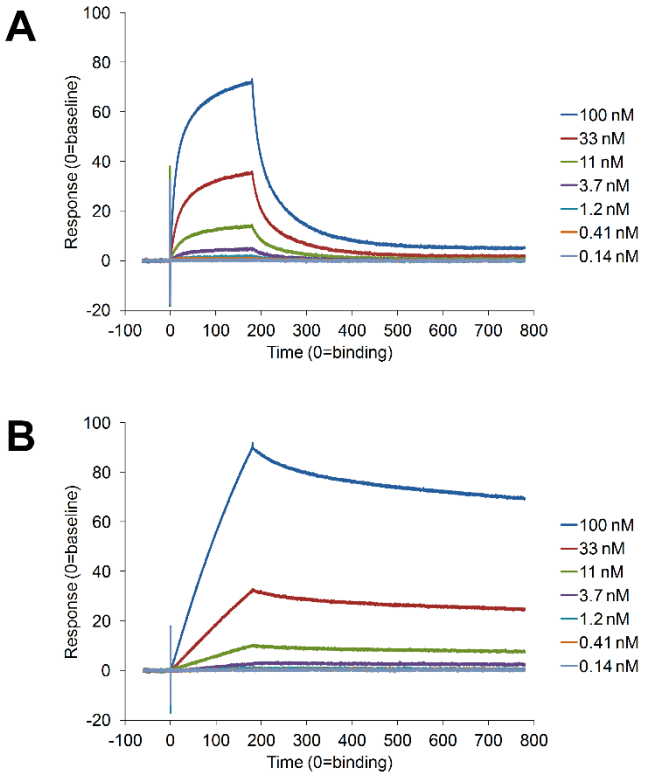

Figure 3. Typical sensorgrams of (A) 15-1-32 and (B) labetuzumab. Each legend indicated the concentration of soluble CEA

Table 1. Binding kinetics of anti-CEA antibody against soluble CEA.

Antibody	k_a ($\times 10^4$) M^{-1} S^{-1}	k_d ($\times 10^{-4}$) S^{-1}	K_D (k_d/k_a) nM
15-1-32	15.6	104	66.3
Labetuzumab	5.08	8.38	16.5

Internalization property of 15-1-32. The internalization property of 15-1-32 on each cell line was evaluated by flow cytometry analysis. The number of internalized 15-1-32 which bound to membrane-bound CEA in each of the time was calculated and shown in Figure 4. About four hundred thousand antibodies were internalized into MKN-45 cells for 24 hours. Although the number of internalized 15-1-32 in KATO-III were less than that in MKN-45, more than two hundred thousand molecules were internalized into each cell. These results indicated that 15-1-32 has well internalizing property into CEA expressing cell.

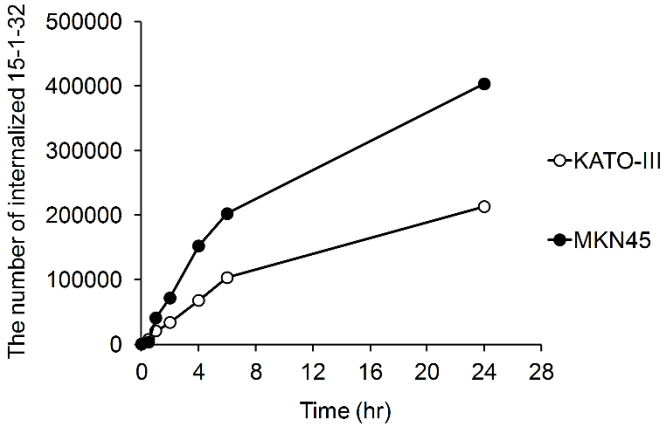

Figure 4. The time-dependent change of the number of internalized 15-1-32 antibody into KATO-III (open circle) and MKN-45 (closed circle).

Reactivity of 15-1-32 to the tumor tissue. To examine the reactivity of 15-1-32 to human gastric cancer tissue by immunohistochemistry, we evaluate 10 surgical specimens to confirm the CEA expression in gastric (Figure 5 upper) and esophageal cancer (Figure 5 lower). Despite the unique binding property of 15-1-32 to soluble CEA, positive staining was observed in 10/10 gastric cancer tissue samples and 6/10 esophageal cancer tissue samples stained with both test antibodies (Table 2). The sites of staining were membrane and/or cytoplasm in tumor cells. Localization of positive staining was apical in adenocarcinoma and squamous cell carcinoma. The frequency of staining was varied in gastric cancer tissue (less than 25% to more than 75%), and almost less than 25% in esophageal cancer tissue. In some esophageal cancer samples, normal esophageal epithelium (mainly apical) also showed positive staining. There was a similar trend with respect to the staining site, intensity, and frequency between 15-1-32 and labetuzumab.

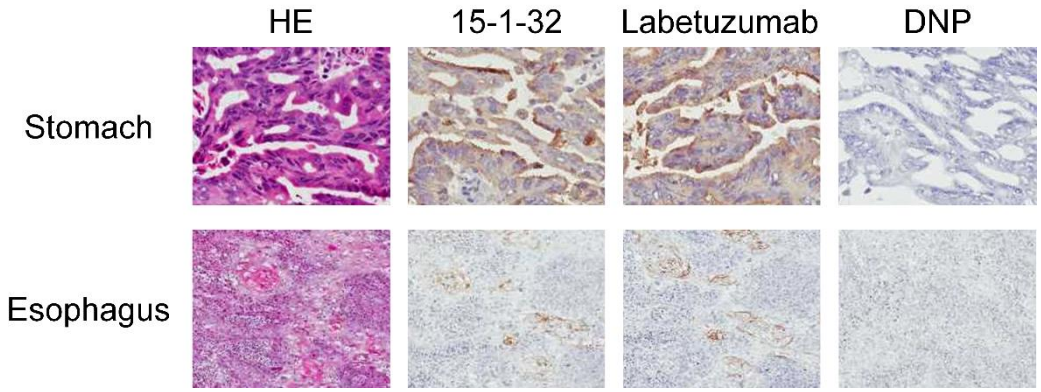

Figure 5. Immunhistochemical staining of CEA with 15-1-32 and labetuzumab. Sections from tumoral stomach adenocarcinoma tissues with an antibody against CEA are shown in the upper panels. Lower panels show esophagus squamous cell carcinoma sections. Anti-DNP was used as negative control. HE stands for Hematoxylin-eosin.

Table 2. Cross-reactivity of anti-CEA antibodies on human stomach and esophagus tumors.

Frozen human tissue								15-1-32			Labetuzumab			Anti-DNP	
NO.	Sex	Age	Organ	Diagnosis	Grade	TNM	Stage	Site	Intensity	Frequency	Site	Intensity	Frequency	Site	Intensity	Frequency
			MKN-45					MC	2+	4	CM	+	4		−	
			LS174T					MC	+	1	C	+	4		−	
			L929-CA9						−			−			−	
081293T2(1)	F	72	Stomach	Adenocarcinoma	G3	T4bN0M0	IIIB	C	2+	4	C	2+	4		−	
081275T2(2)	F	77	Stomach	Adenocarcinoma	G2	T4bN0M0	IIIB	MC	+/2+†	4	MC	+/2+†	4		−	
081274T2(1)	M	66	Stomach	Adenocarcinoma	G1	T2N0M0	IB	MC	+/2+†	2	MC	+/2+†	2		−	
081271T2(2)	F	63	Stomach	Adenocarcinoma	G4	T3N0M0	IIA	C	2+	1	C	2+	1		−	
081202T2(4)	F	67	Stomach	Adenocarcinoma	G3	T3N3bM0	IIIB	C	2+	2	C	2+	2		−	
081200T2(3)	M	70	Stomach	Adenocarcinoma	G2	T3N2M0	IIIA	MC	+/2+†	4	MC	+/2+†	4		−	
081198T2(2)	M	77	Stomach	Adenocarcinoma	G1−2	T1bN0M0	IA	MC	+	1	MC	2+	1		−	
081196T2(1)	M	62	Stomach	Adenocarcinoma	G3	T3N2M1	IV	MC	2+	1	MC	2+	1		−	
081193T2(1)	F	62	Stomach	Adenocarcinoma	G2	T3N0M0	IIA	MC	+/2+†	4	MC	+/2+†	4		−	
081188T2(1)	M	61	Stomach	Adenocarcinoma	G3	T3N3aM0	IIIB	C‡	+	1	MC	+	1		−	
21538T2(2)	M	71	Esophagus	Squamous cell carcinoma	G3	T3N1M0	IIIA	MC‡	2+	1	MC‡	2+	1		−	
21537T2(2)	M	65	Esophagus	Squamous cell carcinoma	G2	T3N2M0	IIIB	MC‡	2+	1	MC‡	2+	1		−	
21534T2(1)	M	52	Esophagus	Squamous cell carcinoma	G3	T3N0M0	IIA	C‡	2+	1	C‡	2+	1		−	
21513T2(2)	M	57	Esophagus	Squamous cell carcinoma	G3	T3N2M0	IIIB	C‡	2+	2	C‡	2+	1		−	
21497T2(2)	M	71	Esophagus	Squamous cell carcinoma	G3	T3N2M0	IIIB	MC‡	+	1	MC‡	+	1		−	
21492T2(3)	M	51	Esophagus	Squamous cell carcinoma	G2	T4aN1M0	IIIC		−			−			−	
21491T2(1)	M	55	Esophagus	Squamous cell carcinoma	G2	T3N1M0	IIIA		−			−			−	
21489T2(2)	M	55	Esophagus	Squamous cell carcinoma	G2	T2N1M0	IIB	MC‡	2+	2	C‡	2+	2		−	
21486T2(1)	M	51	Esophagus	Squamous cell carcinoma	G2	T1bN0M0	IB		−			−			−	
21474T2(3)	M	57	Esophagus	Squamous cell carcinoma	G3	T3N1M0	IIIA		−			−			−	

Site or description of staining; M: membranous, C: cytoplasmic. NA: not applicable.
Criteria of staining intensity; −: negative, 1+: faint/light, 2+: light-medium, 3+: moderate, 4+: dark.
Criteria of staining frequency; − (no labeled cells "-ative"), 1:<25%, 2:>=25% and <50%, 3:>=50% and <75%, 4:>=75%.
†: Apical: 2+, other: +
‡: Positive staining was mainly observed in apical.

The effects of 15-1-32-vcMMAE on CEA-expressing cells in vitro. To enhance the antitumor potency of 15-1-32, we constructed 15-1-32 based ADC. Currently, there are two major tubulin inhibitors are developed as ADC payloads, such as auristatins and maytansine derivatives[21]. We selected auristatin derivative, vcMMAE to conjugate with 15-1-32. We applied novel site specific conjugation technology, Actibody, to control the attached number of the drug to cysteine residues in antibody via thiol reactive molecules such as maleimide[22]. As a result of conjugation, ADC, termed, 15-1-32-vcMMAE, contains 2 molecules vcMMAE per antibody (Figure 6A, B). We also constructed a control ADC, termed labetuzumab-vcMMAE, with Actibody technology (Figure 6C, D).

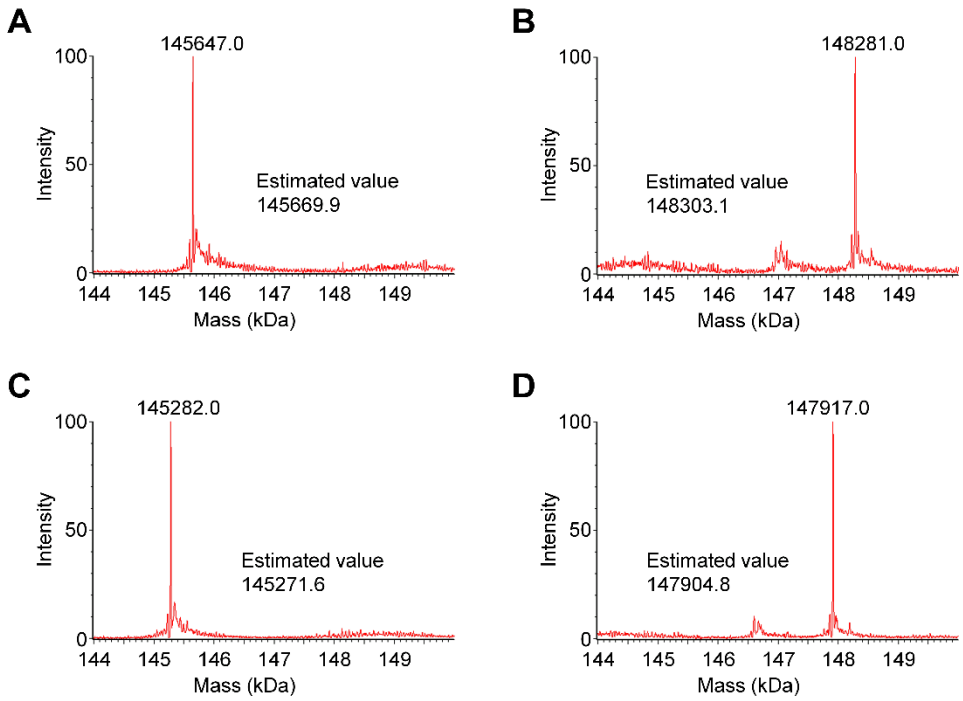

Figure 6. Deconvoluted mass spectra of naked 15-1-32 Actibody (A), 15-1-32-vcMMAE (B), naked labetuzumab Actibody (C), and labetuzumab-vcMMAE (D). The most intense peak in each mass spectrum corresponds to the molecular weight of the antibody.

15-1-32-vcMMAE exerted cytotoxic activity against CEA expressing MKN-45 cells, which led to the death of 60% of all target cells at 10 μg/mL (Figure 7A). Cytotoxic activity of 15-1-32-vcMMAE was almost same as labetuzumab-vcMMAE. To further confirm the influence of soluble CEA, we evaluated the cytotoxicity of 15-1-32-vcMMAE and labetuzumab-vcMMAE in the presence of soluble CEA (Figure 7B). The cytotoxic activity of labetuzumab-vcMMAE was almost canceled in the presence of soluble CEA. On the other hand, 15-1-32-MMAE retained antiproliferative activity on the MKN-45 cells despite of the existence of soluble CEA.

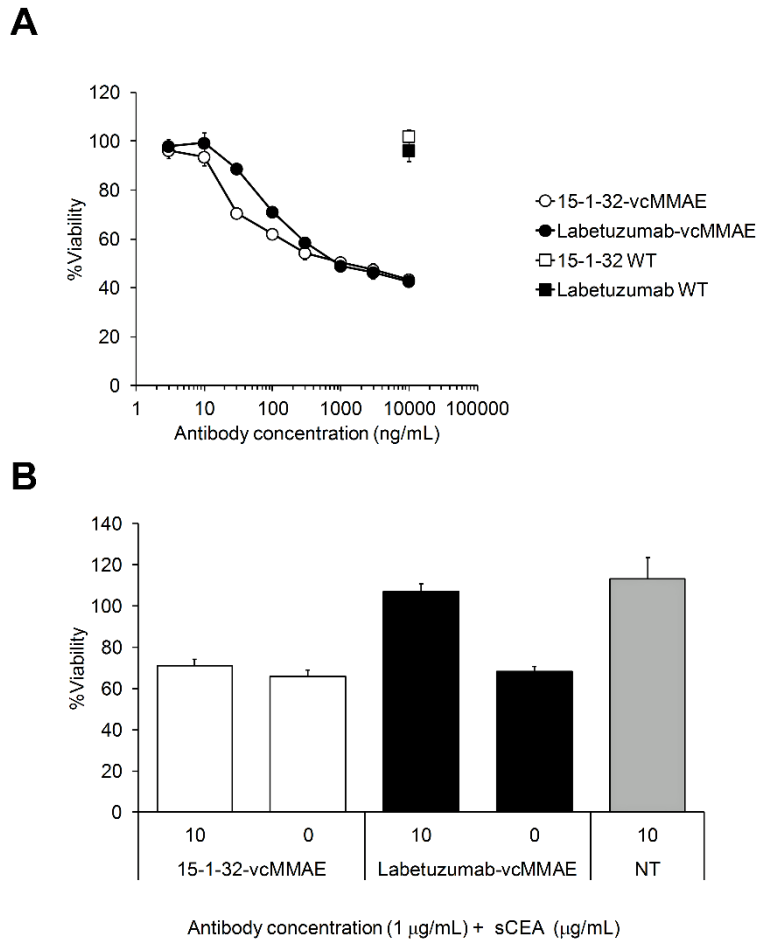

Figure 7. (A) *In vitro* cytotoxicity of 15-1-32-vcMMAE (open circle), labetuzumab-vcMMAE (closed circle), naked 15-1-32 (open square), naked labetuzumab (closed square) on CEA-positive gastric cancer cell lines, MKN-45. (B) Effect of soluble CEA blocking on the cytotoxicity of 15-1-32-vcMMAE and labetuzumab-vcMMAE, against MKN-45 cells. NT stands for not antibody treated.

Discussion

CEA has been reported to be overexpressed in various solid tumors. Although many anti-CEA antibodies have been created and developed since this molecule was discovered, to the best of our knowledge, no anti-CEA antibodies have been approved for clinical use. The functional correlation between CEA and tumorigenesis is still unclear, thus lack of the anti-tumor potency of anti-CEA antibodies could be considered one of the possible problems. Currently, three antibodies are in clinic and all antibodies are enhanced therapeutic potency by new technologies, such as ADC, bispecific antibody and cytokine fusion antibody[4,23]. Addition of new technology to improve the antibody efficacy is an important point for the therapeutic use of anti-CEA antibodies. However, highly secreted soluble CEA is also thought to be a hindrance for the therapeutic use among the anti-CEA antibodies. In this study, we successfully created 15-1-32, a fully human anti-CEA antibody, by immunization of KM mouse[24]. 15-1-32 showed the strongest binding activity to membrane-bound CEA compared with other existing CEA antibodies, while its reactivity to soluble CEA was weak. Thus, 15-1-32 was retained on the cell surface depend on the membrane-bound CEA expression level in the presence of the soluble CEA.

To further investigate the mechanism responsible for this unique binding property of 15-1-32 to soluble CEA, binding kinetics parameters were measured using Biacore biosensor. The kinetics analysis reveals that ka of 15-1-32 is three times higher than existing anti-CEA antibody, labetuzumab. In contrast, kd is 12 times higher than labetuzumab, this suggested that 15-1-32 is highly reactive but easily removal from soluble CEA. Although we could not investigate the kinetics analysis of 15-1-32 to membrane-bound CEA because of the technical difficulty, we speculate that 15-1-32 retained high ka even to the CEA expressed on cell surface, and low kd not to easily

remove from cells. This hypothesis was able to explain 15-1-32 reactivity, such as strongest binding activity to the cell surface membrane-bound CEA and poor binding to soluble CEA. In this study, we could not measure the correct kinetics parameters of PR1A3 because of the lower ka, this suggested both PR1A3 and 15-1-32 are poorly reactive to soluble CEA, however, their binding mechanisms are completely different. To further clarify the binding mechanism, detail epitope analysis may be needed.

To confirm the tumor tissue binding of 15-1-32, we conducted the immunohistochemistry analysis of 15-1-32 and labetuzumab binding in human stomach and esophagus cancer tissue. As a result, positive staining was observed in all stomach cancer tissue and in six out of 10 esophagus cancer. Furthermore, there were similar staining patterns between 15-1-32 and labetuzumab. This suggests that 15-1-32 retains membrane-bound CEA recognition property expressed on tumor tissue and can be applied for future clinical use.

In this study, we generated 15-1-32 based ADC, 15-1-32-vcMMAE, by using our Actibody technology[22], and compared its cytotoxicty with labetuzumab-vcMMAE against CEA expressing MKN-45 cells. The result showed that the cytotoxicity of 15-1-32-vcMMAE was almost the same as labetuzumab-vcMMAE. CEA has been generally reported as a noninternalizing antigen depend on antibody binding[25-27], but many reports also suggested anti-CEA antibodies internalized due to the membrane turnover[28-30]. Furthermore, uptake rates of anti-CEA antibodies were generally similar, independent of affinity, stability against protease digestion and valency[30]. Thus, CEA antibodies might be viable for the cargo of cytotoxic molecule to the tumor tissue for the cancer therapy. In fact, anti-CEA ADC, labetuzumab-SN-38, showed therapeutic effect in preclinical xenograft model and now in phases II clinical trial[31].

Additionaly, we evaluated these ADC activities against tumor cells in the presence of soluble CEA. The cytotoxicity of labetuzumab-vcMMAE was inhibited by presence of soluble CEA, suggesting that the strong coupling between soluble CEA and antibody interfered with binding labetuzumab-vcMMAE membrane-bound CEA. On the other hand, soluble CEA did not have much influence on the cytotoxicity of 15-1-32- vcMMAE because of its unique binding property against soluble and membrane-bound CEA. These results indicate the possibility that 15-1-32 could be suitable for antibody-based drugs especially antibody-drug conjugate compared with labetuzumab. To further clarify the potential of 15-1-32 in ADC, *in vivo* analysis of these antibodies, including pharmacokinetics and pharmacodynamics study in the existence of soluble CEA, have to be required.

In conclusion, we have produced and characterized a novel anti CEA antibody, 15-1-32. Favorable binding properties against membrane-bound CEA, and powerful antitumor effect of vcMMAE conjugate *in vitro* suggest that 15-1-32 has great potential in clinical application in the detection or treatment of CEA-positive tumors.

Experimental Procedures

Materials. Maleimidocaproyl-valine-citrulline-p-aminobenzoyloxycarbonyl-monomethyl auristatin E (vcMMAE) was obtained from MedChem Express (Princeton, NJ). Alexa Fluor 488 (Alexa 488) C5 Maleimide was purchased from Thermo Fisher Scientific (Waltham, MA). Rituximab and anti-2, 4-dinitrophenol (DNP) antibody were internally produced. Human soluble CEA was purchased from HyTest (Turku, Finland). L929 mouse fibroblast cell line was obtained from Riken Cell Bank (Tsukuba, Japan) and cultured at 37°C with 5% CO_2 in MEM supplemented with 10% fetal bovine serum (FBS). The Chinese hamster ovary (CHO) DG44 cell was cultured at 37°C with 5% CO_2 in IMDM supplemented with 10% FBS, 50 μg/mL gentamicin. Expi293F Expression System was purchased from Thermo Fisher Scientific (Waltham, MA). MKN-45 human gastric cancer cell line was obtained from Japanese Collection of Research Bioresources (Osaka, Japan) and cultured at 37°C with 5% CO_2 in RPMI1640 supplemented with 10% FBS. KATO-III human gastric cancer cell line was obtained from Sumitomo Dainippon Pharma (Osaka, Japan) and cultured at 37°C with 5% CO_2 in RPMI1640 supplemented with 10% FBS. Raji human Burkitt's lymphoma cell line was obtained from American Type Culture Collection (Manassas, VA) and cultured at 37°C with 5% CO_2 in RPMI1640 supplemented with 10% FBS. LS174T human colon cancer cell line was obtained from American Type Culture Collection (Manassas, VA) and cultured at 37°C with 5% CO_2 in MEM supplemented with 10% FBS.

Animals. KM mice were obtained from an in house breeding facility. C.B17/Icr-scid Jcl (SCID) mice were purchased from Clea (Tokyo, Japan). All animal studies were performed in accordance with Standards for Proper Conduct of Animal Experiments at

Kyowa Hakko Kirin Co., Ltd. under the approval of the company's Institutional Animal Care and Use Committee. Tokyo Research Park of Kyowa Hakko Kirin co., Ltd. is fully accredited by the Association for the Assessment and Accreditation of Laboratory Animal Care, International.

Generation of transfected cells. Human CEA (GenBank accession No. NM_004363.5) was generated by polymerase chain reaction (PCR), cloned into the INPEP4 (Biogen IDEC, Inc., Cambridge, MA) vector. Human CA9 (GenBank accession No. NM_001216.2) cDNA was cloned into the pKANTEX93 vector. Each expression vector was introduced into L929 cells via electroporation to obtain G418-resistant clones.

Isolation of the anti-CEA mAb. KM mice were i.p. immunized with CEA expressing L929 trasnfectant (1×10^7 cells per head per shot) weekly for 5 weeks. Spleen cells were fused with SP2/0 cells (American Type Culture Collection). Antibody-secreting hybridomas were initially screened by flow cytometry as described below with CEA expressing L929 trasnfectants as positive selection and CEA-null L929 trasnfectants as negative selection. Hybridomas were further selected by competitive flow cytemetry with CEA expressing L929 trasnfectants and soluble CEA. We selected clone 15-1-32 based upon the results of flow cytometry and carried out limiting dilution to isolate a single clone producing a monoclonal antibody.

Antibody and conjugate generation. The heavy- and light-chain variable region cDNAs from the hybridoma cells producing 15-1-32 were isolated by PCR and cloned into the pKANTEX93 vector for production of the recombinant 15-1-32 antibody with

mammalian cells[32]. Existing anti-CEA antibody, PR1A3 and labetuzumab were also cloned into the mammalian expression vectors. Each anti-CEA antibody (15-1-32, PR1A3 and labetuzumab) was stably expressed in DG44 cells and these transfectants were incubated for about 1 week. The culture supernatant was applied onto 1 mL Mab Select SuRe Protein A resin (GE Healthcare, Piscataway, NJ). The resin was washed with 20 mL of D-PBS. The bound antibody was eluted with 5 mL of 100 mM glycine-HCl (pH 3.5) and neutralized using 1 M Tris-HCl (pH 8.0). The buffer exchange into 20 mM Citrate, 150 mM NaCl (pH6.0) was accomplished using Amicon Ultra 4 device (Merck Millipore, Billerica, MA). Actiobody format of 15-1-32 and labetuzumab were genetically spliced into N5KG1-Val Lark vector (Biogen IDEC, Inc., Cambridge, MA) and expressed with Expi293F Expression System and purified as described above. Antibody-Alexa 488 conjugate and vcMMAE conjugate were prepared as described previously[22]. Briefly, antibodies were adjusted to 50 μM with reaction buffer, 20 mM citrate (pH 6.0) and 150 mM NaCl, and conjugated with 10-fold molar excess of Alexa Fluor 488 C5 maleimide at 4°C for overnight. The excess Alexa Fluor 488 C5 maleimide was purified and buffer-exchanged with reaction buffer using Amicon Ultra 4 device. On the other hand, antibdies were adjusted to 30 μM with reaction buffer and conjugated with 10-fold molar excess of vcMMAE in the presence of 20% v/v of acetonitrile at 4°C for overnight. The excess vcMMAE was purified and buffer-exchanged with D-PBS using Amicon Ultra 4 device.

Binding analysis by flow cytometry The specificity of 15-1-32 against CEA was determined by flow cytometry. Adherent MKN-45 and KATO-III cells were detached from the dish with Cell Dissociation Buffer (ThermoFisher), suspended in 96-well round-bottomed plates at a density of 2×10^5 cells/well, and washed with FACS buffer (1% BSA,

2 mM EDTA and 0.05% sodium azide in D-PBS). Floating Raji cells were collected in 96-well round-bottomed plates in the same way. 15-1-32, labetuzumab, 12-140-1 (mouse anti human CEA antibody, LifeSpan BioSciences, Seattle, WA), rituximab and human IgG1 (Sigma-Aldrich, St. Louis, MO) were added to wells at concentrations of 1 μg/mL, and then incubated at 4 °C for 1 h. After washing, secondary antibody (Alexa Fluor 488 Goat Anti-Human or Mouse IgG (H+L) Antibody, Thermo Fisher Scientific, Waltham, MA) was added to each well (1: 2000 diluted in FACS buffer) and incubated at 4 °C for 1 h. After washing, the cells were analyzed using a FACSVerse System (BD Biosciences PharMingen). The competitive analysis was conducted as follows. Alexa488 labeled 15-1-32 was added to MKN-45 cells at concentrations of 800 ng/mL, then incubated with the same volume of 12-140-1 PR1A3, labetuzumab, and human IgG1 at concentrations of 20, 2, 0.2 or 0.02 μg/mL at 4 °C for 1 h. After washing, the cells were analyzed using a FACSVerse System

The binding activity of anti-CEA antibody with or without soluble CEA was also determined by flow cytometry. MKN-45 cells were detached from the dish with Cell Dissociation Buffer (ThermoFisher), suspended in 96-well round-bottomed plates at a density of 2×10^5 cells/well, and washed with FACS buffer. 15-1-32, PR1A3, labetuzumab, and human IgG1 as a negative control, were added to wells at concentrations of 80 ng/mL, then incubated with the same volume of human soluble CEA at concentrations of 200, 20 or 2 μg/mL at 4 °C for 1 h. After washing, secondary antibody was added to each well and incubated at 4 °C for 1 h. After washing, the cells were analyzed using a FACSVerse System.

Internalization analysis of 15-1-32. The internalization of anti-CEA antibody was

determined by modified method as described previously[33]. Firstly, the quantitative determination of cell surface antigens on MKN-45 and KATO-III were conducted. 12-140-1 was added to the cells which collected in the same way as described above at concentrations of 100 nM, and then incubated on ice for 1 hour. After washing with PBS 0.1% BSA-Azide (0.1% BSA and 0.1% sodium azide in D-PBS), FITC-labeled anti-mouse IgG $F(ab')_2$ was added to each well and incubated on ice for 1 hour. Quantification of cell surface CEA expression was done with QIFIKIT (DAKO A/S, Glostrop, Denmark) according to the manufacturer's protocol. Next, internalization of 15-1-32 was evaluated by a quenching method. Alexa 488-labeled 15-1-32 was added to the cells at concentrations of 150 nM and incubated at 37°C with 5% CO_2 for 0.5, 1, 2, 4, 6, and 24 hours. The antibody solution was removed and the cells were washed with ice-cold PBS-Azide (0.1% sodium azide in D-PBS). Then quenching antibody (Anti- Alexa Flour 488, Rabbit IgG, Thermo Fisher Scientific) was added to wells and left on ice for 1 hour (Quenched cells). For unquenched sample, PBS-Azide was added instead of the quenching antibody solution (Unquenched cells). Cells were incubated for 1 hour on ice in Alexa Fluor 488- labeled 15-1-32 followed by incubation for 1 hour on ice in PBS-Azide (initial cells). Cells were incubated for 1 hour on ice in the Alexa Fluor 488-labeled 15-1-32 followed by incubation for 1 hour on ice with the quenching antibody solution (Quenched initial cells). After removing the quenching antibody solution or PBS-Azide, the cells were collected and analyzed by the flow cytometer. Nontreated cells were analyzed as blank cells.

MFI of samples were measured by flow cytometer. Internalized ratio (% initial) of 15-1-32 was calculated by the following equation: Internalized ratio (% initial) = (MFI of Quenched cells − MFI of Quenched initial cells) × 100 ⁄ (MFI of initial cells − MFI

ofblank cells). Internalized number of antibody was obtained by multiplying internalized ratio to number of antibodies bound to cell surface.

Kinetic Analysis of the binding property of anti-CEA antibodies by Biacore. Binding affinity and kinetics analyses were conducted using the Biacore T100 and Human Antibody Capture Kit (GE Healthcare, Piscataway, NJ). The murine anti-human IgG antibody was immobilized on a CM5 sensor chip according to instruction manual. 1.25 μg/mL 15-1-32 or labetuzumab in HBS-EP+ running buffer (10 mM HEPES, pH 7.4, 150 mM NaCl, 3 mM EDTA, 0.005% surfactant P20) was captured for 40 sec at a flow rate of 10 μL/min. A range of concentrations of human soluble CEA (0, 0.14, 0.41, 1.2, 3.7, 11, 33, and 100 nM) in HBS-EP+ running buffer were passed over the captured 15-1-32 or labetuzumab for 180 sec at a flow rate of 30 μL/min during the association phase. At the dissociation phases, HBS-EP+ running buffer was exposed for 600 sec at a flow rate of 30 μL/min. Chip regeneration was accomplished by exposure to 3 M magnesium chloride for 30 sec at a flow rate of 30 μL/min. All kinetic measurements were conducted at 25 °C. Binding kinetic parameters, including the ka, kd, and KD values, were calculated using Biacore evaluation software.

Immunohistochemistry. Frozen samples of 10 stomach adenocarcinoma and 10 esophagus squamous cell carcionma were used as test tissue. MKN-45 and LS174T mouse xenograft were used as positive control tissue, while L929-CA9 mouse xenograft was used as negative control tissue. All tumor samples and xenografts were sectioned at 6 μm, allowed to air-dry for 1 hour, fixed for 10 min at room temperature in acetone and stored at −80°C. Slides were air-dried and treated with sodium azide (1 mM), glucose (10

mM) glucose oxidase (2 U/ml) for 60 min at 37°C. Following a wash in PBS (pH7.2), slides were blocked with avidin and biotin solution (DAKO A/S, Glostrop, Denmark) for 20 min each and blocked with 1% BSA for 10 min. Primary antibodies, 15-1-32, labetuzumab and anti-2,4-dinitrophenol (DNP) antibody (10 µg/ml each), were applied 1 hour at room temperature[34]. Excess primary antibodies were washed off and sections were covered with streptavidin-HRP (NICHIREI BIOSCIENCE INC., Tokyo Japan) for 30 min, where after 3,3'-diaminobenzidine (DAB) was applied for 4 min. Slides were counterstained with hematoxylin, dehydrated and covered slipped for light microscopic evaluation. Slides were graded according to the following criteria, and site of positive staining were also recorded. Staining in cells or tissue was judged as specific, when staining intensity in test antibodies exceed that in the control antibody at the equivalent concentration.

Staining intensity: −; negative, +; faint/ light, 2+; light-medium, 3+; moderate, 4+; dark.

Site of staining: M; membranous, C; cytoplasmic.

Staining frequency: Negative; no labeled cell, Very rare; <25%, Rare; >=25% and <50%, Occasional; >=50% and <75%, Frequent; >=75%.

Proliferation assays. MKN-45 and KATO-III were seeded at a density of 3×10^3 cells/well in clear bottom, white wall 96 well plates (Greiner Bio-One, Kremsmünster, Austria). After 24 hours, dilution of anti-CEA antibody vcMMAE conjugates were added to cells at final concentrations of 10000, 3000, 1000, 300, 100, 30, 10 and 3 ng/mL respectively and incubated at 37°C for 120 hours. Cell viability was then determined using the Cell Titer-Glo luminescent assay (Promega Corp, Madison, WI) following the manufacturer's instructions.

References

1 Cooper, E. H., Turner, R., Steele, L., Neville, A. M. & Mackay, A. M. The contribution of serum enzymes and carcinoembryonic antigen to the early diagnosis of metastatic colorectal cancer. *Br J Cancer* **31**, 111-117 (1975).

2 Gold, P. & Freedman, S. O. Specific carcinoembryonic antigens of the human digestive system. *The Journal of experimental medicine* **122**, 467-481 (1965).

3 Goldstein, M. J. & Mitchell, E. P. Carcinoembryonic antigen in the staging and follow-up of patients with colorectal cancer. *Cancer investigation* **23**, 338-351 (2005).

4 Govindan, S. V. *et al.* Improving the therapeutic index in cancer therapy by using antibody-drug conjugates designed with a moderately cytotoxic drug. *Mol Pharm* **12**, 1836-1847, doi:10.1021/mp5006195 (2015).

5 Meyer, T. *et al.* A phase I trial of radioimmunotherapy with 131I-A5B7 anti-CEA antibody in combination with combretastatin-A4-phosphate in advanced gastrointestinal carcinomas. *Clin Cancer Res* **15**, 4484-4492, doi:10.1158/1078-0432.ccr-09-0035 (2009).

6 Sharkey, R. M. *et al.* A phase I trial combining high-dose 90Y-labeled humanized anti-CEA monoclonal antibody with doxorubicin and peripheral blood stem cell rescue in advanced medullary thyroid cancer. *Journal of nuclear medicine : official publication, Society of Nuclear Medicine* **46**, 620-633 (2005).

7 Shibata, S. *et al.* A phase I study of a combination of yttrium-90-labeled anti-carcinoembryonic antigen (CEA) antibody and gemcitabine in patients with CEA-producing advanced malignancies. *Clin Cancer Res* **15**, 2935-2941, doi:10.1158/1078-0432.ccr-08-2213 (2009).

8 Bramswig, K. H. *et al.* Soluble carcinoembryonic antigen activates endothelial cells and tumor angiogenesis. *Cancer Res* **73**, 6584-6596, doi:10.1158/0008-5472.can-13-0123 (2013).

9 Duffy, M. J. *et al.* Tumor markers in colorectal cancer, gastric cancer and gastrointestinal stromal cancers: European group on tumor markers 2014 guidelines update. *Int J Cancer* **134**, 2513-2522, doi:10.1002/ijc.28384 (2014).

10 Locker, G. Y. *et al.* ASCO 2006 update of recommendations for the use of tumor markers in gastrointestinal cancer. *Journal of clinical oncology : official journal of the American Society of Clinical Oncology* **24**, 5313-5327, doi:10.1200/jco.2006.08.2644 (2006).

11 Gerber, H. P., Koehn, F. E. & Abraham, R. T. The antibody-drug conjugate: an enabling modality for natural product-based cancer therapeutics. *Natural product reports* **30**, 625-639, doi:10.1039/c3np20113a (2013).

12 Panowski, S., Bhakta, S., Raab, H., Polakis, P. & Junutula, J. R. Site-specific antibody drug conjugates for cancer therapy. *MAbs* **6**, 34-45, doi:10.4161/mabs.27022 (2014).

13 Deng, C., Pan, B. & O'Connor, O. A. Brentuximab vedotin. *Clin Cancer Res* **19**, 22-27, doi:10.1158/1078-0432.ccr-12-0290 (2013).

14 LoRusso, P. M., Weiss, D., Guardino, E., Girish, S. & Sliwkowski, M. X. Trastuzumab emtansine: a unique antibody-drug conjugate in development for human epidermal growth factor receptor 2-positive cancer. *Clin Cancer Res* **17**, 6437-6447, doi:10.1158/1078-0432.ccr-11-0762 (2011).

15 Ashraf, S. Q. *et al.* Humanised IgG1 antibody variants targeting membrane-bound carcinoembryonic antigen by antibody-dependent cellular cytotoxicity and

phagocytosis. *Br J Cancer* **101**, 1758-1768, doi:10.1038/sj.bjc.6605355 (2009).

16 Conaghan, P. *et al.* Targeted killing of colorectal cancer cell lines by a humanised IgG1 monoclonal antibody that binds to membrane-bound carcinoembryonic antigen. *Br J Cancer* **98**, 1217-1225, doi:10.1038/sj.bjc.6604289 (2008).

17 Durbin, H. *et al.* An epitope on carcinoembryonic antigen defined by the clinically relevant antibody PR1A3. *Proceedings of the National Academy of Sciences of the United States of America* **91**, 4313-4317 (1994).

18 Stewart, L. M. *et al.* Humanisation and characterisation of PR1A3, a monoclonal antibody specific for cell-bound carcinoembryonic antigen. *Cancer immunology, immunotherapy : CII* **47**, 299-306 (1999).

19 Ishida, T. *et al.* Defucosylated anti-CCR4 monoclonal antibody (KW-0761) for relapsed adult T-cell leukemia-lymphoma: a multicenter phase II study. *Journal of clinical oncology : official journal of the American Society of Clinical Oncology* **30**, 837-842, doi:10.1200/jco.2011.37.3472 (2012).

20 Murakami, M. *et al.* A reference of the GOLD classification of monoclonal antibodies against carcinoembryonic antigen to the domain structure of the carcinoembryonic antigen molecule. *Hybridoma* **14**, 19-28, doi:10.1089/hyb.1995.14.19 (1995).

21 Hamilton, G. S. Antibody-drug conjugates for cancer therapy: The technological and regulatory challenges of developing drug-biologic hybrids. *Biologicals : journal of the International Association of Biological Standardization* **43**, 318-332, doi:10.1016/j.biologicals.2015.05.006 (2015).

22 Shinmi, D. *et al.* One-Step Conjugation Method for Site-Specific Antibody-Drug Conjugates through Reactive Cysteine-Engineered Antibodies. *Bioconjug Chem*

27, 1324-1331, doi:10.1021/acs.bioconjchem.6b00133 (2016).

23 Oberst, M. D. *et al.* CEA/CD3 bispecific antibody MEDI-565/AMG 211 activation of T cells and subsequent killing of human tumors is independent of mutations commonly found in colorectal adenocarcinomas. *MAbs* **6**, 1571-1584, doi:10.4161/19420862.2014.975660 (2014).

24 Ishida, I. *et al.* Production of human monoclonal and polyclonal antibodies in TransChromo animals. *Cloning and stem cells* **4**, 91-102, doi:10.1089/153623002753632084 (2002).

25 Boudousq, V. *et al.* Comparison between internalizing anti-HER2 mAbs and non-internalizing anti-CEA mAbs in alpha-radioimmunotherapy of small volume peritoneal carcinomatosis using 212Pb. *PLoS One* **8**, e69613, doi:10.1371/journal.pone.0069613 (2013).

26 Behr, T. M. *et al.* Therapeutic advantages of Auger electron- over beta-emitting radiometals or radioiodine when conjugated to internalizing antibodies. *European journal of nuclear medicine* **27**, 753-765 (2000).

27 Bryan, J. N. *et al.* Comparative uptakes and biodistributions of internalizing vs. noninternalizing copper-64 radioimmunoconjugates in cell and animal models of colon cancer. *Nuclear medicine and biology* **32**, 851-858, doi:10.1016/j.nucmedbio.2005.05.006 (2005).

28 Ford, C. H., Tsaltas, G. C., Osborne, P. A. & Addetia, K. Novel flow cytometric analysis of the progress and route of internalization of a monoclonal anti-carcinoembryonic antigen (CEA) antibody. *Cytometry* **23**, 228-240, doi:10.1002/(sici)1097-0320(19960301)23:3<228::aid-cyto6>3.0.co;2-e (1996).

29 Shih, L. B. *et al.* Internalization of an intact doxorubicin immunoconjugate.

Cancer immunology, immunotherapy : CII **38**, 92-98 (1994).

30 Schmidt, M. M., Thurber, G. M. & Wittrup, K. D. Kinetics of anti-carcinoembryonic antigen antibody internalization: effects of affinity, bivalency, and stability. *Cancer immunology, immunotherapy : CII* **57**, 1879-1890, doi:10.1007/s00262-008-0518-1 (2008).

31 Jerjian, T. V., Glode, A. E., Thompson, L. A. & O'Bryant, C. L. Antibody-Drug Conjugates: A Clinical Pharmacy Perspective on an Emerging Cancer Therapy. *Pharmacotherapy* **36**, 99-116, doi:10.1002/phar.1687 (2016).

32 Nakamura, K. *et al.* Dissection and optimization of immune effector functions of humanized anti-ganglioside GM2 monoclonal antibody. *Molecular immunology* **37**, 1035-1046 (2000).

33 Austin, C. D. *et al.* Endocytosis and sorting of ErbB2 and the site of action of cancer therapeutics trastuzumab and geldanamycin. *Molecular biology of the cell* **15**, 5268-5282, doi:10.1091/mbc.E04-07-0591 (2004).

34 Motoki, K. *et al.* Enhanced apoptosis and tumor regression induced by a direct agonist antibody to tumor necrosis factor-related apoptosis-inducing ligand receptor 2. *Clin Cancer Res* **11**, 3126-3135, doi:10.1158/1078-0432.ccr-04-1867 (2005).

Chapter 3

TRAIL-R2 superoligomerization induced by human monoclonal agonistic antibody KMTR2

Abstract

The fully human monoclonal antibody KMTR2 acts as a strong direct agonist for tumor necrosis factor-related apoptosis-inducing ligand (TRAIL) receptor 2 (TRAIL-R2), which is capable of inducing apoptotic cell death without cross-linking. To investigate the mechanism of direct agonistic activity induced by KMTR2, the crystal structure of the extracellular region of TRAIL-R2 and a Fab fragment derived from KMTR2 (KMTR2-Fab) was determined to 2.1 Å resolution. Two KMTR2-Fabs assembled with the complementarity-determining region 2 of the light chain via two-fold crystallographic symmetry, suggesting that the KMTR2-Fab assembly tended to enhance TRAIL-R2 oligomerization. A single mutation at Asn53 to Arg located at the two-fold interface in the KMTR2 resulted in a loss of its apoptotic activity, although it retained its antigen-binding activity. These results indicate that the strong agonistic activity, such as apoptotic signaling and tumor regression, induced by KMTR2 is attributed to TRAIL-R2 superoligomerization induced by the interdimerization of KMTR2.

Introduction

Tumor necrosis factor (TNF)-related apoptosis-inducing ligand (TRAIL/Apo2L)[1,2] induces apoptosis in a wide variety of human cancer cell lines, but not in most normal human cells[3,4]. TRAIL activates two distinct receptors, TRAIL-R1 (DR4)[5] and TRAIL-R2 (DR5)[6-8], both of which possess a death domain (DD) in their cytoplasmic tail that can interact with the apoptotic machinery. The assembly and trimerization of TRAIL-R1 and TRAIL-R2 are prerequisites for transducing an apoptosis signal[9,10]. The structure of the extracellular region of TRAIL-R2 (ecTRAIL-R2) in complex with TRAIL has shown that similar to other members of the TNF and TNF receptor superfamily, a TRAIL trimer binds to three receptors[11-13], suggesting that a trimeric ligand−receptor complex is the functional unit for signaling[14]. This trimeric complex has also been determined for ternary (3:3:3) complex with Fab fragment derived from AMG 655 which increases antitumor activity in cooperation with TRAIL[15]. In addition, the structures of ecTRAIL-R2 have been determined for a 2:2 complex with glycoprotein UL141 of human cytomegalovirus[16] and for 1:1 complexes with phage-derived Fabs, YSd1[17], Bdf1[18], and Apomab[19].

Bivalent IgG antibodies normally require cross-linking for further oligomerization to mimic natural ligands. Cross-linking of antibodies with certain reagents, such as secondary antibodies, has been reported to enhance their antitumor effects. For example, Griffith et al.[20] and Chuntharapai et al.[21] reported that the antitumor effects of murine antibodies to TRAIL-R1 and TRAIL-R2 were strongly enhanced in the presence of goat anti-mouse IgG, which aided in antibody cross-linking. We previously reported the generation of several human monoclonal antibodies specific for TRAIL-R1 or TRAIL-R2 that were derived from transchromosomal mice (KM mouse)[22] expressing human immunoglobulin repertoires[23]. We generated a novel anti-TRAIL-R2 monoclonal

antibody, KMTR2, which acts as a direct agonist possessing the ability to induce apoptosis without cross-linking[24].

KMTR2 can oligomerize soluble TRAIL-R2 (fused with the Fc region of IgG) and clusters membrane TRAIL-R2 on cell surfaces without cross-linking, inducing the death of human tumor cells *in vitro* and established tumors *in vivo*[24]. Furthermore, treating tumor-bearing nude mice with KMTR2 significantly suppressed the growth of subcutaneous glioma xenografts and resulted in complete regression[25]. Therefore, specifically targeting the death receptor pathway through TRAIL-R2 using direct agonistic antibodies may provide a novel therapeutic strategy for malignant tumors.

Here we report on the tertiary structure of KMTR2-Fab in complex with ecTRAIL-R2 and describe the mechanism of how this direct agonistic antibody accelerates TRAIL-R2 oligomerization. Based on its crystallographic symmetry, the dimeric complex structure of KMTR2 appeared to be a functional unit for generating a superoligomeric complex. Interference of this interface with an Asn53 to Arg mutation in the light kappa chain of KMTR2 resulted in the loss of the direct agonistic activity but not the binding activity of KMTR2, indicating that interdimerization of KMTR2 is responsible for TRAIL-R2 superoligomerization, leading to the strong agonistic activity of KMTR2.

Results

Overall structure of ecTRAIL-R2 in complex with KMTR2. The tertiary structure of ecTRAIL-R2 in complex with KMTR2-Fab was determined to 2.1 Å resolution by X-ray crystallography (Figure 1A). Although the electron densities of the N-terminal (Ala54−Arg73) and C-terminal (Arg145−Lys181) regions in ecTRAIL-R2 were unclear, the final model included two cysteine-rich domains (CRD1: Ser74−Ser96 and CRD2: Cys97−Gln138), and some part of CRD3 (Cys139−Phe144) of TRAIL-R2 (Figure 1A) and the heavy (Gln1−Ser226, excluding Arg142−Ser145) and light (Glu1−Cys214) chains of KMTR2-Fab. This model also included one N-linked sugar chain bound at Asn73 of the KMTR2 heavy chain and five glycerol molecules, one chloride ion, and 276 water molecules. The overall structure of ecTRAIL-R2 in complex with KMTR2-Fab was similar to that in complex with TRAIL (PDB ID: 1D4V) (11), with an RMSD value of 1.02 Å for all main chain atoms (Figure 1A). Of note, the position of Gly91 in the KMTR2-Fab complex was flipped against that in a TRAIL complex.

The tertiary structure of KMTR2-Fab without ecTRAIL-R2 was also determined to 2.5 Å resolution. Although the electron densities of the central part (Ser102−Tyr106) of complementarity-determining region (CDR) 3 of the heavy chain was unclear, the final model included the heavy (Gln1−Ser226, excluding Ser102−Tyr106 and Ser145−Glu146) and light (Glu1−Cys214) chains, one N-linked sugar chain at Asn73 of the KMTR2 heavy chain, two sulfate and three chloride ions, and 42 water molecules. The overall structure of KMTR2-Fab was conserved regardless of antigen binding, with an RMSD value of 1.17 Å for all main chain atoms (Figure 2).

a

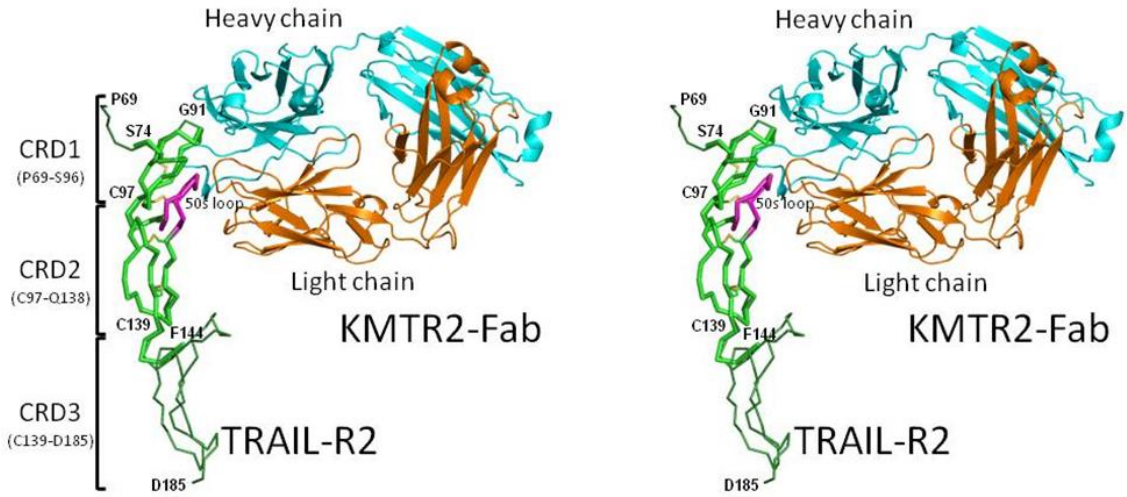
Heavy chain
P69
G91
S74
CRD1
(P69-S96)
C97
50s loop
CRD2
(C97-Q138)
Light chain
C139
F144
KMTR2-Fab
CRD3
(C139-D185)
TRAIL-R2
D185
Heavy chain
P69
G91
S74
C97
50s loop
Light chain
C139
F144
KMTR2-Fab
TRAIL-R2
D185

b

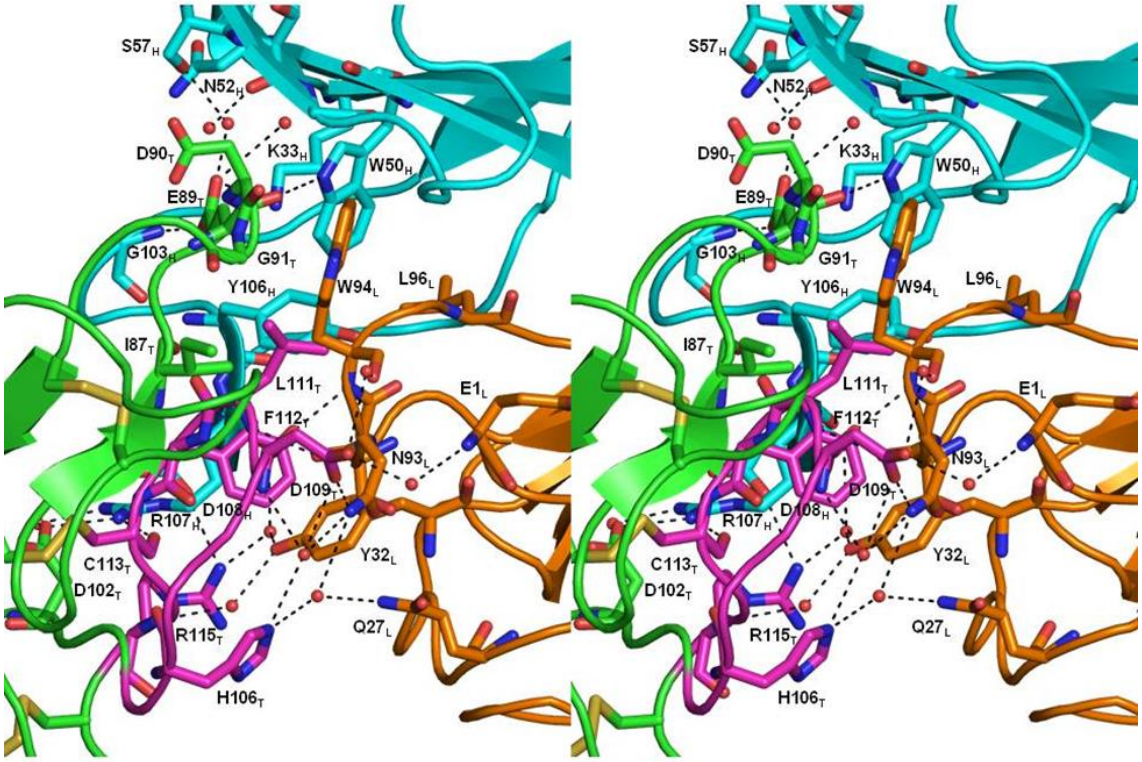
S57H
N52H
D90T
K33H
W50H
E89T
G103H
G91T
Y106H
W94L
L96L
I87T
L111T
E1L
F112T
N93L
D109T
R107H
D108H
C113T
Y32L
D102T
R115T
Q27L
H106T
S57H
N52H
D90T
K33H
W50H
E89T
G103H
G91T
Y106H
W94L
L96L
I87T
L111T
E1L
F112T
N93L
D109T
R107H
D108H
C113T
Y32L
D102T
R115T
Q27L
H106T

Figure 1. Crystal structure of the 1:1 complex between ecTRAIL-R2 and KMTR2-Fab. (a) Overall structure. The TRAIL-R2 molecule and the heavy and light chains of KMTR2 are colored green, cyan, and orange, respectively. A 50s loop and disulfide bonds in TRAIL-R2 are indicated by magenta and a stick model, respectively. The TRAIL-R2 structure in complex with TRAIL (PDB ID: 1D4V, dark green) is superimposed on that of a KMTR2 complex. (b) Close-up view of the interface between ecTRAIL-R2 and KMTR2-Fab. The orientation of this figure is the same as in (a). Residues related to antigen−antibody binding are represented by a stick model. Hydrogen bonds are indicted by dashed lines. Subscripts H, L, and T indicate KMTR2 heavy and light chains and TRAIL-R2, respectively.

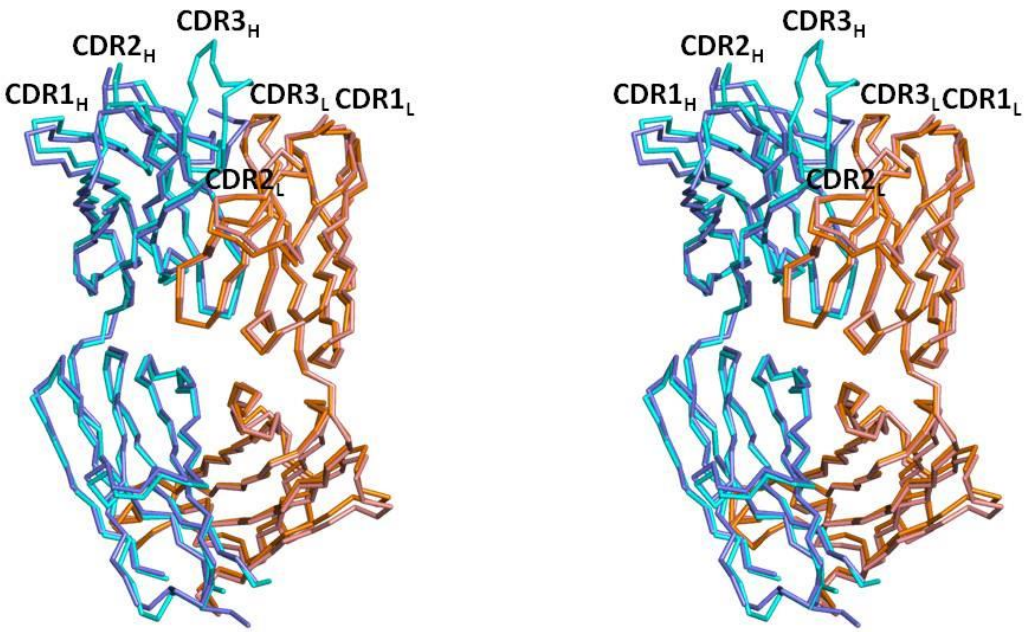

Figure 2. Structural comparison of KMTR2-Fab with (heavy: cyan, light: orange) and without (heavy: purple, light: beige) TRAIL-R2. Two structures were superimposed using all main chain atoms.

TRAIL-R2/KMTR2-Fab interface. KMTR2-Fab recognized CRD1 and CRD2 of TRAIL-R2 in the direction perpendicular to TRAIL-R2 (Figure 1A). The area of the contact region between TRAIL-R2 and KMTR2-Fab was calculated to be 623 $Å^2$, with contributions of 322 $Å^2$ from the heavy chain and 301 $Å^2$ from the light chain of KMTR2. To determine the epitope recognition scheme of KMTR2, residues located within a distance of 4.0 Å between TRAIL-R2 and KMTR2-Fab were determined (summarized in Table 1). KMTR2-Fab recognized two epitopes (epitope-1 and -2) in ecTRAIL-R2 (Figure 1A). Epitope-1 included Ile87, Glu89, Asp90, and Gly91 in CRD1, which was mostly recognized by CDR1−3 of the heavy chain (Figure 1B, Table 1). The side chain Glu89 atoms of TRAIL-R2 interacted with Lys33 in CDR1, Gly103 in CDR3, and Trp50, Asn52, Ser57 in CDR2 in the heavy chain of KMTR2 via direct and water-mediated hydrogen bonds. The aromatic Trp94 ring in CDR3 of the light chain exhibited a stacking interaction parallel to the peptide surface of Asp90−Gly91 of TRAIL-R2, which was the greatest positional difference compared with that in a TRAIL complex (Figure 1A). The side chain (Cβ atom) of Trp94 in CDR3 of the light chain was also positioned within a distance of 4.0 Å against the side chain atoms of Ile87 in epitope-1.

Epitope-2 comprised Asp102 and some residues in a “50s loop” (Thr105−Arg115) in CRD2, one of the two natural ligand recognition sites, and interacted with CDR1 and CDR3 of the light chain and CDR3 of the heavy chain (Figure 1B, Table 1). A hydrogen bond network was generated between epitope-2 (His106 and Asp109) and the light chain of KMTR2 (Gln27 in CDR1, Asn93 and Trp94 in CDR3, and Glu1). The Arg107 side chain in CDR3 of the heavy chain intruded into the 50s loop of TRAIL-R2 and participated in recognizing epitope-2 (Asp102, Phe112, Cys113, and Arg115) by hydrogen bonding and van der Waals interactions. The hydroxyl oxygen atom of the

Tyr32 side chain in CDR1 of the light chain interacted with the main chain amide and side chain guanidino group of Arg115 in the 50s loop via water-mediated hydrogen bonds. The side chains of Leu111 and Phe112 were wedged between two tyrosine residues (Tyr32 in CDR1 of the light chain and Tyr106 in CDR3 of the heavy chain), which provided van der Waals interactions. The side chain atoms of Leu111 were also located within a distance of 4.0 Å against three residues (Asn93, Trp94, and Lue96) in CDR3 of the light chain.

We compared the structures described above with other TRAIL-R2 structures in complex with other Fab fragments. In addition to the KMTR2-Fab structure, the crystal structures of phage-derived Fab fragments, YSd1 (PDB ID: 1ZA3)[17], Bdf1 (PDB ID: 2H9G)[18], and Apomab (PDB ID: 4OD2)[19], were previously determined. Apomab exhibits some agonistic activity (EC50: approximately 100 ng/ml) without using a cross-linking reagent[19]. Recently, the crystal structure of Fab fragment derived from AMG 655 was reported (PDB ID: 4N90). AMG 655 has no activity in the absence of cross-linking, but increases it in cooperation with TRAIL.

Table 1. Related residues of antigen-antibody binding.

TRAIL-R2			distance		KMTR2			
epitope	**residue**	**atom**			**atom**	**residue**	**CDR**	**chain**
1	Ilu87	Cγ2	3.73		Cβ	Trp94	3	L
	Glu89	O	2.96	h	Nε1	Trp50	2	H
		Cδ	3.89		Cε	Lys33	1	
		Oε1	3.07	h	Nζ			
			2.72	h	N	Gly103	3	
		Oε2	3.24	h	Nζ	Lys33	1	
			water mediated	h	Nε1	Trp50	2	
			water mediated	h	N	Asn52		
			water mediated	h	Oγ	Ser57		
	Asp90	N	water mediated	h	O	Thr58		
		Cβ	3.84		Cα	Gly59		
		C	3.91		Cε2	Trp94	3	L
	Gly91	Cα	3.61		Cδ1			
2	Asp102	Oδ2	2.97	h	Nη1	Arg107	3	H
			water mediated	h	Nη2			
	His106	Nε2	water mediated	h	Nε2	Gln27	1	L
			water mediated	h	Nδ2	Asm93	3	
	Asp109	N	water mediated	h				
		O	2.85	h	N	Trp94		
		Oδ1	2.65	h	Nδ2	Asn93		
		Oδ2	water mediated	h	O	Trp94		
			water mediated	h	N	Glu1	—	
	Leu111	N	2.87	h	O	Ser92	3	
		Cβ	3.96		Cε1	Tyr106	3	H
		Cδ1	3.82		Cβ	Trp94	3	L
		Cδ2	3.67		C	Asn93		
			3.7		Cδ1	Leu96		
	Phe112	Cδ1	3.71		Cδ1	Tyr106	3	H
			3.55		Cβ	Arg107		
		Cε2	3.52		Cε1	Tyr32	1	L
		Cζ	3.73		Cα	Ser92	3	
	Cys113	O	2.78	h	Nη1	Arg107	3	H
	Arg115	N	water mediated	h	Oη	Tyr32	1	L
		Cγ	3.27		Cζ	Arg107	3	H
		Nη1	3.24	h	Oδ2	Arg108		
			water mediated	h	Oη	Tyr32	1	L
			water mediated	h	O	Arg107	3	H

h: hydrogen bond (within 3.6 Å between donor and acceptor).

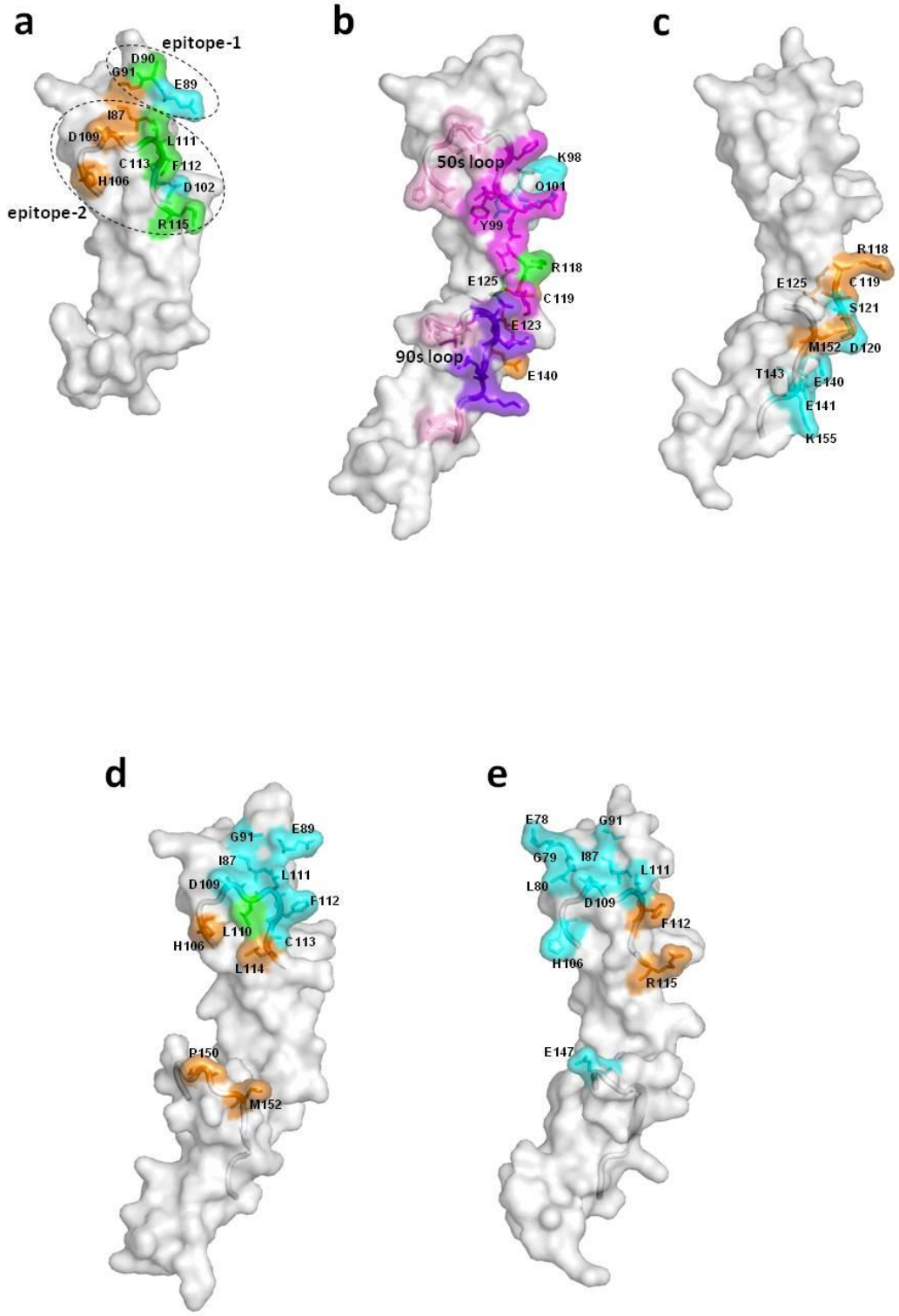
a
epitope-1
D90
G91
E89
I87
D109
L111
C113
F112
H106
D102
epitope-2
R115
b
50s loop
K98
Q101
Y99
R118
E125
C119
E123
90s loop
E140
c
R118
E125
C119
S121
M152
D120
T143
E140
E141
R155
d
E89
G91
I87
L111
D109
F112
L110
H106
C113
L114
P150
M152
e
E78
G91
G79
I87
L111
L80
D109
F112
H106
R115
E147

Fugure 3. Comparison of the structural epitopes of TRAIL-R2 for binding to (a) KMTR2, (b) AMG 655, (c) Apomab, (d) Bdf1, and (e) Ysd1. ecTRAIL-R2 is shown as a molecular surface model. Residues recognized by light, heavy, and both chains of Fab are drawn as a stick model and colored orange, cyan, and green, respectively. Residues recognized by TRAIL are colored in magenta (by TRAIL molecule in 1:1 complex), pink (by TRAIL molecule in neighbor complex), and purple (by both TRAIL molecules) in (b).

KMTR2 recognized the N-terminal region of TRAIL-R2 with a contact area of 623 $Å^2$ (Figure 3A) that involved both epitope-1 and -2, which was less than half of the contact area (1427 $Å^2$) of the interface of a 3:3 complex of TRAIL and TRAIL-R2 (Figure3B). Epitope-2 for KMTR2 involved the 50s loop region, which was a TRAIL recognition site in CRD2. Apomab interacted with the C-terminal region of ecTRAIL-R2, which was nearly perpendicular to that recognized by KMTR2 (Figure 3C). Epitope recognition by Apomab did not have any overlaps in CRD1 and CRD2 with that by KMTR2, but had a little overlap with the TRAIL recognition site, a 90s loop, in CRD3. AMG 655 interacted with ecTRAIL-R2 in the same direction of recognition by Apomab (Figure 3B). Epitope recognition by AMG 655 mostly overlapped in CRD3 with that by Apomab. In contrast, epitope recognition by Bdf1 and Ysd1, which have little or no agonistic activity[19], predominantly overlapped in CRD1 and CRD2 with that by KMTR2 (Figure 3D and 3E). The contact area (623 $Å^2$) between TRAIL-R2 and KMTR2 was smaller than those with Ysd1 (715 $Å^2$), Bdf1 (851 $Å^2$), and Apomab (805 $Å^2$). Thus, this suggested that antigen recognition by CRD1 and CRD2 was insufficient to determine the direct agnostic activity of KMTR2.

Interaction between two KMTR2-Fab fragments in crystal packing. Next, we focused on the crystal packing of ecTRAIL-R2/KMTR2-Fab complex because an oligomer configuration rendered by crystallographic symmetry often corresponds to the following biological assemblies. For a 1:1 complex structure between ecTRAIL-R2 (PDB ID: 1D4V), a 3:3 configuration via three-fold crystallographic symmetry reflects an activated TRAIL-R2 state. Based on two-fold crystallographic symmetry, we have also elucidated a 2:2 structure for the signaling complex between granulocyte colony-stimulating factor (GCSF) and its receptor (GCSF-R), with reference to several mutational analyses[26].

The 2:2 complex structure between ecTRAIL-R2 and KMTR2-Fab rendered by crystallographic symmetry is shown in Figure 4A (unobserved CRD3 structure in TRAIL-R2 was constructed by superimposition with another TRAIL-R2 structure). Two KMTR2-Fab molecules interacted with CDR2 of the light chain via two-fold crystallographic symmetry, and consequently, two TRAIL-R2 molecules were situated in parallel within a C-terminal distance of 20 Å. It is believed that this adjacent configuration of extracellular regions results in access to each DD in the intracellular regions of TRAIL-R2 molecules, leading to activation of a caspase-dependent apoptotic pathway[6].

Table 2 lists the contact pairs within 4 Å (3.6 Å for detecting hydrogen bonds) between two KMTR2-Fab fragments. The contact region mainly consisted of the region from Tyr49 to Arg61 located in CDR2 of the light chain, including six direct hydrogen bonding interactions and four van der Waals interactions, which may have partly accounted for the strong interaction between two KMTR2-Fab fragments (Figure 4B). In particular, Arg54 in CDR2 of the light chain primarily contributed to the interaction between two KMTR2-Fab fragments, with three direct and five water-mediated hydrogen bonds.

a

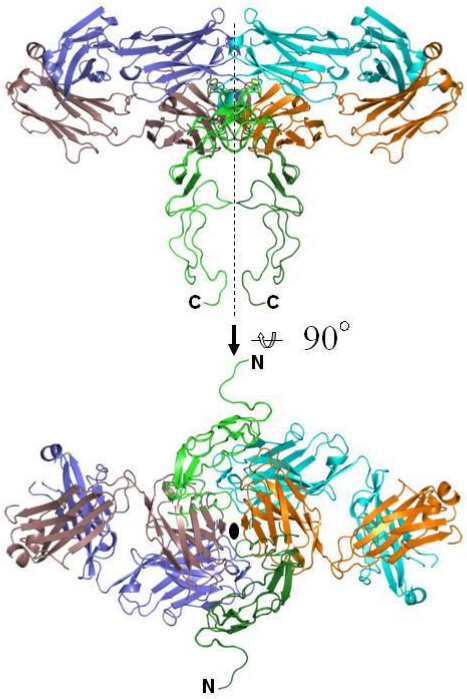
C
C
90°
N
N

b

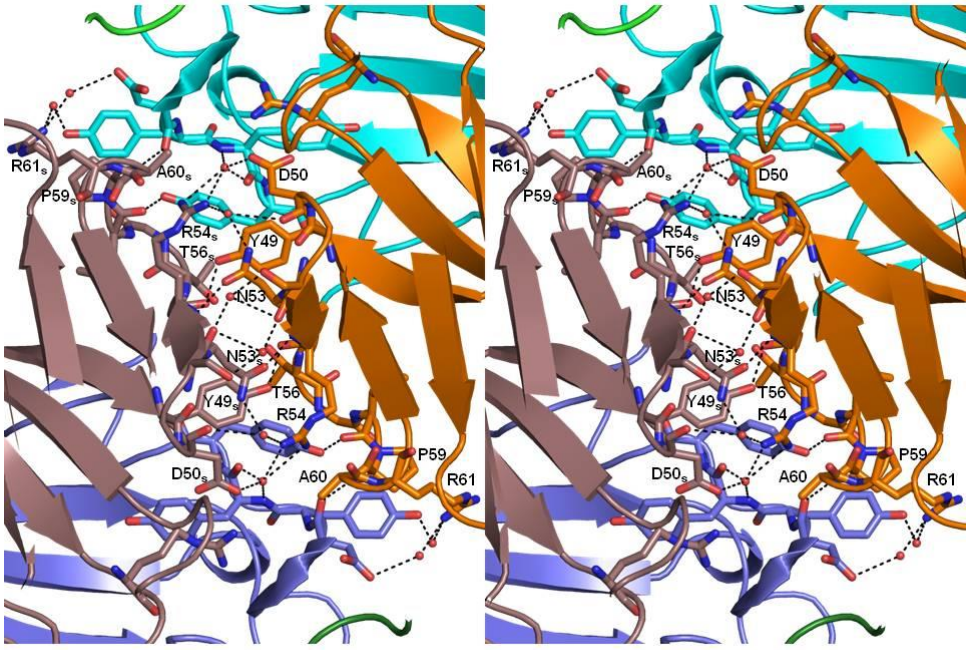
R61s
A60s
D50
P59s
R54s
T56s
Y49
N53
N53s
Y49s
T56
R54
P59
D50s
A60
R61
R61s
A60s
D50
P59s
R54s
T56s
Y49
N53
N53s
Y49s
T56
R54
P59
D50s
A60
R61

Figure 4. Dimeric structure of an ecTRAIL-R2/KMTR2-Fab complex rendered by crystallographic two-fold symmetry. The heavy and light chains of neighboring molecules rendered by crystallographic symmetry are colored purple and brown, respectively. (a) Overall structure. Dashed lines and ellipse indicate the two-fold axis. (b) Close-up view of the interface between two KMTR2-Fab molecules. Residues related to the interaction between two KMTR2-Fab molecules are represented by a stick model.

Table 2. Residues related to antibody−antibody binding via crystallographic symmetry.

				distance		**Symmetry**			
chain	**CDR**	**residue**	**atom**			**atom**	**residue**	**CDR**	**chain**
H	1	Gly26	O	3.5	h	Oε1	Glu1	―	H
L	2	Tyr49	Oη	2.59	h	O	Arg54	2	L
		Asp50	Oδ2	water mediated	h	Nη1			
			O	water mediated	h	Nη2			
		Ser52	Oγ	water mediated	h	O	Ser52		
		Asn53	Oδ1	2.9	h	N	Arg54		
			Nδ2	water mediated	h	Nη2			
		Arg54	Nη1	3.59	h	O	Asp108	3	H
				water mediated	h	O	Tyr110		
				water mediated	h	Nη1	Arg91	3	L
		Thr56	Cα	3.95		Cδ2	Tyr111	3	H
		Gly57	Cα	3.47		Cζ			
			N	3.12	h	Oη			
		Ile58	O	2.75	h	Oη			
		Pro59	Cβ	3.52		Cζ	Tyr109		
		Ala60	N	2.99	h	O	Asp108		
			Cβ	3.99		Cα			
		Arg61	Nη1	water mediated	h	Oδ1			
				water mediated	h	Oη1	Tyr109		

h: hydrogen bond (within 3.6 Å between donor and acceptor).

Binding and apoptosis-inducing activities of KMTR2 and its LkN53R mutant. We assumed that Fab dimerization based on this two-fold symmetry was essential for the direct agonistic activity of KMTR2. To confirm whether the interaction between two KMTR2-Fab fragments via crystallographic symmetry was essential for KMTR2 apoptotic activities, we attempted to incorporate a bulky residue into this interface to disrupt this interaction. We designed a mutant, Asn53 to Arg, in the light kappa chain of KMTR2 (LkN53R) to prevent dimerization at this site. Because Asn53 in CDR2 of the light chain was located near the two-fold axis between the two KMTR2-Fab fragments, the Asn53 to Arg mutation should have resulted in introducing both steric hindrance and charge repulsion from the associations of four positive charges, two from Arg53 after mutation and two from Arg54 (Figure 4B).

We first examined the effect of this mutation on the binding activity with TRAIL-R2. As determined by flow cytometry analysis, both KMTR2 and its LkN53R mutant specifically bound to endogenous TRAIL-R2 in Colo205 cells (Figure 5A). The fluorescence signal intensity of KMTR2 was similar to that of the LkN53R mutant at concentrations of both 100 ng/mL and 1000 ng/mL. The signal intensities of both KMTR2 and the LkN53R mutant increased in a concentration-dependent manner. In addition, ELISA analysis showed that both KMTR2 and the LkN53R mutant resulted in similar dose-dependent increases in absorbance after binding to ecTRAIL-R2 fused with Fc and reached saturation at an antibody concentration of 200 ng/mL (Figure 5B). These results indicated that the Asn53 to Arg mutation had little effect on binding activity.

a

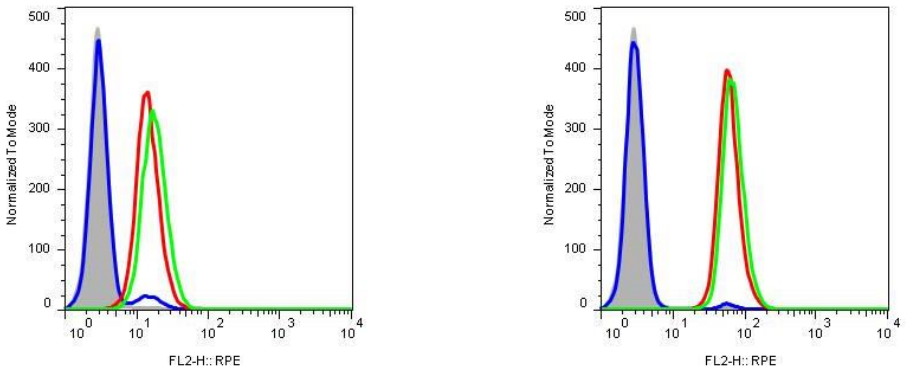

b

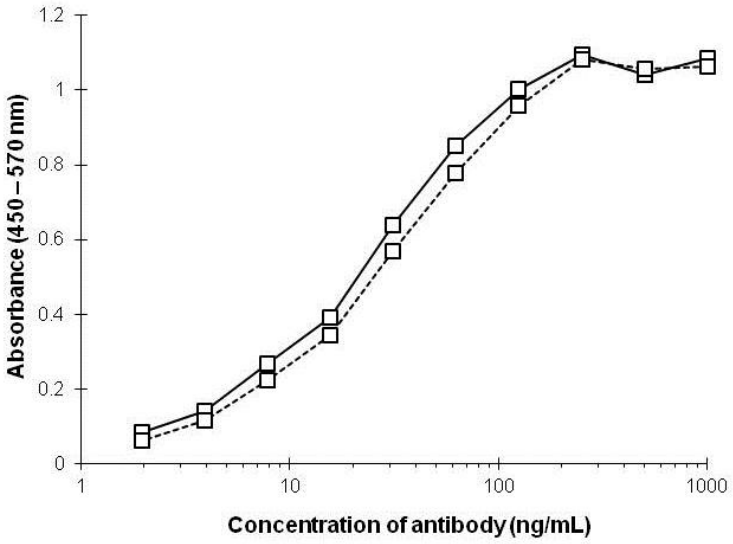

Figure 5. Binding activities of KMTR2 and its mutant (LkN53R) to TRAIL-R2. (a) Flow cytometry results. Antibody concentrations are 100 ng/mL (left) and 1000 ng/mL (right). X-axis indicates R-phycoerythrin (RPE) fluorescence signal intensity. Data for KMTR2, LkN53R mutant, and anti-DNP (negative control) are shown as green, red, and blue lines, respectively. Gray-colored histogram is the control (2nd-PE). (b) ELISA results. Data for KMTR2 and the LkN53R mutant are shown as solid and dashed lines, respectively.

Effect on LkN53R mutation on TRAIL-R2 oligomerization. Next, we examined the effect of this mutation on TRAIL-R2 oligomerization. Size exclusion chromatography showed that KMTR2 can oligomerize ecTRAIL-R2:Fc (Figure 6A, upper). The immune complex (ecTRAIL-R2:Fc/KMTR2) was eluted in the void volume fraction. In contrast, the ecTRAIL-R2:Fc/LkN53R complex was eluted within 250 kDa (Figure 6A, lower), which was estimated by reference to previous SEC-light scattering analysis[24]. The formation of immune complexes on the surface of Colo205 cells was visualized by confocal microscopy. Consistent with the idea that KMTR2 induces receptor clustering, Colo205 cells incubated with KMTR2 formed specific patches (Figure 6B, upper). In contrast, the LkN53R mutant showed dispersed staining on Colo205 cells (Figure 6B, lower). These results indicated that the LkN53R mutation abolishes the higher oligomerization of TRAIL-R2.

Apoptosis-inducing activities of KMTR2 and LkN53R. We examined whether the LkN53R mutant resulted in a loss of apoptosis-inducing activity without cross-linking. KMTR2 exhibited concentration-dependent inhibition on the proliferation of Colo205 cells (EC_{50} = 6−7 ng/mL) (Figure 7A) even in the absence of cross-linking reagent. In contrast, the LkN53R mutant exhibited no inhibitory activity at any concentration. However, both antibodies induced apoptosis in a concentration-dependent manner and with similar activities in the presence of a cross-linking regent, although the LkN53R mutant activity was less than the activity of KMTR2 even if a cross-linking reagent was used (Figure 7A; KMTR2: EC_{50} = 4−5 ng/mL; LkN53R: EC_{50} = 10−20 ng/mL). In addition, IgG monomer of KMTR2 induced marked caspase-3/7 activation of the same level as cross-linked KMTR2 at concentration of 100 and 1,000 ng/mL (Figure 7B). In

contrast, the LkN53R mutant exhibited caspase-3/7 activation only when the cross-linking reagent was added. These results indicated that the LkN53R mutant did not have agonistic activity without cross-linking and strongly suggested that the LkN53R mutant interfered with KMTR2 Fab dimerization, which resulted in a loss of its direct agonistic activity.

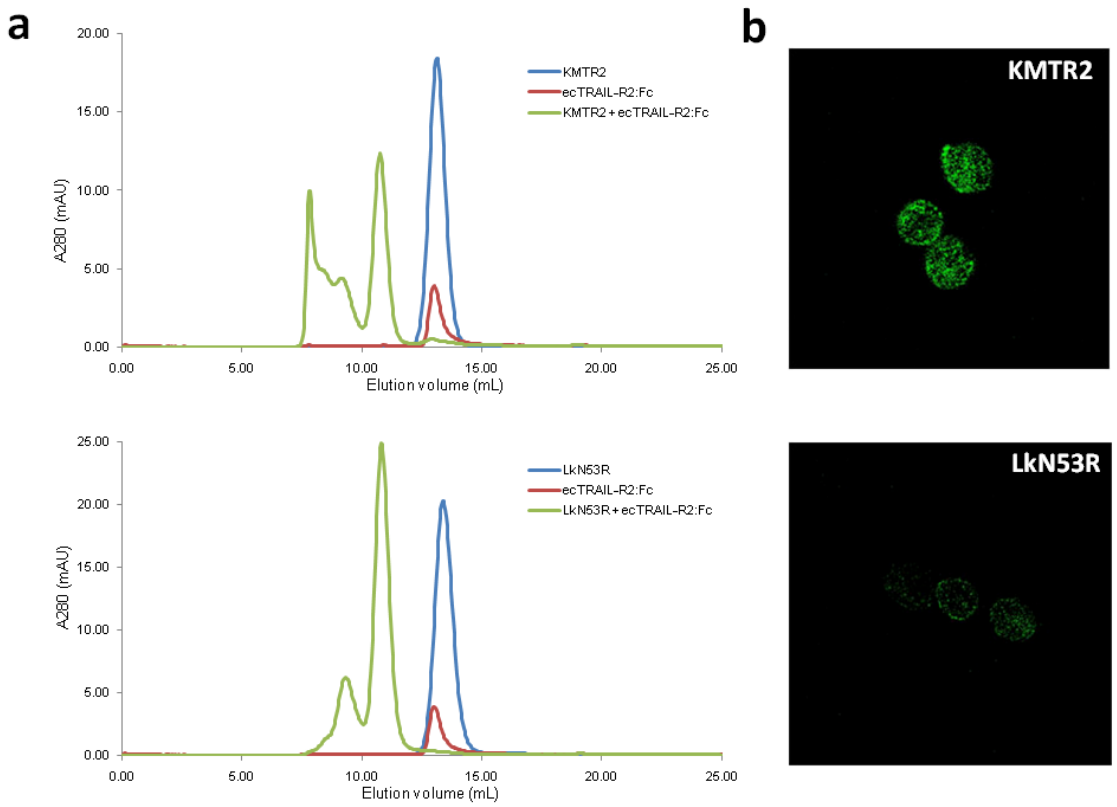

Figure 6. .Immune complex analysis of TRAIL-R2 and monomer antibody. (a) Size exclusion chromatogram. KMTR2 (upper) or the LkN53R mutant (lower) was mixed with ecTRAIL-R2:Fc fusion protein at the molar ratio of 1:1 and then loaded to Superdex 200 10/300 GL gel filtration column. Monomer antibodies and ecTRAIL-R2:Fc were also loaded independently. (b) Cell surface TRAIL-R2 immune complexes on Colo205 cells visualized by confocal microscopy (× 40). Cells were incubated with monomer KMTR2 (upper) and the LkN53R mutant (lower) at 37°C for one hour and then labeled with Alexa488.

a

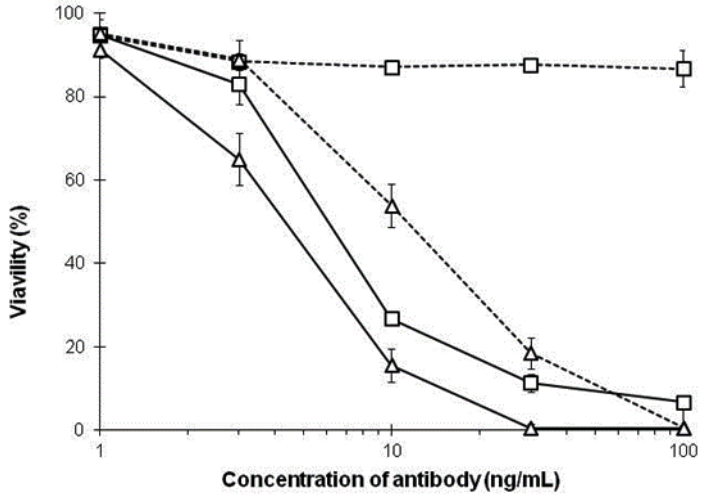

b

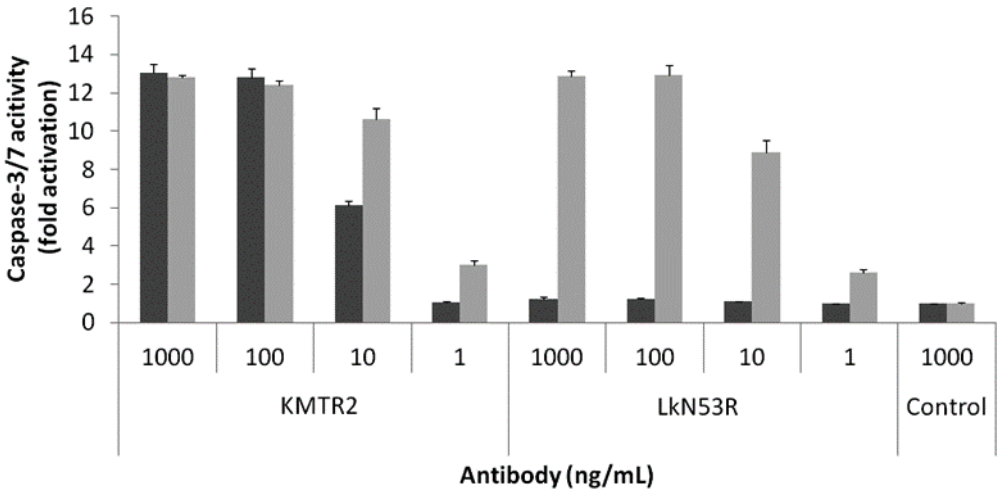

Figure 7. Apoptosis-inducing activity of KMTR2 and the LkN53R mutant. (a) Dose-dependent responses of apoptosis-inducing activity by a purified monomer fraction of KMTR2 without (open squares) and with (open triangles) cross-linking. Data for KMTR2 and the LkN53R mutant are shown as solid and dashed lines, respectively. (b) Effector caspase activity of Colo205 was assessed 2 hours after the treatment with a monomer fraction of KMTR2, LkN53R, and anti-DNP (negative control) without (dark gray) and with (light gray) cross-linking.

Discussion

Our results suggested that the 2:2 configuration shown in Figure 4A was an essential unit for sufficient KMTR2 direct agonistic activity. In the KMTR2-Fab structure without TRAIL-R2, CDR2 of the KMTR2 light chain was also involved in the interaction with neighboring molecules via crystallographic symmetry (Figure 8). There were some interaction residues between each CDR2 of the light chain; however, its binding mode was quite different from that in complex with TRAIL-R2. In the presence of TRAIL-R2, the unique sequence at CDR2 of the light chain in KMTR2 was responsible for its association with KMTR2, which resulted in effective superoligomerization and activation of potent apoptotic signaling via TRAIL-R2.

Our previous results using SEC-light scattering analysis showed that the molecular mass of the ecTRAIL-R2:Fc/KMTR2 complex eluted in the void fraction (Figure 6A, upper) was 5,130 kDa[24]. This mass corresponds to approximately twenty 2:2 complexes between KMTR2 and ecTRAIL-R2 (Fc regions of antibody and antigen were included in this calculation). We assumed that TRAIL-R2 superoligomerization induced by KMTR2 would appear in its crystallographic packing. Several 2:2 complexes on the same layer in a crystal lattice were extracted (Figure9A). In the vertical direction, each 2:2 complex (shown within rounded rectangles) was linked with another unit of the 2:2 complex via an interface between two TRAIL-R2 molecules (shown within dotted circles).

It is known that many receptors that belong to the TNF receptor superfamily exist as preassembled oligomers on a cell surface[27,28]. TRAIL-R2 also generates a ligand-independent assembly with TRAIL-R4, which acts as a decoy receptor[29]. TNF receptor-1 and -2 form a self-complex of homodimers or homotrimers as preassembled oligomers on a cell surface[27,30]. During the ligand-independent assembly of TNF receptors, each

receptor associates with others via CRD1[27], and a parallel dimer of TNF receptor-1 through a CRD1−CRD1 interaction has been confirmed in its crystal structure (Figure 10)[31]. A similar CRD1−CRD1 interaction was also observed in the crystal packing between TRAIL-R2 molecules (Figure 9B), in which the CRD1−CRD1 interface was constructed via two-fold crystallographic symmetry (shown within dotted circles in Figure 9A). The side chain of Lys98 interacted with two main chain carbonyl oxygen atoms in neighboring symmetric molecule by hydrogen bonding. The aromatic ring of Tyr99 and two sequential prolines (Pro82 and Pro83) in neighboring molecule were situated in positions which permit van der Waals interaction. In addition, two sequential threonin residues (Thr130 and Thr131) formed a hydrogen bond network with identical residues in neighboring molecule via several water molecules. The mutation study for TNF receptor-1 showed that the serial Lys-Tyr residues (Lys19 and Tyr20) in CRD-1 were essential for the ligand-independent self-association and signal transduction[27] (however, in the crystal structure[31], Tyr20 was located far from neighboring molecule as shown in Figure 10). These information suggests that the symmetric TRAIL-R2 dimer may be ligand-independent homo dimer.

These findings suggest that KMTR2 acts as a bridge between preassembled TRAIL-R2 dimers and results in the linear oligomerization observed in its crystal packing, in which the distance between each TRAIL-R2 dimer is approximately 70 Å. This distance corresponds to that in both dimer and trimer models of TNF receptor-2 proposed as the signaling oligomers of TNF/TNF receptor-2 complexes[30]. With respect to the adjacent relationship between the linear packing of ecTRAIL-R2/KMTR2, there is no direct packing interaction between 2:2 complexes (Figure 9A). The distances between the C-terminals of the KMTR2-Fab heavy chain in this linear packing are, however,

approximately 45 Å apart (Figure 9A). Because the distance between the C terminals of Fab was 45 Å in the crystal structure of IgG, this distance (45 Å) enables these two Fab fragments to exist as two "arms" in one intact IgG molecule.

Based on these considerations, we propose the clustering mechanism of TRAIL-R2 provided by KMTR2 shown as Figure 9C. Although the enhanced clustering (trimer model) of TRAIL-R2 is proposed from the structure of TRAIL/TRAIL-R2/AMG 655-Fab ternary complex[15], KMTR2 constructs such clustering without TRAIL, and consequently, shows a strong direct agonistic activity. The schematic clustering model drawn in Figure 9C shows that four TRAIL-R2 molecules localize in parallel within 70 Å on cell surface. Such conformation of receptors may allow the adjacent positioning of the intracellular death domains (DDs) sufficient for activating the caspase-dependent apoptotic pathway. In crystal structures of the death-inducing signaling complex (DISC) formed by Fas receptor and Fas-associaetd death domain protein, 4[32] and 5–7[33] Fas-DDs composed the DISC, which activates caspases. It is believed that superoligomerization of receptors with methodological clustering (~70 Å and parallel direction) induced by KMTR2 is essential for transducing an apoptosis signal.

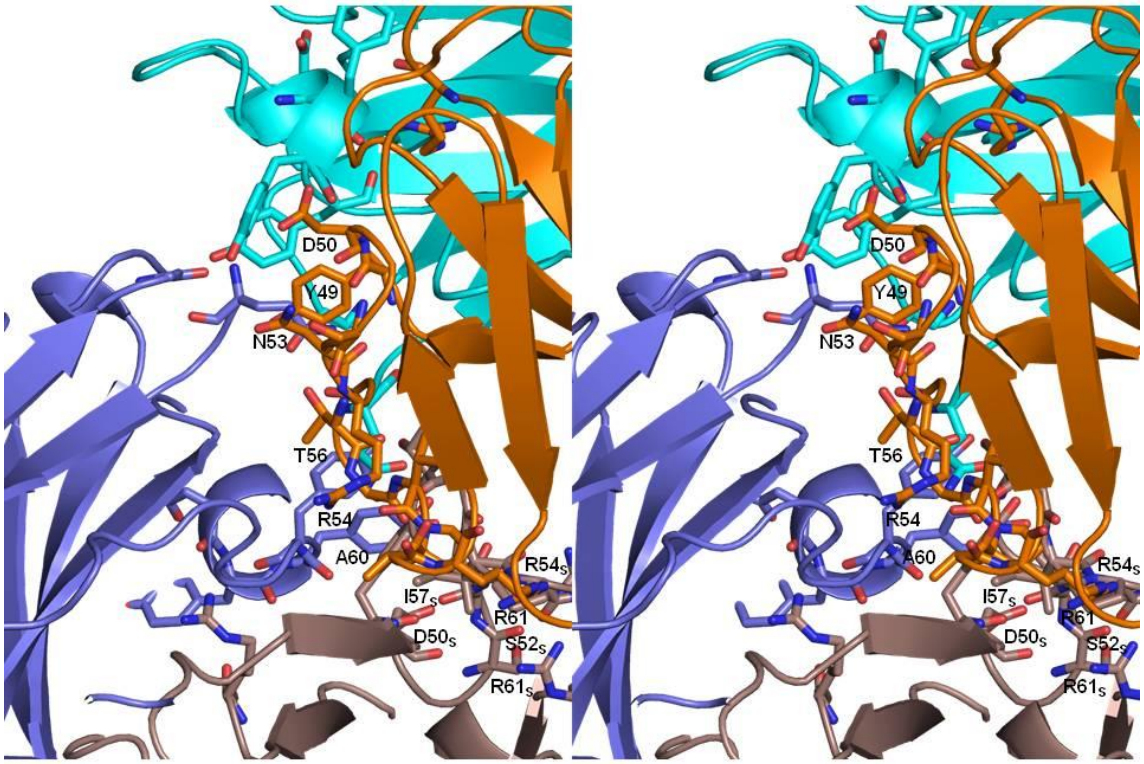

Figure 8. Close-up view of the interface between two KMTR2-Fab molecules in a structure without ecTRAIL-R2 rendered by crystallographic symmetry. KMTR2-Fab molecule (heavy: cyan, light: orange) at right is shown in the same position as that in Figure 4B.

a

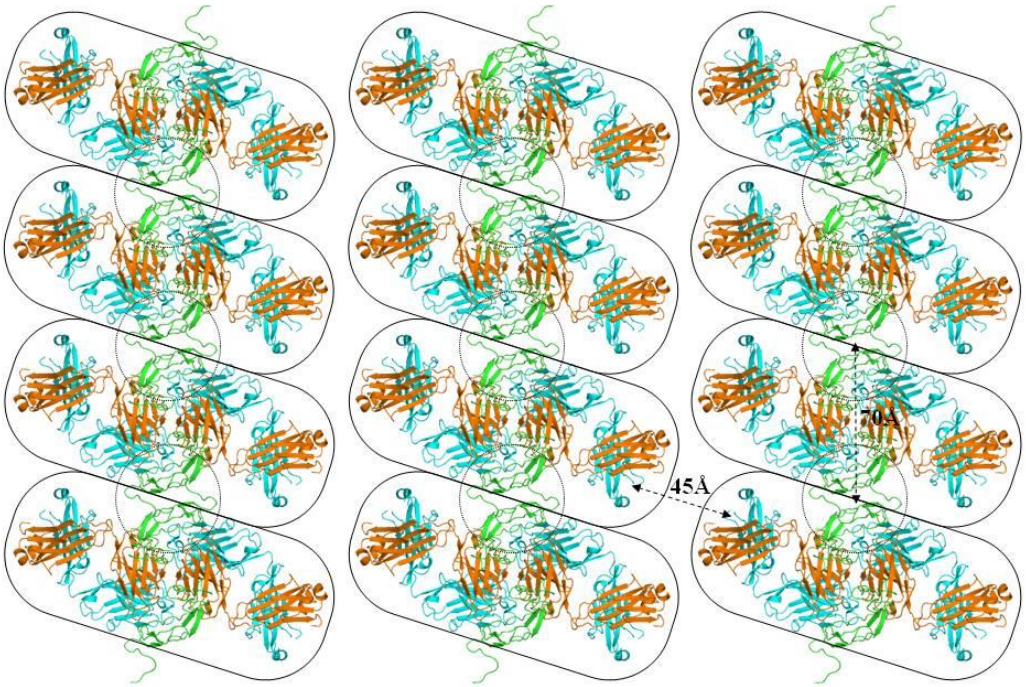
45Å
70Å

b

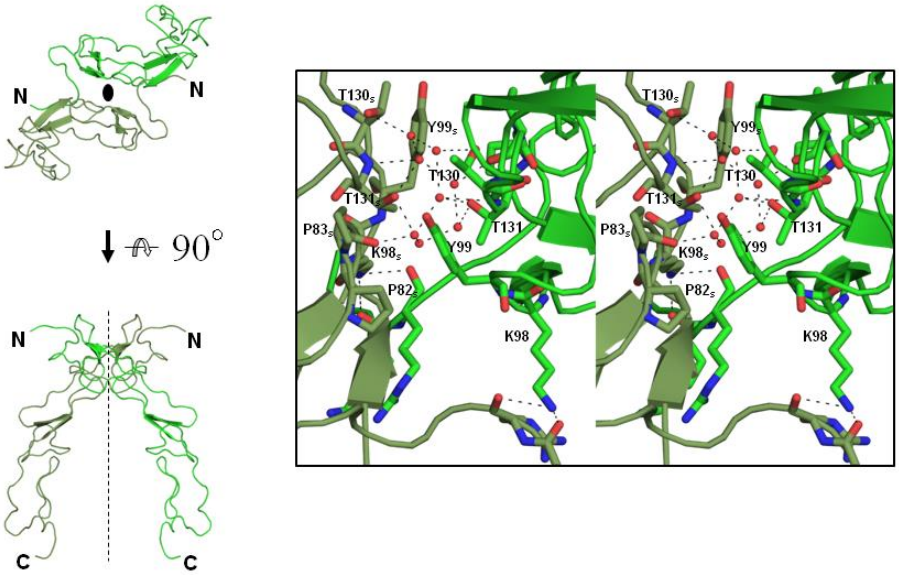
N
N
90°
N
N
C
C
T130s
Y99s
T130
T131
P83s
K98s
Y99
T131
P82s
K98
T130s
Y99s
T130
T131
P83s
K98s
Y99
T131
P82s
K98

c

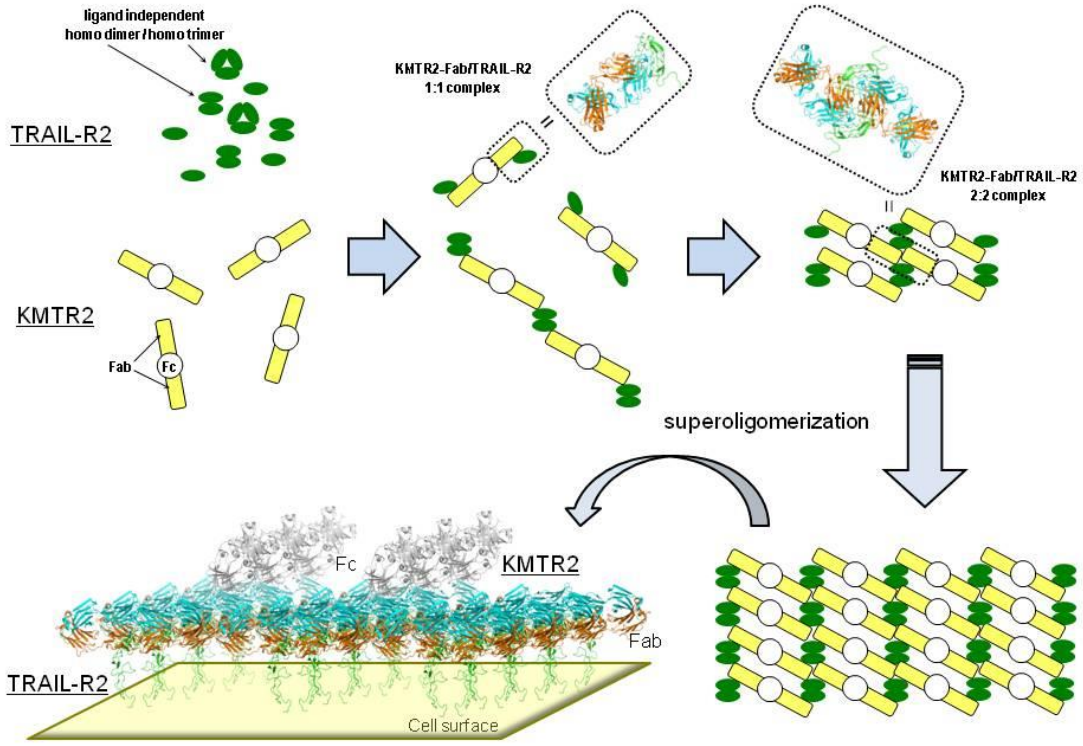

Figure 9. TRAIL-R2 oligomerization induced by KMTR2. (a) Oligomeric structure of an ecTRAIL-R2/KMTR2-Fab complex on a layer in a crystal lattice. The 2:2 complexes and TRAIL-R2 dimers rendered by another two-fold symmetry are enclosed by rounded rectangles and dotted circles, respectively. (b) Close-up view of a TRAIL-R2 dimer enclosed by a dotted circle in (a). (c) Model for TRAIL-R2 superoligomerization by KMTR2. The intact model structure of KMTR2 which was constructed with reference to the crystal structure of an intact IgG2a monoclonal antibody (PDB ID: 1IGT)[34].

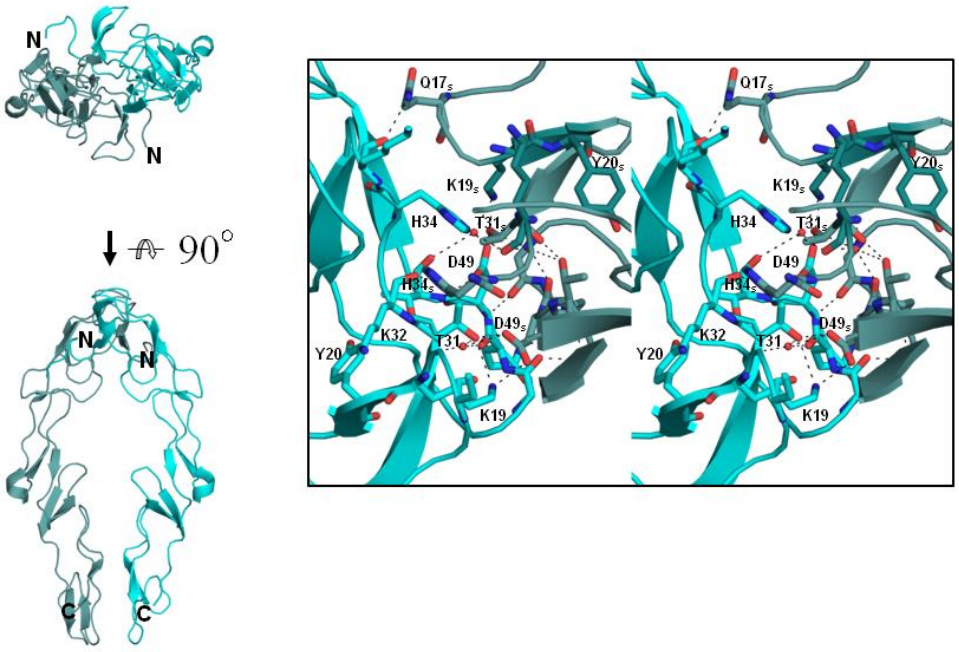

Figure 10. Cristal structure of TNF receptor-1 dimer. A close-up view of the interface between two receptor molecules id drawn in the box figure (stereo representation).

Experimental Procedures

Materials. Anti-human IgG polyclonal antibody was purchased from Sigma-Aldrich Japan K.K. (Tokyo, Japan) and used as crosslinking reagent for *in vitro* assay. Human IgG labeling kit was purchased from Molecular Probes (Eugene, OR) and used for confocal microscopy analysis. Control human antibody to 2,4-dinitrophenol (DNP) was prepared in our laboratory from Chinese hamster ovary (CHO) cells transfected with variable region of the hybridoma-derived antibody and the framework of IgG1 according to the method described below. Colo205 human colorectal adenocarcinomawas obtained from American Type Culture Collection (Rockville, MD). Colo205 cells were maintained in RPMI 1640 supplemented with 10% fetal bovine serum (FBS) and streptomycin.

ecTRAIL-R2 and mutant preparation. The extracellular region (residues Ala54−Lys181) of human TRAIL-R2 fused with the Fc region of human IgG1 was prepared in our laboratory from stably transfected CHO cells with a vector that contains cDNA encoding the extracellular domain of TRAIL-R2 fused to Fc portion of human IgG1. A FLAG sequence (DYKDDDDK) was inserted between ecTRAIL-R2 and Fc. The ecTRAIL-R2:Fc fusion protein was purified using a HiTrap rProtein A FF column (GE Healthcare, Piscataway, NJ) for affinity chromatography and then digested using a recombinant enterokinase cleavage kit (Novagen) according to the supplier's protocol. ecTRAIL-R2 and Fc were purified by cation-exchange chromatography on a TSKgel SP-5PW column (4.5 × 75 mm, TOSOH, Tokyo, Japan) after removing enterokinase with capture agarose. ecTRAIL-R2 and Fc were separated using a linear gradient of 0 − 0.5 M NaCl in 20 mM sodium acetate (pH 5.0).

KMTR2 and mutant preparation. KMTR2 generation was performed as reported previously. An anti-TRAIL-R2 fully human monoclonal antibody KMTR2 was expressed in CHO cells and purified with protein A (Amersham Biosciences Corp., Piscataway, NJ) by standard methods from culture supernatant of CHO cells.

Single amino acid substitution (Asn53 → Arg) in the light kappa chain of KMTR2 was introduced using the primers 5′ -GAT GCA TCC AGA AGG GCC ACT GG-3′ and 5′ -CCA GTG GCC CTT CTG GAT GCA TC-3′ . Site-directed mutagenesis was conducted using a N5KG4-KMTR2 vector and a QuikChange site-directed mutagenesis kit (Stratagene, La Jolla, CA) according to the supplier’ s protocol. After site-directed mutagenesis, the N5KG4-KMTR2 vector with substituted Asn53 to Arg in the light kappa chain (LkN53R) was transformed in Escherichia coli DH5α cells, and the LkN53R mutant was expressed and purified using the same procedures as used for KMTR2.

KMTR2 Fab fragment was prepared by papain (Boehringer Ingelheim, Germany) digestion at the hinge region of KMTR2 to remove the Fc region. Antibodies were incubated for 1 hour under both non-reducing and reducing (10 mM cysteine) conditions, after which they were incubated with activated papain for 24 hours. Fab and Fc fragments were separated by cation-exchange chromatography on a TSKgel SP-5PW column using a linear gradient of 0−0.5 M NaCl in 20 mM sodium acetate (pH 5.0).

ecTRAIL-R2/KMTR2-Fab complex preparation. ecTRAIL-R2 was mixed with an excess amount of KMTR2-Fab and incubated at room temperature (RT) for 1 hour to form the ecTRAIL-R2/KMTR2-Fab complex. The ecTRAIL-R2/KMTR2-Fab complex was purified by gel filtration using a Superdex 200 HR 10/30 column (Amersham Pharmacia Biotech AB, Uppsala, Sweden) equilibrated with 20 mM HEPES buffer (pH

7.2) with 0.2 M NaCl at a flow rate of 0.3 mL/min. The observed mass of the eluted complex by multi-angle light scattering using mini-DAWN (Wyatt Technologies, Santa Barbara, CA) indicated that ecTRAIL-R2 and KMTR2-Fab had formed a 1:1 stoichiometric complex.

Crystallization. Crystallization was kindly conducted by Dr. Tamada. Purified ecTRAIL-R2/KMTR2-Fab complexes and KMTR2-Fab fragments were concentrated to 5 mg/mL in 20 mM HEPES buffer (pH7.2) that contained 0.2 M NaCl. Initial screening of crystallization conditions was performed using Crystal Screen 1 & 2 and PEG/Ion Screen 1 & 2 (Hampton Research, Riverside, CA) by vapor diffusion against the reservoir solution. Microcrystals of ecTRAIL-R2/KMTR2-Fab were obtained from condition 7 in PEG/Ion Screen 1. Crystallization conditions were finally refined to 75 mM calcium chloride dihydrate (pH 5.1) containing 7.5% (w/v) PEG3350 to yield prism-shaped crystals with a dimension of approximately 0.02 × 0.04 × 0.15 mm. Prism-shaped crystals of KMTR2-Fab with a dimension of approximately 0.05 × 0.05 × 0.2 mm were obtained from condition 33 [200 mM sodium sulfate decahydrate, pH 6.6, with 20% (w/v) PEG3350] in PEG/Ion Screen 1 after the initial crystallization screening.

Data collection, phasing, and refinement. Data collection, phasing, and refinement was also kindly conducted by Dr. Tamada. Diffraction data for ecTRAIL-R2/KMTR2-Fab complexes and KMTR2-Fab fragments were acquired in a cold nitrogen gas stream at 100 K and recorded on an ADSC Quantum 315 at BL41XU at the SPring-8 facility (Hyogo, Japan), with a total oscillation range of 180°. The oscillation angle and exposure time per frame were 1.0° and 10 s, respectively. Intensity data for ecTRAIL-R2/KMTR2-

Fab complexes and KMTR2-Fab fragments were processed with HKL2000[35] to 2.1 Å and 2.5 Å resolution, respectively. The crystals of ecTRAIL-R2/KMTR2-Fab complexes and KMTR2-Fab fragments belonged to space group *I*222 with unit cell dimensions of a = 145, b = 152, and c = 65 Å and $C222_1$ with unit cell dimensions of a = 153, b = 165, and c = 66 Å, respectively. The Matthews coefficients of ecTRAIL-R2/KMTR2-Fab complexes and KMTR2-Fab fragments were 2.77 $Å^3$/Da and 4.26 $Å^3$/Da assuming one 1:1 complex and Fab in the asymmetric unit corresponding to solvent contents of 56% and 71%, respectively. Initial phase information was obtained by molecular replacement analysis with PHASER[36] using a Fab structure of human IgG1 anti-HIV-1 (PDB ID: 1HZH)[37] and a structure of an ecTRAIL-R2 in 1:1 complex structure with TRAIL (PDB ID: 1D4V) as search models. The atomic model was built and modified with COOT[38]. The final models for ecTRAIL-R2/KMTR2-Fab complexes and KMTR2-Fab fragments were refined to crystallographic R-factors of 18.8% and 18.8% (free R-factors = 22.4% and 22.4%) to 2.1 Å and 2.5 Å resolution using TLS and restrained refinement with REFMAC[39], respectively. Statistics for data collection and refinement are summarized in Table 3. Figures 1, 2, 3, 4, 8 and 10, were prepared using the PyMOL Molecular Graphics System (DeLano Scientific, San Carlos, CA, USA).

Flow cytometry. The human colorectal adenocarcinoma cell line Colo205 (ATCC No. CCL-222) was cultured in RPMI 1640 medium supplemented with 10% FBS in 96-well round-bottomed plates (BD Biosciences PharMingen, San Jose, CA) at a density of 5×10^5 cells/well. KMTR2, LkN53R mutant, and an anti-DNP monoclonal antibody IgG1 (anti-DNP) as a negative control were added to wells at concentrations of 100 or 1000 ng/mL and then incubated with R-phycoerythrin (RPE)-labeled goat anti-human IgG

(Southern biotech) at 4°C for 1 hour. After washing, the cells were analyzed using a FACSCalibur (BD Biosciences PharMingen).

ELISA. Purified ecTRAIL-R2:Fc fusion proteins were added to a flat-bottomed plate at 25 ng/well and incubated at RT for 1 hour. The wells were then blocked with blocking buffer (Pierce, Rockford, IL) at RT for 30 min. After three washes with wash buffer (Tris-buffered saline with 0.1% Tween-20), KMTR2, KMTR2 mutants, and anti-DNP as negative control were added to the wells at concentrations of 2−1000 ng/mL and incubated at RT for 1 hour. The plate was washed three times with wash buffer; thereafter, a horseradish peroxidase-labeled secondary antibody, goat anti-human kappa polyclonal antibody (dilution 1:2000; Biosource International), was added to each well, followed by incubation at RT for 1 hour. The plate was washed three times with wash buffer, after which TMB substrate (DAKO Japan, Kyoto, Japan) was added. The enzymatic reaction was stopped by adding 0.5 mol/L of sulfonic acid and absorbance was measured at 450 nm (reference wavelength of 570 nm) using a microplate reader.

Size exclusion chromatography. KMTR2 and the LkN53R mutant antibodies were mixed with ecTRAIL-R2:Fc in D-PBS at the molar ratio of 1:1. The mixture was incubated for 30 min at 37°C and then loaded to Superdex 200 10/300 GL gel filtration column (GE Healthcare, Piscataway, NJ) equilibrated with D-PBS. The protein complexes of each fraction were detected by UV absorbance at 280 nm.

Confocal microscopic analysis. Colo205 cells were seeded in collagen I two-well CultureSlides (BD Biosciences PharMingen, San Jose, CA) at 2×10^5 cells per well and

cultured overnight at 37°C under 5% CO2. Cells were incubated with gel filtration fractionated monomeric KMTR2 or the LkN53R mutant at a concentration of 100 ng/mL for 1.5 hour at 37°C under 5% CO2. After washing by ice-cold 1% FBS-D-PBS, Alexa 488-labeled Fab fragment specifically recognizing human IgG (Zenon Human IgG Labeling kits, Molecular Probes) was added for 30 min on ice. Cells were washed and mounted in Fluoromount-G (Southern-Biotech, Birmingham, AL) and visualized with confocal microscope (Carl Zeiss, Oberkochen, Germany), × 40 objective lens.

Proliferation assay. Colo205 cells were seeded in a 96-well flat-bottomed plate at a density of 1×10^4 cells/well and cultured overnight at 37°C under 5% CO2. KMTR2 and LkN53R mutant antibodies were added to the wells at concentrations of 1−100 ng/mL, after which the cells were cultured for an additional 2 days. Cross-linked KMTR2 was prepared by adding goat anti-human IgG (gamma-chain specific; Sigma-Aldrich) at a concentration of 10 μg/mL for 0.5−1 hour after adding KMTR2. Cell viability was determined by an MTS dye reduction assay using a CellTiter 96 aqueous non-radioactive cell proliferation assay kit (Promega Corp., Madison, WI) and calculated as follows:

Cell viability (%) = 100 × (a − b)/(c − b),

where a = absorbance of a sample well, b = absorbance of a blank well, and c = absorbance of medium-treated cells. Each measurement was repeated three times with similar results. The EC50 value for each antibody was defined as the concentration that reduced cell viability by 50%.

Caspase assay. Colo205 cells were seeded in 96-well flat-bottomed plate (Greiner Bio-One, Kremsmünster, Austria) at 1×10^4 cells per well and cultured overnight at 37°C

under 5% CO2. KMTR2, the LkN53R mutant and anti-DNP (as negative control) antibodies were added to each well at 1, 10, 100, and 1,000 ng/mL (anti-DNP: 1,000 ng/mL only) and subsequently incubated for 8 hour. Cells were added with or without goat anti-human IgG at a concentration of 10 μg/mL. Eight hours after the addition of antibodies, caspase-3/7 activity was measured by Caspase-Glo 3/7 Assay kit (Promega Corp., Madison, WI).

Table 3. Data collection and refinement statistics.

	ecTRAIL-R2/KMTR2-Fab	KMTR2-Fab
Crystal Data		
Space group	*I*222	$C222_1$
Cell constants (Å)	a = 145, b = 152, c = 65.0	a = 153, b = 165, c = 65.3
Data Collection		
Resolution (Å)	46.73−2.10 (2.18−2.10)	38.25−2.50 (2.59−2.50)
Reflections (total/unique)	195,258/39,887	173,069/27,370
Redundancy	4.9 (2.7)	6.3 (3.9)
Mosaicity	0.54	0.38
I/σ(I)	12.1 (1.9)	27.6 (3.8)
R_{merge}[1]	0.080 (0.294)	0.063 (0.396)
Completeness (%)	94.9 (84.2)	95.4 (81.1)
Refinement		
Resolution (Å)	46.73−2.10 (2.16−2.10)	38.25−2.51 (2.58−2.51)
Used reflections	39,887	27,361
R_{cryst}[2]	0.188 (0.285)	0.188 (0.321)
R_{free}[3]	0.224 (0.323)	0.224 (0.377)
No. of atoms	4,199	3,418
protein	3,878	3,349
sugar chain	14	14
glycerol, ion	31	13
water	276	42
Mean B value ($Å^2$)	32.8	78.27
ecTRAIL-R2	37.2	–
KMTR2-Fab heavy chain	32.7	74.2
KMTR2-Fab light chain	30.6	82.4
r.m.s. deviation		
bond lengths (Å)	0.008	0.012
bond angle (°)	1.36	1.70

Values for highest resolution shells are shown in parentheses.

[1] $R_{merge} = \Sigma|I(h) - |/\Sigma I(h)$, where is the mean value of reflection h for all measurements of I(h).

[2] $R_{cryst} = \Sigma||Fobs| - |Fcalc||/\Sigma|Fobs|$, where Fobs and Fcalc are observed and calculated structure factor amplitudes, respectively.

[3] R_{free} is the same as Rcryst, except for a 5% subset of all reflections.

References

1 Wiley, S. R. *et al.* Identification and characterization of a new member of the TNF family that induces apoptosis. *Immunity* **3**, 673-682 (1995).

2 Pitti, R. M. *et al.* Induction of apoptosis by Apo-2 ligand, a new member of the tumor necrosis factor cytokine family. *The Journal of biological chemistry* **271**, 12687-12690 (1996).

3 Walczak, H. *et al.* Tumoricidal activity of tumor necrosis factor-related apoptosis-inducing ligand in vivo. *Nature medicine* **5**, 157-163, doi:10.1038/5517 (1999).

4 Ashkenazi, A. *et al.* Safety and antitumor activity of recombinant soluble Apo2 ligand. *The Journal of clinical investigation* **104**, 155-162, doi:10.1172/jci6926 (1999).

5 Pan, G. *et al.* The receptor for the cytotoxic ligand TRAIL. *Science (New York, N.Y.)* **276**, 111-113 (1997).

6 Walczak, H. *et al.* TRAIL-R2: a novel apoptosis-mediating receptor for TRAIL. *The EMBO journal* **16**, 5386-5397, doi:10.1093/emboj/16.17.5386 (1997).

7 Chaudhary, P. M. *et al.* Death receptor 5, a new member of the TNFR family, and DR4 induce FADD-dependent apoptosis and activate the NF-kappaB pathway. *Immunity* **7**, 821-830 (1997).

8 Screaton, G. R. *et al.* TRICK2, a new alternatively spliced receptor that transduces the cytotoxic signal from TRAIL. *Curr Biol* **7**, 693-696 (1997).

9 Ashkenazi, A. Targeting death and decoy receptors of the tumour-necrosis factor superfamily. *Nature reviews. Cancer* **2**, 420-430, doi:10.1038/nrc821 (2002).

10 LeBlanc, H. N. & Ashkenazi, A. Apo2L/TRAIL and its death and decoy receptors. *Cell Death Differ* **10**, 66-75, doi:10.1038/sj.cdd.4401187 (2003).

11 Mongkolsapaya, J. *et al.* Structure of the TRAIL-DR5 complex reveals mechanisms conferring specificity in apoptotic initiation. *Nature structural biology* **6**, 1048-1053, doi:10.1038/14935 (1999).

12 Hymowitz, S. G. *et al.* Triggering cell death: the crystal structure of Apo2L/TRAIL in a complex with death receptor 5. *Molecular cell* **4**, 563-571 (1999).

13 Cha, S. S. *et al.* Crystal structure of TRAIL-DR5 complex identifies a critical role of the unique frame insertion in conferring recognition specificity. *The Journal of biological chemistry* **275**, 31171-31177, doi:10.1074/jbc.M004414200 (2000).

14 Ashkenazi, A. & Dixit, V. M. Death receptors: signaling and modulation. *Science (New York, N.Y.)* **281**, 1305-1308 (1998).

15 Graves, J. D. *et al.* Apo2L/TRAIL and the death receptor 5 agonist antibody AMG 655 cooperate to promote receptor clustering and antitumor activity. *Cancer Cell* **26**, 177-189, doi:10.1016/j.ccr.2014.04.028 (2014).

16 Nemcovicova, I., Benedict, C. A. & Zajonc, D. M. Structure of human cytomegalovirus UL141 binding to TRAIL-R2 reveals novel, non-canonical death receptor interactions. *PLoS pathogens* **9**, e1003224, doi:10.1371/journal.ppat.1003224 (2013).

17 Fellouse, F. A. *et al.* Molecular recognition by a binary code. *Journal of molecular biology* **348**, 1153-1162, doi:10.1016/j.jmb.2005.03.041 (2005).

18 Li, B. *et al.* Activation of the proapoptotic death receptor DR5 by oligomeric peptide and antibody agonists. *Journal of molecular biology* **361**, 522-536, doi:10.1016/j.jmb.2006.06.042 (2006).

19 Adams, C. *et al.* Structural and functional analysis of the interaction between the

agonistic monoclonal antibody Apomab and the proapoptotic receptor DR5. *Cell Death Differ* **15**, 751-761, doi:10.1038/sj.cdd.4402306 (2008).

20 Griffith, T. S. *et al.* Functional analysis of TRAIL receptors using monoclonal antibodies. *J Immunol* **162**, 2597-2605 (1999).

21 Chuntharapai, A. *et al.* Isotype-dependent inhibition of tumor growth in vivo by monoclonal antibodies to death receptor 4. *J Immunol* **166**, 4891-4898 (2001).

22 Ishida, I. *et al.* Production of human monoclonal and polyclonal antibodies in TransChromo animals. *Cloning and stem cells* **4**, 91-102, doi:10.1089/153623002753632084 (2002).

23 Mori, E. *et al.* Human normal hepatocytes are susceptible to apoptosis signal mediated by both TRAIL-R1 and TRAIL-R2. *Cell Death Differ* **11**, 203-207, doi:10.1038/sj.cdd.4401331 (2004).

24 Motoki, K. *et al.* Enhanced apoptosis and tumor regression induced by a direct agonist antibody to tumor necrosis factor-related apoptosis-inducing ligand receptor 2. *Clin Cancer Res* **11**, 3126-3135, doi:10.1158/1078-0432.ccr-04-1867 (2005).

25 Nagane, M., Shimizu, S., Mori, E., Kataoka, S. & Shiokawa, Y. Predominant antitumor effects by fully human anti-TRAIL-receptor 2 (DR5) monoclonal antibodies in human glioma cells in vitro and in vivo. *Neuro-oncology* **12**, 687-700, doi:10.1093/neuonc/nop069 (2010).

26 Tamada, T. *et al.* Homodimeric cross-over structure of the human granulocyte colony-stimulating factor (GCSF) receptor signaling complex. *Proceedings of the National Academy of Sciences of the United States of America* **103**, 3135-3140, doi:10.1073/pnas.0511264103 (2006).

27 Chan, F. K. *et al.* A domain in TNF receptors that mediates ligand-independent receptor assembly and signaling. *Science (New York, N.Y.)* **288**, 2351-2354 (2000).

28 Siegel, R. M. *et al.* Fas preassociation required for apoptosis signaling and dominant inhibition by pathogenic mutations. *Science (New York, N.Y.)* **288**, 2354-2357 (2000).

29 Clancy, L. *et al.* Preligand assembly domain-mediated ligand-independent association between TRAIL receptor 4 (TR4) and TR2 regulates TRAIL-induced apoptosis. *Proceedings of the National Academy of Sciences of the United States of America* **102**, 18099-18104, doi:10.1073/pnas.0507329102 (2005).

30 Mukai, Y. *et al.* Solution of the structure of the TNF-TNFR2 complex. *Science signaling* **3**, ra83, doi:10.1126/scisignal.2000954 (2010).

31 Naismith, J. H., Devine, T. Q., Brandhuber, B. J. & Sprang, S. R. Crystallographic evidence for dimerization of unliganded tumor necrosis factor receptor. *The Journal of biological chemistry* **270**, 13303-13307 (1995).

32 Scott, F. L. *et al.* The Fas-FADD death domain complex structure unravels signalling by receptor clustering. *Nature* **457**, 1019-1022, doi:10.1038/nature07606 (2009).

33 Wang, L. *et al.* The Fas-FADD death domain complex structure reveals the basis of DISC assembly and disease mutations. *Nature structural & molecular biology* **17**, 1324-1329, doi:10.1038/nsmb.1920 (2010).

34 Harris, L. J., Larson, S. B., Hasel, K. W. & McPherson, A. Refined structure of an intact IgG2a monoclonal antibody. *Biochemistry* **36**, 1581-1597, doi:10.1021/bi962514+ (1997).

35 Otwinowski, Z. & Minor, W. [20] Processing of X-ray diffraction data collected

in oscillation mode. *Methods in enzymology* **276**, 307-326, doi:10.1016/s0076-6879(97)76066-x (1997).

36 McCoy, A. J., Grosse-Kunstleve, R. W., Storoni, L. C. & Read, R. J. Likelihood-enhanced fast translation functions. *Acta crystallographica. Section D, Biological crystallography* **61**, 458-464, doi:10.1107/s0907444905001617 (2005).

37 Saphire, E. O. *et al.* Crystal structure of a neutralizing human IGG against HIV-1: a template for vaccine design. *Science (New York, N.Y.)* **293**, 1155-1159, doi:10.1126/science.1061692 (2001).

38 Emsley, P. & Cowtan, K. Coot: model-building tools for molecular graphics. *Acta crystallographica. Section D, Biological crystallography* **60**, 2126-2132, doi:10.1107/s0907444904019158 (2004).

39 Murshudov, G. N., Vagin, A. A. & Dodson, E. J. Refinement of macromolecular structures by the maximum-likelihood method. *Acta crystallographica. Section D, Biological crystallography* **53**, 240-255, doi:10.1107/s0907444996012255 (1997).

General conclusion

In these studies, the technologies and characters which have possibilities of improving the efficacy of monoclonal antibody therapeutics were evaluated.

One-step conjugation method for site-specific antibody-drug conjugates through reactive cysteine engineered antibodies.

The ADC is a therapeutic modality consisting of a monoclonal antibody attached to a cytotoxic, small-molecule payload which can enhance the activity of antibodies. This study examined that the novel cysteine engineered antibody, IgG-Lc-Q124C (named active thiol antibody: Actibody), which was introduced engineered cysteine residues at the position with the lowest Accessible Surface Area (ASA). Actibody was easily prepared by just substituion with cysteine at Gln124 (Kabat numbering) in light chain of aimed antibody. Furthermore, Actibody retained high thiol reactivity itself and made it possible to perform one-step conjugation without any pretreatment. Actibody based ADC of trastuzumab, Tra-IgG-Lc-Q124C-vcMMAE, exhibited *in vitro* cytotoxicy similar to common cysteine engineered antobpdy-drug conjugate, Tra-IgG-Lc-V205C-vcMMAE, through reduction-reoxidization process. These results suggested that Actibody could be applied to site-specific ADC.

In this study, a simple and efficient method was also created to enhance the stability of Lc-Q124C-conjugates in human plasma, in which reaction is performed on anion exchange resin at pH 9.5. The result showed that succinimide hydrolyzed Lc-Q124C (hy-Lc-Q124C) conjugate was produced after short time exposure (6 hours) onto anion exchange resin and following buffer exchange. Additionally, hy-Tra-IgG-Lc-Q124C-

vcMMAE exhibited similar efficacy than that of Tra-IgG-Lc-V205C-vcMMAE. These findings together suggest that Actibody provides easy way for preparing and analyzing site-specific conjugate, and shed light on the progress on analysis of functional molecules as in the form of antibody-conjugated.

Novel anticarcinoembryonic antigen antibody-drug conjugate has antitumor activity in the existence of soluble antigen.

In this study, 15-1-32, a fully human anti- CEA antibody, was successfully created. 15-1-32 showed the strongest binding activity to membrane-bound CEA compared with other existing CEA antibodies, while its reactivity to soluble CEA was weak. Thus, 15-1-32 was retained on the cell surface depend on the membrane-bound CEA expression level in the presence of the soluble CEA. From the results of immunohistochemistry analysis, the specificity, intensity, and frequency of 15-1-32 against human stomach and esophagus cancer tissue were similar to those of labetuzumab, which is the parental antibody of IMMU-130 in phase II clinical trials for the colorectal cancers. This suggests that 15-1-32 retains membrane-bound CEA recognition property expressed on tumor tissue and can be applied for future clinical use.

15-1-32 based ADC, 15-1-32-vcMMAE, by using our Actibody technology was evaluated. Cytotoxic activity of 15-1-32-vcMMAE was almost same as labetuzumab-vcMMAE against CEA expressing MKN45 cells. Furthermore, in contrast to labetuzumab-vcMMAE, soluble CEA did not have much influence on the cytotoxicity of 15-1-32- vcMMAE because of its unique binding property against soluble and membrane-bound CEA. These results indicate that favorable binding properties against membrane-bound CEA, and powerful antitumor effect of vcMMAE conjugate *in vitro*

suggest that 15-1-32 has great potential in clinical application in the detection or treatment of CEA-positive tumors.

TRAIL-R2 Superoligomerization Induced by Human Monoclonal Agonistic Antibody KMTR2.

The fully human monoclonal antibody KMTR2 acts as a strong direct agonist for TRAIL-R2, which is capable of inducing apoptotic cell death without cross-linking. In this study, the mechanism of direct agonistic activity of KMTR2 was evaluated by analyzing the crystal structure of the complex of extracellular region of TRAIL-R2 and the KMTR2-Fab fragment. The 2.1 Å resolution crystal structure of complex was determined and two KMTR2-Fabs assembled via the CDR2 of the light chain each other. This association mode was quite different from that in complex without TRAIL-R2. These results suggested that the KMTR2-Fab assembly identified in complex with TRAIL-R2 tended to enhance TRAIL-R2 oligomerization.

To validate that the Fab dimerization based on this two-fold symmetry was essential for the direct agonistic activity of KMTR2, a single mutation at Asn53 to Arg located in the light chain CDR2 of KMTR2 (LkN53R) was evaluated. The results showed that LkN53R lost its apoptotic activity, although it retained its antigen-binding activity. These results indicate that the strong agonistic activity, such as apoptotic signaling and tumor regression, induced by KMTR2 is attributed to TRAIL-R2 superoligomerization induced by the interdimerization of KMTR2.

List of publications

1. **One-Step Conjugation Method for Site-Specific Antibody-Drug Conjugates through Reactive Cysteine-Engineered Antibodies.**

   Daisuke Shinmi, Eri Taguchi, Junko Iwano, Tsuyoshi Yamaguchi, Kazuhiro Masuda, Junichi Enokizono, and Yasuhisa Shiraishi

   Bioconjug. Chem., 27, 1324-1331, 2016.

2. **Novel anticarcinoembryonic antigen antibody-drug conjugate has antitumor activity in the existence of soluble antigen.**

   Daisuke Shinmi, Ryosuke Nakano, Keisuke Mitamura, Minami Suzuki-Imaizumi, Junko Iwano, Yuya Isoda, Junichi Enokizono, Yasuhisa Shiraishi, Emi Arakawa, Kazuma Tomizuka, and Kazuhiro Masuda

   Cancer Med., 6, 798–808., 2017.

3. **TRAIL-R2 Superoligomerization Induced by Human Monoclonal Agonistic Antibody KMTR2.**

   Taro Tamada, **Daisuke Shinmi**, Masahiro Ikeda, Yasushi Yonezawa, Shiro Kataoka, Ryota Kuroki, Eiji Mori, and Kazuhiro Motoki

   Sci. Rep., 5, 17936, 2015.

Other publications

1. **Identification of highly reactive cysteine residues at less exposed positions in the Fab constant region for site-specific conjugation.**

   Yasuhisa Shiraishi, Takashige Muramoto, Kazutaka Nagatomo, **Daisuke Shinmi**, Emiko Honma, Kazuhiro Masuda, and Motoo Yamasaki

   Bioconjug. Chem., 26, 1032-1040. 2015.

2. **Genetically encoded fluorescent thermosensors visualize subcellular thermoregulation in living cells.**

   Shigeki Kiyonaka, Taketoshi Kajimoto, Reiko Sakaguchi, **Daisuke Shinmi**, Mariko Omatsu-Kanbe, Hiroshi Matsuura, Hiromi Imamura, Takenao Yoshizaki, Itaru Hamachi, Takashi Morii, and Yasuo Mori

   Nat. Methods, 10, 1232-1238, 2013

3. **Efficient antibody production upon suppression of O mannosylation in the yeast Ogataea minuta.**

   Kousuke Kuroda, Kazuo Kobayashi, Yoshinori Kitagawa, Taishiro Nakagawa, Haruhiko Tsumura, Toshihiro Komeda, **Daisuke Shinmi**, Eiji Mori, Kazuhiro Motoki, Kazumi Fuju, Teruyuki Sakai, Koichi Nonaka, Takeshi Suzuki, Kimihisa Ichikawa, Yasunori Chiba, and Yoshifumi Jigami

   Appl. Environ. Microbiol., 74, 446-453, 2008

4. **Oligo-Asp tag/Zn(II) complex probe as a new pair for labeling and fluorescence**

imaging of proteins.

Akio Ojida, Kei Honda, **Daisuke Shinmi**, Shigeki Kiyonaka, Yasuo Mori, and Itaru Hamachi

J. Am. Chem. Soc., 128, 10452-10459, 2006

Reprinted with permission from Bioconjugate Chem., 2016, 27, 1324-1331. Copyright (2016) American Chemical Society.

10.1021/acs.bioconjchem.6b00133

10.1002/cam4.1003

10.1038/srep17936.